

Magnetic pyrochlore oxides

Jason S. Gardner*

NIST Center for Neutron Research, National Institute of Standards and Technology Gaithersburg, MD 20899-6102 and Indiana University, 2401 Milo B. Sampson Lane, Bloomington, IN 47408-1398, USA

Michel J. P. Gingras†

Department of Physics and Astronomy, University of Waterloo, Waterloo, ON, N2L 3G1 and Canadian Institute for Advanced Research, 180 Dundas St. W., Toronto, ON, M5G 1Z8, Canada

John E. Greedan‡

Department of Chemistry and Brockhouse Institute for Materials Research, McMaster University, Hamilton, ON, L8S 4M1, Canada

(Dated: February 3, 2022)

Within the past 20 years or so, there has occurred an explosion of interest in the magnetic behavior of pyrochlore oxides of the type $A_2^{3+}B_2^{4+}O_7$ where A is a rare-earth ion and B is usually a transition metal. Both the A and B sites form a network of corner-sharing tetrahedra which is the quintessential framework for a geometrically frustrated magnet. In these systems the natural tendency to form long range ordered ground states in accord with the Third Law is frustrated, resulting in some novel short range ordered alternatives such as spin glasses, spin ices and spin liquids and much new physics. This article attempts to review the myriad of properties found in pyrochlore oxides, mainly from a materials perspective, but with an appropriate theoretical context.

Contents

I Introduction

I. Overview	2
II. Motivation for the study of frustration	3
III. Historical Perspective	4
IV. Theoretical Background	5

II Materials

V. Crystal Structure	8
A. Space Group and Atomic Positions	8
B. Local Environment of the A and B -Sites	9
C. Alternative Views of the Pyrochlore Structure	10
D. Phase Stability	10
VI. Sample Preparation and Characterisation	11
VII. Metal Insulator Transitions in the Oxide Pyrochlores	11

III Experimental Results

VIII. Long-Range Ordered Phases	13
A. $Gd_2Ti_2O_7$ and $Gd_2Sn_2O_7$	13
B. $Er_2Ti_2O_7$	15
C. $Tb_2Sn_2O_7$	16
D. $A_2Ru_2O_7$ ($A = Y, Gd, Dy, Ho, Er$ and Tl)	17
E. $A_2Mn_2O_7$ ($A = Sc, Y, Tb - Lu$ and Tl)	19
1. $Tl_2Mn_2O_7$	19
2. $Y_2Mn_2O_7$	20
3. $Ho_2Mn_2O_7$ and $Yb_2Mn_2O_7$	22
F. $A_2Ir_2O_7$ ($A = Nd - Yb$)	23
G. $A_2Mo_2O_7$ ($A = Gd, Nd$ and Sm)	25
1. $Gd_2Mo_2O_7$	25
2. $Nd_2Mo_2O_7$	26
3. $Sm_2Mo_2O_7$	27
4. $A_2(MoB)_2O_7$	27
IX. Spin Glass Phases	28
A. $Y_2Mo_2O_7$ and $Tb_2Mo_2O_7$	29
1. $Y_2Mo_2O_7$	29
2. $Tb_2Mo_2O_7$	31
3. Other $A_2Mo_2O_7$	32
X. Spin Ice Phases	33
A. $Dy_2Ti_2O_7$ and $Ho_2Ti_2O_7$	35
B. $A_2Sn_2O_7$ ($A = Pr, Dy$ and Ho)	40
C. $Ho_{2+x}Ti_{2-x}O_{7-\delta}$: stuffed spin ice	40
XI. Spin Liquid Phases	41
A. $Tb_2Ti_2O_7$	41
B. $Yb_2Ti_2O_7$	44
C. $Er_2Sn_2O_7$	44
D. $Pr_2Ir_2O_7$	45
XII. External Perturbations	45
A. Magnetic Field	46
1. $Gd_2Ti_2O_7$	46
2. Kagome ice	46
3. $Tb_2Ti_2O_7$	47
B. High Pressure	47
1. $Tb_2Ti_2O_7$	48

*Electronic address: jsg@nist.gov

†Electronic address: gingras@gandalf.uwaterloo.ca

‡Electronic address: greedan@univmail.cis.mcmaster.ca

IV Conclusions

Acknowledgements

References

Part I

Introduction

I. OVERVIEW

Competing interactions, or frustration, are common in systems of interacting degrees of freedom. The frustration arises from the fact that each of the interactions in competition tends to favor its own characteristic spatial correlations. A more operational definition classifies a system as frustrated whenever it cannot minimize its total classical energy by minimizing the interaction energy between each pair of interacting degrees of freedom, pair by pair. Frustration is ubiquitous in condensed matter physics. It arises in liquid crystals, in superconducting Josephson junction arrays in a magnetic field, in molecular crystals such as solid N_2 , and in magnetic thin films. Frustration is important outside the realm of condensed matter physics in, for example, the competition between nuclear forces and long-range electrostatic Coulomb interactions between protons which is believed to lead to the formation of a so-called “nuclear pasta” state of spatially modulated nuclear density in stellar interiors. This enhances the scattering cross-section for neutrinos with nuclear matter and may be a factor in the mechanism of supernovae explosions. Yet, perhaps, the most popular context for frustration is in magnetic systems. This review is concerned with the many interesting and often exotic magnetic and thermodynamic phenomena that have been observed over the past twenty years in a broad family of geometrically frustrated magnetic materials, the pyrochlore oxides. Before launching into the review per se, we first briefly outline what is meant by geometric magnetic frustration and comment on the scientific motivation for investigating geometrically frustrated magnetic systems.

Although the details will be provided later, here we give the reader a brief introduction to the key issues in frustrated magnetic systems. One can distinguish two classes of frustrated magnetic systems: those in which the frustration is *geometric* and those in which it is *random*. The simplest example of geometric frustration is that of Ising spins which can only point in two possible (up or down) directions, interacting via nearest-neighbor antiferromagnetic exchange and which lie at the vertices of an equilateral triangle as shown in Fig. 1. Under those conditions, it is impossible for the three spins to align mutually antiparallel to each other. When many triangles

are condensed to form an edge-sharing triangular lattice, a massive level of configurational spin disorder results, giving rise to an extensive residual zero temperature entropy and no phase transition down to absolute zero temperature (Houtappel, 1950; Wannier, 1950). This example is one of geometric frustration since it is the regular periodic structure of the (here triangular) space lattice that imposes the constraint inhibiting the development of a long range ordered state given antiferromagnetic interactions between the spins. The same system with Ising spins on a triangular lattice, but with ferromagnetic interactions, is not frustrated and displays a second order phase transition to long range order at nonzero temperature.

One can distinguish two types of random frustration. The first one arises due to competing interactions among degrees of freedom in full thermodynamic equilibrium, as in the case of liquid crystals and the nuclear pasta mentioned above. Although it is not commonly referred to as such, one could speak of “dynamical frustration” or “annealed frustration”, by analogy to annealed disorder. Since there is rarely only one type of interaction setting a sole characteristic length scale in any realistic system, annealed frustration is really the norm. In this context, the most dramatic signature of dynamical frustration occurs when multiple length scales develop, as in modulated phases of condensed matter, for example the case of stripes in the copper oxide superconducting materials, or in the case of reentrant phase transitions, as in some liquid crystal materials. In other words, a system with competing interactions will often attempt to resolve the underlying frustration by developing non-trivial spatial correlations, such as modulated structures, whenever full dynamical equilibrium is maintained. We will return below to the topic of multiple dynamical degrees of freedom and annealed frustration when we discuss the role that lattice degrees of freedom may play in geometrically frustrated magnetic systems.

The other case of random frustration arises when the randomness is “quenched”, i.e. frozen in. This occurs when a subset of the degrees of freedom evolve on a time scale that is, for all practical purposes, infinitely long compared to the predominant degrees of freedom under focus. Consider the example above of the triangular lattice Ising antiferromagnet. There, the position of the atoms is quenched and only the magnetic (spin) degrees of freedom are dynamical. This is an example of quenched frustration. However, the frustration in that case is said to be *geometric*, not random. Quenched random frustration arises in systems where the frozen degrees of freedom (e.g. positions of the magnetic atoms) are not related by periodic translational invariance. One example of random frustration is that of magnetic iron (Fe) atoms in a gold (Au) matrix. In AuFe, the interaction between the Fe moments is mediated by conduction electrons via the RKKY (Rudermann-Kittel-Kasuya-Yoshida) $J_{\text{RKKY}}(r)$ interaction, which can be either ferromagnetic or antiferromag-

netic depending on the distance r between two magnetic Fe atoms. Depending on their relative separation distance, some trios of Fe spins will have either one or three of their J_{RKKY} interactions antiferromagnetic, and will therefore be frustrated. Because the atomic positions are frozen-in, this is an example of *quenched random frustration*. Quenched random frustration is a crucial ingredient in the physics of spin glass materials (Binder and Young, 1986). These systems exhibit a transition between a paramagnetic state of thermally fluctuating spins to a glass-like state of spins frozen in time, but random in direction. Random frustration can also arise when the magnetic moments in an otherwise disorder-free geometrically frustrated system are diluted, or substituted, with non-magnetic atoms (Binder and Young, 1986; Villain, 1979).

While it is common to invoke exchange interactions between spins as the source of their magnetic coupling, there are cases, discussed in some detail below, where magnetostatic dipole-dipole interactions play a crucial role. Because of their long-range nature and angular dependence, dipolar interactions are intrinsically frustrated, irrespective of the lattice dimensionality or topology. Indeed, two dipole moments μ_1 and μ_2 at positions \mathbf{r}_2 and \mathbf{r}_1 ($\mathbf{r}_{12} = \mathbf{r}_2 - \mathbf{r}_1$) reach their minimum energy for $\mu_1 \parallel \mu_2 \parallel \mathbf{r}_{12}$. Obviously, this condition cannot be met for any system of more than two dipole moments that are not all located on a perfectly straight line. As a result, even systems where long-range collinear ferromagnetism is due to dipolar interactions, are in fact frustrated, and display quantum mechanical zero point fluctuations (Corruccini and White, 1993; White *et al.*, 1993). This example illustrates that even systems which achieve a seemingly simple, conventional long range order can be subject to frustration of their underlying microscopic interactions. Being intrinsically frustrated, the introduction of randomness via the substitution of dipole-carrying atoms by non-magnetic (diamagnetic) species, can lead for sufficiently large dilution to a spin glass phase (Binder and Young, 1986; Villain, 1979).

II. MOTIVATION FOR THE STUDY OF FRUSTRATION

Magnetism and magnetic materials are pervasive in everyday life, from electric motors to hard disk data storage. From a fundamental perspective, magnetic materials and theoretical models of magnetic systems have, since the original works of Ising and Potts, offered physicists perhaps the best test bench to investigate the broad fundamental concepts, even at times universal ones, underlying collective phenomena in nature. The reasons for this are threefold. Firstly, from an experimental perspective, magnetic materials present themselves in various aspects. They can be metallic, insulating or semi-conducting. As well, the magnetic species may reside on crystalline lattices which are spatially anisotropic, providing examples of quasi-one or quasi-two dimensional

systems and permitting an exploration of the role that spatial dimensionality plays in phase transitions. Secondly, and perhaps most importantly, magnetic materials can be investigated via a multitude of experimental techniques that can probe many aspects of magnetic and thermodynamic phenomena by exploring spatial and temporal correlations over a range of several decades of length or time scales. Finally, from a theoretical view point, magnetic materials can often be described by well-defined microscopic Hamiltonian models which, notwithstanding the mathematical complexity commonly associated in solving them, allow in principle to develop a theoretical framework that can be used to interpret experimental phenomena. This close relationship between theory and experiment has been a key characteristic of the systematic investigation of magnetism since its incipency. Such a symbiotic relationship between experiment and theory has been particularly strong in the context of investigations of frustrated magnetism systems. Indeed, a number of experimental and theoretical studies in frustrated magnetic systems were originally prompted by theoretical proposals. We briefly mention two. The first pertains to the proposal that frustrated antiferromagnets with a non-collinear ordered state may display a transition to a paramagnetic state belonging to a different (“chiral”) universality class from conventional $O(N)$ universality for collinear magnets (Kawamura, 1988). The second, perhaps having stimulated the largest effort, is that some frustrated quantum spin systems may lack conventional semi-classical long-range order altogether and possess instead a quantum disordered “spin liquid” state breaking no global spin or lattice symmetries (Anderson, 1973, 1987).

Systems where magnetic moments reside on lattices of corner-sharing triangles or tetrahedra are subject to geometric magnetic frustration, as illustrated in Fig. 1, and are expected to be ideal candidates for exhibiting large quantum mechanical spin fluctuations and the emergence of novel, exotic, magnetic ground states.

The cubic pyrochlore oxides, $A_2B_2O_7$, have attracted significant attention over the past twenty years because the A and B ions reside on two distinct interpenetrating lattices of corner-sharing tetrahedra as shown in Fig. 2. Henceforth, we shall refer to the lattice of corner-sharing tetrahedra simply as the pyrochlore lattice, as has become customary since the mid 1980’s. If either A , B or both are magnetic, and the nearest-neighbor exchange interaction is antiferromagnetic, the system is highly geometrically frustrated. As a result, antiferromagnetically coupled classical Heisenberg spins on the pyrochlore lattice do not develop long range order at any nonzero temperature, opening up new avenues for novel, intrinsically quantum mechanical, effects to emerge at low temperatures.

In all real systems, interactions beyond isotropic nearest-neighbor exchange are at play. Exchange beyond nearest-neighbors, symmetric and antisymmetric (Dzyaloshinskii-Moriya) exchange, dipolar interactions

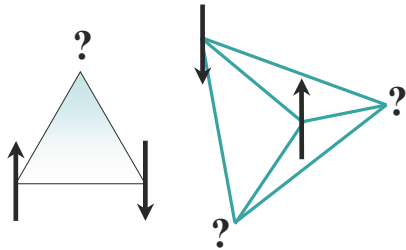


FIG. 1 Antiferromagnetically coupled spins arranged on a triangle or tetrahedron are geometrically frustrated.

and magnetoelastic couplings are all concrete examples of corrections to the isotropic nearest-neighbor exchange part of the Hamiltonian, \mathcal{H}_H . These additional interactions, \mathcal{H}' , are typically weaker than \mathcal{H}_H and, often, two or more terms in \mathcal{H}' compete to dictate the development of the spin-spin correlations as the system is cooled from the paramagnetic phase. The specific details pertaining to the material under consideration determine whether the perturbations \mathcal{H}' are able, ultimately, to drive the system into a semi-classical long-range ordered state, or whether quantum fluctuations end up prevailing. It is for this reason that many magnetic pyrochlore oxides have been found to display a gamut of interesting and unconventional magnetic and thermodynamic behaviors. Examples of phenomena exhibited by $A_2B_2O_7$ materials include spin glass freezing in $Y_2Mo_2O_7$, spin liquid behavior in $Tb_2Ti_2O_7$, disordered spin ice (not to be confused with spin glass) phenomenology in $Ho_2Ti_2O_7$ and $Dy_2Ti_2O_7$, ordered spin ice in $Tb_2Sn_2O_7$, order-by-disorder in $Er_2Ti_2O_7$, unconventional anomalous Hall effect in metallic $Nd_2Mo_2O_7$, superconductivity in $Cd_2Re_2O_7$ and the Kondo-like effect in $Pr_2Ir_2O_7$, to name a few.

The above examples illustrate the broad diversity of phenomena exhibited by pyrochlore oxides. There exist a number of general reviews concerned with pyrochlore structure materials such as those by Subramanian *et al.* (1983), Greedan (1992a), and Subramanian and Sleight (1993) and more focused reviews for example on the rare earth titanates, (Greedan, 2006). As well, pyrochlore structure materials are often featured in more general reviews of geometrically frustrated magnetic materials, such as those by Ramirez (1994), Schiffer and Ramirez (1996), Greedan (2001) and others (Diep, 1994, 2004; Gaulin, 1994). The purpose of this article is to provide, given the space limitations, a comprehensive review of both experimental and theoretical investigations of the $A_2B_2O_7$ materials over the past twenty years or so. Whenever possible, we outline what we perceive as promising avenues for future work. Thus, space limitations preclude detailed discussion of other very interesting highly frustrated magnetic materials based on lattices

of corner-shared triangles such as kagome systems and garnets, or the spinels and Laves phases, which are also based on the pyrochlore lattice. However, we will refer to those materials in specific contexts whenever appropriate in order to either contrast or relate to the behavior observed in the pyrochlore oxides.

This review is organized as follows: after a brief historical overview and some generalities on geometrically frustrated magnets we review and discuss experimental data from the most static (i.e. long range ordered phases) to the most dynamic (i.e. spin liquid phases). Then follows a brief section on the superconducting compounds found among pyrochlore oxides, although frustration has not been demonstrated to play a role here. Finally, we report on salient results from experiments performed under the influence of applied magnetic field or pressure. We conclude the review by a brief discussion of perceived avenues for future research.

III. HISTORICAL PERSPECTIVE

The term frustration, meaning the inability of a plaquette of spins with an odd number of antiferromagnetic bonds to adopt a minimum energy collinear spin configuration, first appeared in a paper on spin glasses by Toulouse (1977) and soon after, in one by Villain (1977). However, it is said that the concept of frustration as a key ingredient in the physics of spin glasses was first introduced by Anderson who apparently wrote on a blackboard at a summer school in Aspen in 1976 “*Frustration is the name of the game*” (Chandra and Coleman, 1995; Harrison, 2004). It is interesting that the notion of frustration, random frustration to be more precise, had to await the discovery of spin glasses before it was introduced in magnetism.

Indeed, geometrically frustrated antiferromagnets, without being labeled as such, had been studied much earlier. In 1950, Wannier (1950) and Houtappel (1950) investigated the exact solution of the Ising antiferromagnet on the triangular lattice, finding that no transition to long range order occurs at positive temperature and that the system possesses an extensive ground state entropy. Soon after, following on a previous work by Néel (1948), Yafet and Kittel (1952) investigated the problem of antiferromagnetic spin arrangements in spinel ferrite materials and the role of magnetic interactions between the octahedral and the tetrahedral sites in determining the ground state spin structure, where the octahedral sites form a pyrochlore lattice. Motivated by the problem of magnetic ordering for spins on the octahedral sites of normal spinels and the related one of ionic ordering in inverse spinels, Anderson (1956) investigated the physics of antiferromagnetically coupled Ising spins on what we now recognize as the pyrochlore lattice. This work appears to have been the first to identify clearly the peculiar magnetic properties of this system and, in particular, noted the existence of a macroscopic number of ground

states, and the connection with the problem of the zero point proton entropy in hexagonal water ice previously investigated by Pauling (1935). We will return to the connection between geometrically frustrated Ising spins on the pyrochlore lattice and the water ice problem later.

Quantum mechanics made its first noticeable entry in the realm of geometrically frustrated magnetism in 1973 when Anderson (1973) proposed that a regular two-dimensional triangular lattice of spins $S = 1/2$ coupled via nearest-neighbor antiferromagnetic exchange could, instead of displaying a three sublattice 120 degree Néel ordered state, possess an exotic *resonating valence bond* liquid of spin singlets. This proposal was further examined and its conclusion supported by more detailed calculations by Fazekas and Anderson (1974). While Anderson (1973) had written that there were no experimental realizations of an $S = 1/2$ antiferromagnet with isotropic exchange, the situation would change dramatically almost twenty-five years later with the 1987 discovery of the copper-oxide based high-temperature superconductors, some of which possess a parent insulating state with antiferromagnetically coupled $S = 1/2$ spins (Anderson, 1987).

The discovery of spin glasses by Cannella and Mydosh (1972) prompted a flurry of experimental and theoretical activity aimed at understanding the nature of the observed spin freezing and determining whether a true thermodynamic *spin glass* phase transition occurs in these systems. Particularly relevant to this review, Villain (1979) investigated the general problem of insulating spin glasses and the role of weak dilution of the B -site pyrochlore lattice in spinels. The extensive ground state degeneracy characterizing this system for classical Heisenberg spins interacting via nearest-neighbor antiferromagnetic exchange J was noted. He speculated that such a system would remain in a paramagnetic-like state down to zero temperature, giving rise to a state at temperatures $T \ll J$ that he called a *collective paramagnet* – a classical spin liquid of sorts. Villain (1979) also considered the case of tetragonal spinels where there are two exchange couplings, J and J' , perpendicular and parallel to the tetragonal axis. More recently, theoretical (Tchernyshyov *et al.*, 2002; Yamashita and Ueda, 2000) and experimental (Lee *et al.*, 2000) studies have investigated the cubic to tetragonal distortion in spinels, which leads to a relief of the magnetic frustration and allows the system to develop long range magnetic order. Villain discussed how the effect of a *weak* dilution of the magnetic moments may be dramatically different in the case of cubic spinels compared to those with a slight tetragonal distortion. In particular, he argued that in the case of the cubic spinel, weak dilution would leave the system a collective paramagnet, while for the tetragonal spinel the ground state would be glassy.

While there had been some experimental studies on non-collinear magnets between the work of Villain and the mid-to-late 1980's (Coey, 1987), the high level of research activity in the field of frustrated magnetism re-

ally only started following the discovery of the unconventional magnetic properties of $\text{SrCr}_{9-x}\text{Ga}_{3+x}\text{O}_{19}$ (SCGO) by Obradors *et al.* (1988). In the context of oxide pyrochlores, the topic of this review, experimental and theoretical interests developed in the mid-1980's with reports of spin glass behavior in the apparently well-ordered material $\text{Y}_2\text{Mo}_2\text{O}_7$ and accelerated rapidly after 1990.

IV. THEORETICAL BACKGROUND

The amount of theoretical work dedicated to the topic of highly frustrated systems, particularly quantum spin systems, has exploded over the past ten years. It is beyond our scope here to discuss more than a fragment and in fact the field is so active that a dedicated review would at this time be warranted. Short of such being available, we refer the reader to a somewhat recent book edited by Diep (2004) and a forthcoming one by edited by Mila (2008). In this section, we merely present the simplest and most generic theoretical arguments of relevance to the pyrochlore systems. The focus of the discussion is on the effects of perturbations on a nearest-neighbor Heisenberg pyrochlore antiferromagnet.

One simple and highly convenient measure of the level of frustration in magnetic system is the so-called *frustration index* f (Ramirez, 1994), defined as

$$f \equiv \frac{|\theta_{\text{CW}}|}{T^*}. \quad (1)$$

Here θ_{CW} is the Curie or Curie-Weiss temperature, defined from the high temperature paramagnetic response of the system, i.e. the high temperature, linear part of the inverse DC susceptibility. The temperature T^* is the critical temperature T_c (or Néel temperature, T_N) at which the system ultimately develops long range spin order. In the case of freezing into a glassy state, which may correspond to a genuine thermodynamic spin glass transition, T^* would be the freezing temperature T_f . The more frustrated a system is, the lower T^* is compared to θ_{CW} , hence an ideal spin liquid system would have $f = \infty$. In most real materials there are, however, perturbative interactions, \mathcal{H}' that ultimately intervene at low temperature and lead to the development of order out of the spin liquid state. The rest of this section discusses some of the most common perturbations.

Anderson (1956) and Villain (1979) were the first to anticipate the absence of long range order at nonzero temperature in the Ising (Anderson, 1956) and Heisenberg (Villain, 1979) pyrochlore antiferromagnet. The Hamiltonian for the Heisenberg antiferromagnet model is

$$\mathcal{H}_H = -J \sum_{\langle i,j \rangle} \mathbf{S}_i \cdot \mathbf{S}_j, \quad (2)$$

where we take for convention that $J < 0$ is antiferromagnetic while $J > 0$ is ferromagnetic. The spins \mathbf{S}_i can be,

at least within the model, taken either as classical and of fixed length $|\vec{S}_i| = 1$ or quantum. A model with $n = 1$, $n = 2$ or $n = 3$ components of \vec{S} corresponds to the Ising, XY and Heisenberg model, respectively. Since the pyrochlore lattice has cubic symmetry, the Ising and XY models with a uniform global Ising easy axis direction \hat{z} or XY global plane are not physical. One can however, define local \hat{z}_i Ising directions or local XY planes with normal \hat{z}_i that are parallel to the four cubic $\langle 111 \rangle$ directions.

A mean field theory calculation for the Heisenberg Hamiltonian by Reimers *et al.* (1991a) provided indirect confirmation of Anderson and Villain's result by finding that a nearest-neighbor model with classical Heisenberg spins on the pyrochlore lattice has two (out of four) branches of exactly degenerate soft (critical) modes throughout the Brillouin zone. In other words, there is an extensive number of soft modes in this system and no unique state develops long range order at the mean field critical temperature. In early Monte Carlo simulations, Reimers (1992) found no sign of a transition in this system, either to long range order or to a more complex type, such as nematic order, down to a temperature of $J/20$, where J is the nearest-neighbor antiferromagnetic exchange constant. This conclusion was confirmed in numerical studies by Moessner and Chalker (1998,a). This behavior of the nearest-neighbor pyrochlore antiferromagnet differs markedly from that of the nearest-neighbor classical Heisenberg antiferromagnet on the two-dimensional kagome lattice where co-planar order-by-disorder develops as the temperature drops below $\sim J/100$ (Chalker *et al.*, 1992; Reimers and Berlinsky, 1993). However, the Mermin-Wagner-Hohenberg theorem forbids a phase transition at nonzero temperature in the kagome Heisenberg antiferromagnet. While no transition is seen in the pyrochlore Heisenberg system (Moessner and Chalker, 1998,a; Reimers, 1992), the pyrochlore lattice with easy-plane (XY) spins, where the easy planes are perpendicular to the local $\langle 111 \rangle$ directions, displays a phase transition to long range order (Bramwell *et al.*, 1994; Champion *et al.*, 2003). Finally, in agreement with Anderson's prediction (Anderson, 1956), Monte Carlo simulations find that the Ising antiferromagnet, or equivalently the Ising ferromagnet with local $\langle 111 \rangle$ directions, which is the relevant model to describe spin ice materials, does not order down to the lowest temperature (Harris *et al.*, 1998).

Moessner and Chalker (1998,a) investigated the conditions under which an n -component classical spin \vec{S}_i with $|\vec{S}_i| = 1$ arranged on a lattice of corner-sharing units of q sites and interacting with $q - 1$ neighbors in each unit can exhibit thermally-induced order-by-disorder. Their analysis allows one to rationalize why the Heisenberg $n = 3$ kagome antiferromagnet develops co-planar order and why the XY pyrochlore antiferromagnet (with spins in a global XY plane) develops collinear order (Moessner and Chalker, 1998). From their analysis, one would predict a phase transition to long range nematic order

for $q = 3, n = 3$ in three spatial dimensions. Interestingly, such a situation arises in the $S = 1/2$ $\text{Na}_4\text{Ir}_3\text{O}_8$ hyperkagome (Okamoto *et al.*, 2007) and $\text{Gd}_3\text{Ga}_5\text{O}_{12}$ garnet (Dunsiger *et al.*, 2000; Petrenko *et al.*, 1998; Schiffer *et al.*, 1994, 1995a; Yavors'kii *et al.*, 2006). Moving away from the strictly nearest-neighbor model, one would generally expect interactions beyond nearest-neighbors to drive a transition to an ordered state, at least for classical spins (Reimers, 1992). While this has been studied via Monte Carlo simulations (Mailhot and Plumer, 1993; Reimers *et al.*, 1992), it has not been the subject of very many investigations. In that context, we note that a paper by Pinettes *et al.* (2002) studies a classical Heisenberg pyrochlore antiferromagnet with an additional exchange interaction J' that interpolates between the pyrochlore lattice ($J' = 0$) and the face-centered cubic lattice ($J' = J$). It is found that for J'/J as low as $J'/J \sim 0.01$, the system orders into a collinear state whose energy is greater than the classical incommensurate ground state predicted by mean field theory. A Monte Carlo study of another classical model of a pyrochlore lattice with antiferromagnetic nearest-neighbor exchange and ferromagnetic next nearest-neighbor exchange finds an ordered state with mixed ordered and dynamical character (Tsuneishi *et al.*, 2007). Because the pyrochlore lattice lacks bond inversion symmetry, Dzyaloshinsky-Moriya (DM) spin-spin interactions arising from spin-orbit coupling are allowed by symmetry and can give rise to various ordered states depending on the orientation of the DM vector (Elhajal *et al.*, 2005).

As we will discuss below, a number of pyrochlore materials exhibit glassy behavior where the spins freeze at low temperature into a state where their orientation is random in space, but frozen in time (Binder and Young, 1986). It is not yet fully understood whether this glassy behavior is due to the intrinsic nature of the systems considered, as is the case for the spin ices, or if it originates from random disorder (e.g. antisite disorder, random bonds or other) as in conventional random disorder spin glasses (Binder and Young, 1986). Only a very few theoretical studies have explored the effect of random disorder in antiferromagnetic pyrochlores with classical Heisenberg spins and with small and homogeneously random deviations of exchange J_{ij} from the average antiferromagnetic exchange J (Bellier-Castella *et al.*, 2001; Saunders and Chalker, 2007). Interestingly, random bonds on a single tetrahedron lift the degeneracy and drive an order-by-(random)-disorder to a collinear spin arrangement. However, on the lattice, the system remains frustrated and there is no global order-by-disorder (Bellier-Castella *et al.*, 2001). Considering this model in more detail, Saunders and Chalker (2007) find compelling evidence of a conventional spin glass transition. Sagi *et al.* (2005) have investigated how coupling with the spins to the lattice may lead to a freezing behavior and trapping of the spins into metastable states in an otherwise disorder-free nearest-neighbor classical pyrochlore antiferromagnet. Villain (1979) discussed the

role of non-magnetic impurities on the pyrochlore lattice antiferromagnet. He argued that the collective paramagnetic behavior of the otherwise disorder-free system should survive up to a finite concentration of impurities. A similar conclusion was reached on the basis of heuristic arguments and simulations for the site-diluted two-dimensional kagome Heisenberg antiferromagnet (Shender *et al.*, 1993). It would be valuable if the problems of site-disorder and dilute random bonds in the antiferromagnetic pyrochlore lattice were explored in more detail. We note in passing that the problem of disorder in quantum variants of the kagome Heisenberg antiferromagnet has attracted some attention (Läuchli *et al.*, 2007).

In insulating $A_2B_2O_7$, where A is a 4f rare-earth trivalent ion, the inter-rare-earth exchange interactions are often small, contributing only $10^0 - 10^1$ K to the Curie-Weiss θ_{CW} temperature. This is because the unfilled magnetically active 4f orbitals are strongly shielded by the 5s, 5p and 5d orbitals and their direct exchange overlap or superexchange overlap is small. At the same time, trivalent rare earths often possess large magnetic moments and hence the magnetostatic dipole-dipole energy scale is significant compared to θ_{CW} and needs to be incorporated into Eq. (2),

$$\mathcal{H}_{\text{int}} = -\frac{1}{2} \sum_{(i,j)} \mathcal{J}_{ij} \mathbf{J}_i \cdot \mathbf{J}_j + \left(\frac{\mu_0}{4\pi} \right) \frac{(g_L \mu_B)^2}{2r_{\text{nn}}^3} \sum_{(i,j)} \frac{(\mathbf{J}_i \cdot \mathbf{J}_j - 3\mathbf{J}_i \cdot \hat{\mathbf{r}}_{ij} \hat{\mathbf{r}}_{ij} \cdot \mathbf{J}_j)}{(r_{ij}/r_{\text{nn}})^3}. \quad (3)$$

Here we have taken the opportunity to generalize Eq. (2) to the case where the total angular momentum $\mathbf{J}_i = \mathbf{L}_i + \mathbf{S}_i$ is included. g_L is the Landé factor and $\mathbf{r}_j - \mathbf{r}_i = |\mathbf{r}_{ij}| \hat{\mathbf{r}}_{ij}$, where \mathbf{r}_i is the position of magnetic ion i . In general, one needs to include the role of the single-ion crystal field, \mathcal{H}_{cf} , to the full Hamiltonian, $\mathcal{H} = \mathcal{H}_{\text{cf}} + \mathcal{H}_{\text{int}}$.

A mean field study of \mathcal{H}_{int} , with $\mathcal{H}_{\text{cf}} = 0$ and with only nearest-neighbor antiferromagnetic \mathcal{J}_{nn} and dipolar interactions of approximately 20% the strength of \mathcal{J}_{nn} , was done by Raju *et al.* (1999) to investigate the type of order expected in $\text{Gd}_2\text{Ti}_2\text{O}_7$. The assumption $\mathcal{H}_{\text{cf}} = 0$ is a reasonable first approximation for $\text{Gd}_2\text{Ti}_2\text{O}_7$ since the electronic ground state of Gd^{3+} is $^8S_{7/2}$ with $L = 0$. Raju *et al.* (1999) argued that this model has an infinite number of soft modes with arbitrary ordering wave vector along [111] and that the transition at ~ 1 K could possibly proceed via order-by-disorder. However, Palmer and Chalker (2000) argued that quartic terms in the mean field Ginzburg-Landau theory would select a $\mathbf{k}_{\text{ord}} = 000$ ordering wavevector at the critical temperature T_c that also corresponds to the zero temperature classical ground state. Subsequent mean field calculations (Cépas and Shastry, 2004; Enjalran and Gingras, 2003) showed that there are in fact two very closely spaced transitions and that the transition at the highest temperature is at a unique ordering wave vector

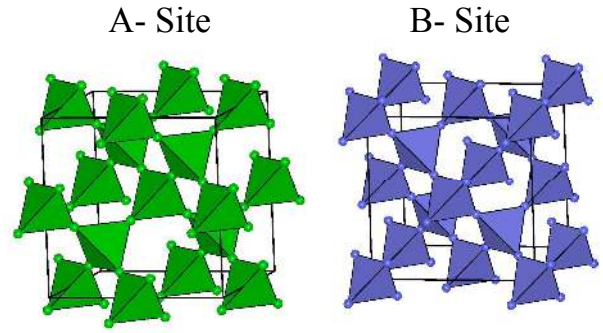


FIG. 2 The A and B sublattices of the cubic pyrochlore materials. Either or both sublattices can be magnetic.

($\mathbf{k}_{\text{ord}} = \frac{1}{2}\frac{1}{2}\frac{1}{2}$) that had been missed in previous calculations (Palmer and Chalker, 2000; Raju *et al.*, 1999). A Monte Carlo simulation (Cépas *et al.*, 2005) found a single first order transition. It appears likely that the small temperature separation between the two transitions that is predicted by mean field theory is not resolved in the Monte Carlo simulation. Irrespective of the subtleties associated with the transition, it is generally accepted that the classical ground state of the nearest-neighbor pyrochlore Heisenberg antiferromagnet with weak dipolar interactions is the so-called Palmer-Chalker ground state (Cépas and Shastry, 2004; Del Maestro and Gingras, 2004, 2007; Enjalran and Gingras, 2003; Palmer and Chalker, 2000; Wills *et al.*, 2006). Starting from the Palmer-Chalker ground state, a $1/S$ expansion calculation shows that all conventional magnetic spin-wave-like excitations of this system are gapped and that the $1/S$ quantum fluctuations are negligible (Del Maestro and Gingras, 2004, 2007). For Ho and Dy-based pyrochlore oxides, the crystal field Hamiltonian \mathcal{H}_{cf} produces a single-ion ground state doublet and the system maps onto a classical dipolar Ising model. We shall return to this model when reviewing the problem of spin ice in Section X.

Another important perturbation of relevance to real materials is the coupling between spin and lattice degrees of freedom. Spin-lattice coupling can lead to a redistribution of the frustration among the magnetic bonds such that the energy cost for distorting the lattice is more than compensated by the energy difference between that of the more strongly coupled antiparallel spins on the compressed bonds compared to the higher energy (frustrated, parallel) spins on the dilated bonds (Tchernyshyov *et al.*, 2002; Yamashita and Ueda, 2000). It is anticipated that such coupling can lead to a global lifting of magnetic degeneracy and drive a transition to long range magnetic order that is accompanied by a cubic to tetragonal lattice deformation. Villain (1979) had also discussed a number of significant differences in the thermodynamic properties and the response to random disorder of a tetragonal spinel compared to that of a cubic spinel. The problems

of magnetic order, lattice distortion, coupling to an external magnetic field and magnetization plateaus in oxide spinels are currently very topical ones (Bergman *et al.*, 2006; Lee *et al.*, 2000; Penc *et al.*, 2004; Tchernyshyov *et al.*, 2002). However, in pyrochlore oxides, interest in the role of the lattice degrees of freedom is just starting to attract attention (Ruff *et al.*, 2007; Sagi *et al.*, 2005).

We close with a brief discussion of the quantum $S = 1/2$ pyrochlore Heisenberg antiferromagnet. This is obviously an extremely difficult problem and there is no consensus yet about the nature of the ground state. It appears to have been first studied by Harris *et al.* (1991) who found indicators that the system may form a dimerized state at low temperature. By applying perturbation theory to the density matrix operator, Canals and Lacroix (1998, 2000) found evidence for a quantum spin liquid in the $S = 1/2$ pyrochlore antiferromagnet. From exact diagonalizations on small clusters, they also found that the singlet-triplet gap is filled with a large number of singlets, similar to what is observed in the $S = 1/2$ kagome lattice antiferromagnet (Lecheminant *et al.*, 1997). Calculations using the contractor-renormalization (CORE) method (Berg *et al.*, 2003) find a ground state that breaks lattice symmetry, analogous to that suggested by Harris *et al.* (1991), and with a singlet-triplet gap filled with singlets, similar to Canals and Lacroix (1998). Moving away from strictly numerical approaches, analytical calculations based on large- N (Moessner *et al.*, 2006; Tchernyshyov *et al.*, 2006) and large- S expansions (Hizi and Henley, 2007) as well as variational calculations away from an exact dimer covering ground state solution (Nussinov *et al.*, 2007) have all been very recently carried out.

Part II

Materials

While this review is focused on the three dimensional pyrochlore lattice, which is shown in Fig. 2, there are of course other lattice types which provide the conditions for geometric frustration. Among these, in two spatial dimensions are the edge-sharing and corner-sharing triangular lattices - the latter best known as the Kagome lattice - and in three spatial dimensions one has garnets, langasites and face centered cubic lattices among others. There exists a considerable and important literature devoted to these materials which lies, unfortunately, outside the scope of this work.

A network of corner-sharing tetrahedra is found in several common mineral types in nature. The octahedrally coordinated B -site of the spinel class of minerals (AB_2O_4) forms a network of corner-sharing tetrahedra. The A - and the B -site can be filled by many ions, but when the B -site is occupied by a trivalent magnetic transition metal ion, magnetic frustration can play a role in its bulk properties. The trivalent chromates have re-

Atom	Wyckoff Position	Point Symmetry	Minimal Coordinates
A	$16d$	$\bar{3}m$ (D_{3d})	$\frac{1}{2}, \frac{1}{2}, \frac{1}{2}$
B	$16c$	$\bar{3}m$ (D_{3d})	$0, 0, 0$
O	$48f$	mm (C_{2v})	$x, \frac{1}{8}, \frac{1}{8}$
O'	$8b$	$43m$ (T_d)	$\frac{3}{8}, \frac{3}{8}, \frac{3}{8}$

TABLE I The crystallographic positions for the space group, $Fd\bar{3}m$ (No. 227) suitable for the cubic pyrochlore $A_2B_2O_6O'$ with origin at $16c$.

cently sparked considerable interest (Lee *et al.*, 2000, 2002; Matsuda *et al.*, 2007; Ueda *et al.*, 2005) in this area of magnetic frustration. Another common family of materials that contain a network of corner-sharing tetrahedra are the cubic Laves phases, such as YMn_2 (Ballou, 2001; Shiga *et al.*, 1993).

As already emphasized, in this review, we will restrict ourselves to the cubic pyrochlore oxides with the general formula $A_2B_2O_7$, where A is a trivalent rare earth which includes the lanthanides, Y and sometimes Sc, and B is either a transition metal or a p-block metal ion. It should be mentioned here that it is possible to form $A_2^{2+}B_2^{5+}O_7$ (2+,5+) pyrochlores, however these are not common and have not been studied in great detail. Most of this manuscript will deal with the (3+,4+) variety of pyrochlores, but when appropriate the (2+,5+) will be discussed.

V. CRYSTAL STRUCTURE

A. Space Group and Atomic Positions

Pyrochlore materials take their name from the mineral $NaCaNb_2O_6F$ pyrochlore, the structure of which was first reported by Gaertner (1930). The name, literally “green fire”, alludes to the fact that the mineral shows a green color upon ignition. Most synthetic pyrochlores of interest here are oxides that crystallize in the space group $Fd\bar{3}m$ (No. 227). As pointed out by Subramanian and Sleight (1993), confusion can exist due to the fact that there exist four possible choices for the origin. Currently, standard practice is to formulate oxide pyrochlores as $A_2B_2O_6O'$ and to place the B ion at $16c$ (the origin of the second setting for $Fd\bar{3}m$ in the International Tables of Crystallography), A at $16d$, O at $48f$ and O' at $8b$ as shown in Table I. Note that there is only one adjustable positional parameter x for the O atom in $48f$. There are at least two important implications of these structural details. One concerns the topology of the $16c$ and $16d$ sites and the other the coordination geometry of the O ligands about the two metal sites. Both the $16c$ and $16d$ sites form a three dimensional array of corner-sharing tetrahedra as shown in Fig. 2, thus giving rise to one of the canonical geometrically frustrated lattices.

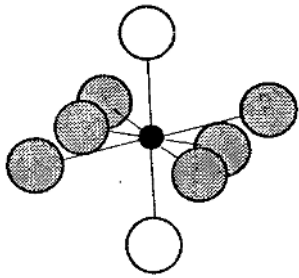


FIG. 3 The coordination geometry of the A -site by O (shaded spheres) and O' (open spheres) atoms. The $O' - A - O'$ unit is oriented normal to the average plane of a puckered six-membered ring. This bond is one of the shortest seen between a rare earth and oxygen ions.

B. Local Environment of the A and B -Sites

The coordination geometry about the two metal sites is controlled by the value of x for the O atom in the $48f$ site. For $x = 0.3125$ one has a perfect octahedron about $16c$ and $x = 0.375$ gives a perfect cube about $16d$. In fact x is usually found in the range 0.320 to 0.345 and the two geometries are distorted from the ideal polyhedra. For a typical pyrochlore the distortion about the B ion or $16c$ site is relatively minor. The $\bar{3}m(D_{3d})$ point symmetry requires that all six $B - O$ bonds must be of equal length. The $O - B - O$ angles are distorted only slightly from the ideal octahedral values of 90° ranging between 81° and 100° . The distortion of the A site geometry from an ideal cube is on the other hand very large. This site is depicted in Fig. 3 and is best described as consisting of a puckered six-membered ring of O atoms with two O' atoms forming a linear $O' - A - O'$ stick oriented normal to the average plane of the six-membered ring. The $A - O$ and $A - O'$ bond distances are very different. While typical $A - O$ values are 2.4 - 2.5 Å, in accord with the sum of the ionic radii, the $A - O'$ bonds are amongst the shortest known for any rare earth oxide, ≈ 2.2 Å. Thus, the A -site has very pronounced axial symmetry, the unique axis of which is along a local $\langle 111 \rangle$ direction. This in turn has profound implications for the crystal field at the A -site which determines much of the physics found in the pyrochlore materials.

Recall that the spin-orbit interaction is large in rare earth ions and the total angular momentum, $\mathbf{J} = \mathbf{L} + \mathbf{S}$ is a good quantum number. For a given ion one can apply Hund's rules to determine the isolated (usually) electronic ground state. Electrostatic and covalent bonding effects originating from the local crystalline environment, the so-called crystal field (CF), lift the $2J + 1$ degeneracy of the ground state. A discussion of modern methods for calculation of the CF for f-element ions is beyond the scope of this review but is described in several monographs for example, one by H ufner (1978). For our purposes we will assume that the single ion energy levels and wave functions, the eigenvectors and eigenenergies of

the CF Hamiltonian \mathcal{H}_{cf} have been suitably determined either through ab initio calculations or from optical or neutron spectroscopy (see for example Rosenkranz *et al.* (2000) and more recently Mirebeau *et al.* (2007)).

\mathcal{H}_{cf} can be expressed either in terms of the so-called tensor operators or the “operator equivalents” due to Stevens (1952). The two approaches are contrasted by H ufner (1978). While the tensor operators are more convenient for ab-initio calculations, the latter are better suited to our purposes here. In this formalism, \mathcal{H}_{cf} is expressed in terms of polynomial functions of the J_{iz} and $J_{i\pm}$, with $J_{i\pm} = J_{ix} \pm J_{iy}$, which are components of the \mathbf{J}_i angular momentum operator. The most general expression for \mathcal{H}_{cf} is:

$$\mathcal{H}_{cf} = \sum_i \sum_{l,m} B_l^m O_l^m(\mathbf{J}_i), \quad (4)$$

where, for example, the operator equivalents are $O_2^0 = 3J_z^2 - J(J+1)$ and $O_6^0 = J_+^6 + J_-^6$. The full CF Hamiltonian for $\bar{3}m(D_{3d})$ point symmetry involves a total of six terms for $l = 2, 4$ and 6 (Greedan, 1992a). In fact, due to the strong axial symmetry of the A -site, described previously, it can be argued that the single $l = 2$ term, B_2^0 , plays a major role in the determination of the magnetic anisotropy of the ground state. In the Stevens formalism, $B_2^0 = A_2^0 \langle r^2 \rangle \alpha_J (1 - \sigma_2)$, where A_2^0 is a point charge lattice sum representing the CF strength, $\langle r^2 \rangle$ is the expectation value of r^2 for the 4f electrons, σ_2 is an electron shielding factor and α_J is the Stevens factor (Stevens, 1952). This factor changes sign in a systematic pattern throughout the lanthanide series, being positive for $A = \text{Sm, Er, Tm}$ and Yb and negative for all others. So, the sign of B_2^0 depends on the product $\alpha_J A_2^0$ and A_2^0 is known from measurements of the electric field gradient from for example ^{155}Gd M ossbauer studies to be positive for pyrochlore oxides (Barton and Cashion, 1979). Thus, B_2^0 should be positive for $A = \text{Sm, Er, Tm}$ and Yb and negative for all others. From the form of B_2^0 above, it is clear that states of different $|M_J\rangle$ do not mix and that the energy spectrum will consist of a ladder of states with either $|M_{J(\min)}\rangle$ ($B_2^0 > 0$) or $|M_{J(\min)}\rangle$ ($B_2^0 < 0$) as the ground state. Note that the former constitutes an easy plane and the latter an easy axis with respect to the quantization axis which is $\langle 111 \rangle$ for pyrochlores. A comparison of the known anisotropy for the $\text{A}_2\text{Ti}_2\text{O}_7$ and $\text{A}_2\text{Sn}_2\text{O}_7$ materials, that is, easy axis for $A = \text{Pr, Nd, Tb, Dy}$ and Ho and easy plane for $A = \text{Er}$ and Yb with the sign of B_2^0 shows a remarkable agreement with this very simple argument. [Note that only the Stevens formalism works here. The tensor operator definition of B_2^0 is $B_2^0 = A_2^0 \langle r^2 \rangle$, so this quantity is always positive for pyrochlore oxides, independent of the rare earth A . We do not maintain that the actual ground state wave function can be obtained within such a simple model (although the agreement for $A = \text{Dy}$ and Ho is remarkable), rather, that the overall anisotropy can be predicted without a detailed calculation.]

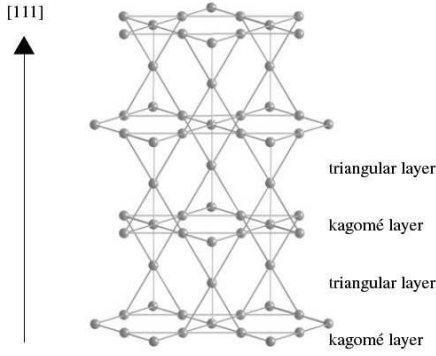


FIG. 4 Alternating kagome and triangular planar layers stacked along the $[111]$ direction of the pyrochlore lattice.

C. Alternative Views of the Pyrochlore Structure

An important feature of the pyrochlore structure relevant to the central theme of this review is the fact that the $16c$ or $16d$ sites form layers stacked along the $[111]$ direction as shown Fig. 4. From this perspective, the pyrochlore lattice is seen to consist of alternating kagome and triangular planar layers. As well, from the viewpoint of chemical bonding, the pyrochlore structure can be described as either an ordered defect fluorite (CaF_2) or as two interpenetrating networks, one of composition B_2O_6 , which is a network of corner-sharing metal-oxygen octahedra (topologically equivalent to that found in the perovskite structure) and the other of composition A_2O' , which forms a zig-zag chain through the large channels formed by the B_2O_6 network. These models have been described in detail in several of the previous reviews and the discussion here focuses on a few important issues. While there is a topological relationship with the perovskites, the pyrochlore lattice is considerably more rigid. For example the $B-O-B$ angle in which the O atom is shared between two octahedra is restricted to a very narrow range in pyrochlores, usually from about 127° to 134° , with only little influence from the size of the A ion. On the other hand this angle can range from 180° to 140° in perovskites and there is a strong variation in the radius of the A ion. The interpenetrating network description allows an understanding of the formation of so-called defect or “rattling” pyrochlores, such as KOs_2O_6 , in which the entire A_2O' network is missing and where the large K^+ ion occupies the $8b$ site which is normally occupied by O' in the standard pyrochlore structure. The disordered fluorite model is useful in cases where a disordered, defect fluorite structure phase competes with the ordered pyrochlore, such as for the $A_2\text{Zr}_2\text{O}_7$ series where A/B site mixing is observed.

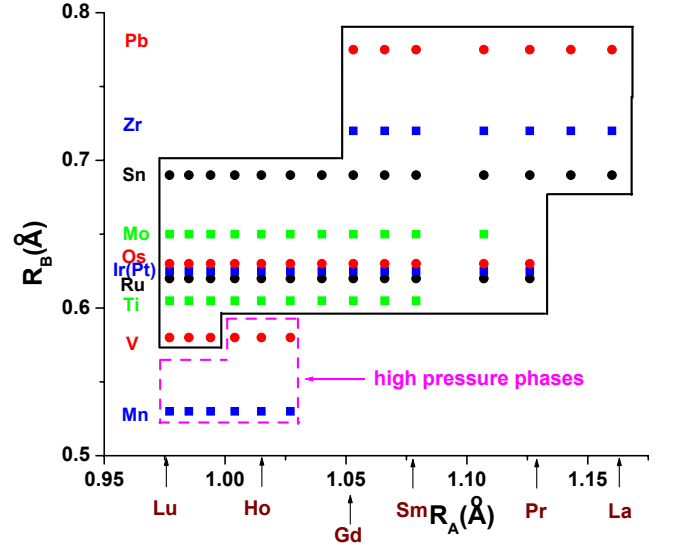


FIG. 5 A structure-field or stability-field map for $A_2B_2O_7$ materials. The $B = \text{Pt}$ series are also high pressure phases. Adapted from Subramanian and Sleight (1993).

D. Phase Stability

There are over 15 tetra-valent ions that can reside on the B-site of a cubic pyrochlore at room temperature. Pyrochlore oxides of most interest here are formed with a rare earth ion in the A-site and transition or p-block elements in the B-site. The rare earth elements form a series in which the trivalent state predominates and through which the ionic radius decreases systematically with increasing atomic number (the so-called lanthanide contraction). Nonetheless, it is uncommon to find that the pyrochlore phase is stable for all A for a given B.

The most efficient way to display the range of stability of pyrochlores in the space of the ionic radii is through a structure-field map or structure-stability map. Figure 5 is an abridged version of a comprehensive map published by Subramanian and Sleight (1993). First it is worth noting that the $B = \text{Sn}$ series is the only one to form for all rare earths. There would also appear to be minimal and maximal ionic radius ratios, A^{3+}/B^{4+} , which define the stability limits for pyrochlore phases of this type. For B ions with very small radii, such as Mn^{4+} , the pyrochlore phase can be prepared only using high pressure methods. This is in strong contrast to perovskites of the type $A^{2+}\text{Mn}^{4+}\text{O}_3$ which can be prepared easily under ambient oxygen pressures. The first series stable under ambient pressure is that for $B = \text{V}$, but only for the three smallest members, Lu, Yb and Tm. The series can be extended using high pressure synthesis (Troyanchuk, 1990). For the largest B ion, Pb^{4+} , the smallest rare earth for which a stable pyrochlore is found appears to be Gd. Thus, an ambient pressure stability range defined in terms of radius ratios, A^{3+}/B^{4+} , (RR) would extend

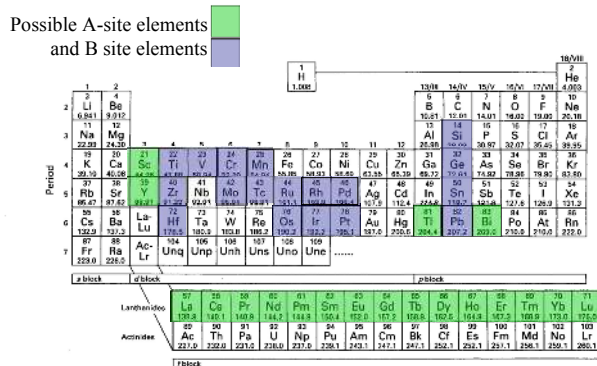


FIG. 6 Elements known to produce the (3+,4+) cubic pyrochlore oxide phase.

between 1.36 and 1.71 with marginal stability expected as those limits are approached. There are exceptions, for example $\text{Pr}_2\text{Ru}_2\text{O}_7$ is clearly stable with a RR of 1.82, yet $\text{Pr}_2\text{Mo}_2\text{O}_7$ does not exist with a $\text{RR} = 1.73$.

Also of relevance to this review are issues of defect formation in pyrochlores. This is an active area of research in materials science where defect pyrochlores which show high ionic conductivities are of interest. While the defect levels are often small and difficult to quantify via experiment, some computational guidelines have appeared recently (Minervini *et al.*, 2002). The general trend is that defect concentrations are predicted to increase as the RR approaches its lower limit, for example as the B radius increases within any given series, and that the predicted levels are generally of the order of 1% or less.

VI. SAMPLE PREPARATION AND CHARACTERISATION

Polycrystalline samples of pyrochlore oxides readily form by a standard solid state process, where stoichiometric proportions of high purity (> 99.99%) rare earth and transition metal oxides are calcined at 1350°C over several days in air with intermittent grindings. Elements known to exist in the cubic (3+,4+) pyrochlore phase are highlighted in the periodic table shown in Fig. 6. Several series of compounds with particularly volatile elements, like tin, require excess material to account for losses during the heating processes and others require heating under special atmospheres to form the desired oxidation state. For example the molybdates require a vacuum furnace or a reducing atmosphere to form the Mo^{4+} state and the rare earth manganese (IV) oxide pyrochlores are not stable at ambient pressure and require a high pressure synthesis technique (Subramanian *et al.*, 1988). Specialized growth conditions will be discussed below, as relevant. When high chemical homogeneity is required, the sol-gel method (Kido *et al.*, 1991) has been successful.

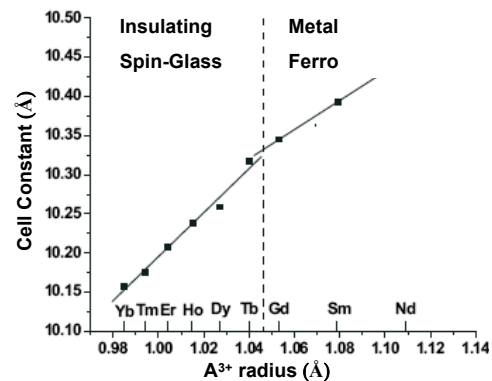


FIG. 7 Variation of unit cell constant and physical properties of the series $A_2\text{Mo}_2\text{O}_7$ with the A^{3+} radius (Ali *et al.*, 1989)

Crystals of a several oxide pyrochlores were grown in the 60's and 70's by flux methods (Wanklyn, 1968). The size and quality of the crystals grown by these methods vary, and it is often difficult to obtain voluminous crystals, especially for neutron scattering experiments. The 'floating zone' method of crystal growth was first used by Gardner *et al.* (1998) to produce large single crystals of $\text{Tb}_2\text{Ti}_2\text{O}_7$. Later the entire titanate series was produced by others (Balakrishnan *et al.*, 1998; Tang *et al.*, 2006; Zhou *et al.*, 2007) and within the last few years, groups have started to grow many other pyrochlores in image furnaces including molybdates, ruthenates and stannates (Miyoshi *et al.*, 2002; Taguchi *et al.*, 2002; Wiebe *et al.*, 2004). Single crystals have also been produced by several other methods including vapour transport (He *et al.*, 2006), hydrothermal techniques (Chen and Xu, 1998) and KF flux (Millican *et al.*, 2007).

Powder samples of the β -pyrochlores ("defect" pyrochlores) are formed at lower temperature ($\approx 500^\circ\text{C}$) in an oxidizing atmosphere (Yonezawa *et al.*, 2004). Small single crystals are also available (Schuck *et al.*, 2006).

Most oxide pyrochlores are cubic at room temperature with a lattice parameter between 9.8 Å and 10.96 Å (Subramanian *et al.*, 1983). Of these, the titanates are probably the most studied, followed by the zirconates, but many are still poorly represented in the literature. Both the titanate and zirconate pyrochlores were first reported by Roth (1956). Since then, over 1000 papers have been published on the two families.

VII. METAL INSULATOR TRANSITIONS IN THE OXIDE PYROCHLORES

Two types of metal-insulator (MI) transitions occur in the oxide pyrochlore family. First, are those that, as a function of a thermodynamic variable (e.g. temperature, magnetic field, pressure) change their transport properties, for example $\text{Tl}_2\text{Mn}_2\text{O}_7$ (Fujinaka *et al.*, 1979). Secondly, there are the *series* of compounds where the room

temperature character changes from metal to insulator as the rare earth ion changes, for example the molybdate (Greedan *et al.*, 1986) or iridate series (Yanagishima and Maeno, 2001). There appears to be very little controversy over the first class of MI transition, however for the second type, the exact position of this transition is a topic of debate. For example, in the molybdenum pyrochlore series, studies of their bulk properties have indicated a strong correlation with the magnetism and electrical transport properties, i.e., the ferromagnets were metallic while the paramagnets were insulating (Ali *et al.*, 1989; Greedan *et al.*, 1987). Indeed, the dependence on the lattice constant, a_0 , on the A^{3+} radius showed a distinct break at the MI boundary; see Fig. 7. In some subsequent studies however, the Gd phase is clearly insulating (Cao *et al.*, 1995; Kézsmárki *et al.*, 2004). The initial studies were carried out on polycrystalline samples, prepared between 1300 - 1400°C and in at least one case, in a CO/CO₂ “buffer gas” mixture which fixes the oxygen partial pressure during synthesis (Greedan *et al.*, 1986). Several subsequent studies have used single crystals grown by various methods above 1800°C, including melt and floating zone growths (Kézsmárki *et al.*, 2004; Moritomo *et al.*, 2001; Raju and Gougeon, 1995). While the polycrystalline samples have been fairly well characterized, including elemental analysis, thermal gravimetric weight gain and measurement of the cubic lattice constant, a_0 , this is less true of the single crystals. The differences between poly and single crystalline samples can be monitored most simply using the unit cell constant as illustrated in Fig. 8 in which unpublished data (Raju and Gougeon, 1995) for a selection of single crystals of Gd₂Mo₂O₇ are plotted. Note that as a_0 increases the samples become more insulating. From accurate structural data for the powders and single crystals, it has been determined that the increase in a_0 correlates with an increase in the Mo - O distance as shown Fig. 8. The most likely origin of this systematic increase is the substitution of the larger Mo³⁺ (0.69 Å) for the smaller Mo⁴⁺ (0.64 Å) which can arise from oxygen deficiency in the crystals resulting in the formula Gd₂Mo_{2-2x}Mo_{2x}O_{7-x}. Note that other defect mechanisms, such as vacancies on either the A or Mo sites would result in the oxidation of Mo⁴⁺ to the smaller Mo⁵⁺ (0.61 Å) which would lead to a reduction in a_0 . Further evidence for this mechanism comes from the fact that the crystal with the intermediate cell constant in Fig. 8 was obtained from the most insulating crystal by annealing in a CO/CO₂ buffer gas at 1400°C for 1-2 days. Thus, insulating single crystals of Gd₂Mo₂O₇ are oxygen deficient. This analysis is fully consistent with the report of Kézsmárki *et al.* (2004) who find that “Gd₂Mo₂O₇” is insulating but can be doped into the metallic state by 10 percent Ca substitution on the Gd site. Ca-doping will of course add holes to the Mo states which compensate for the electron doping due to the oxygen deficiency in the “as grown” crystals. After considering all the studies, we conclude that the MI boundary for stoichiometric A₂Mo₂O₇ is indeed between A = Gd and Tb.

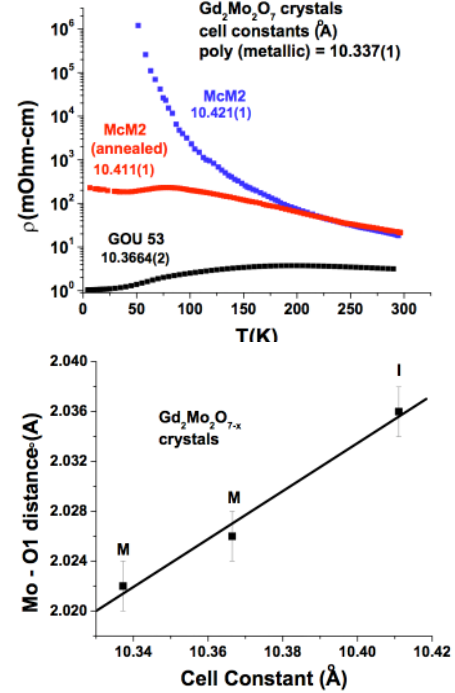


FIG. 8 Top: Comparison of electrical resistivity data for three single crystals of Gd₂Mo_{2-2x}Mo_{2x}O_{7-x} as a function of unit cell constant, a_0 . Bottom: Variation of the Mo - O distance with increasing cell constant for Gd₂Mo₂O_{7-x} crystals.

Single crystals for the other ferromagnetic metals, A = Nd and Sm, are also reported and these are subject to the same oxygen deficiency and electron doping but, as they are farther from the MI boundary, the effects on the physical properties are less drastic. For example the transport, optical and magnetic properties, reported by Cao *et al.* (1995) for Sm₂Mo₂O₇ were for a crystal with $a_0 = 10.425(1)$ Å compared with the polycrystal with $a_0 = 10.391(1)$ Å. While the material is still metallic (albeit a poor metal), the ferromagnetic Curie temperature is reduced by ≈ 30 K relative to the powder, to 65 K. Note also the ZFC/FC divergence below 50 K which suggests a spin glassy component. Very similar results were reported for other A = Sm single crystals, $a_0 = 10.4196(1)$ Å, for example by Park *et al.* (2003) and by Moritomo *et al.* (2001), which also show $T_c \sim 65$ K and a ZFC/FC divergence below 20 K.

The oxide pyrochlores can display a wide range of bulk properties including oxygen ion conductivity, superconductivity, ferroelectricity and unusual magnetic behavior (e.g. spin liquid and spin ice). However these are intimately related to their stoichiometry, electrical and crystallographic properties, as shown in the previous paragraphs. Whenever possible, we encourage one to measure, and report, these basic properties at room temperature or as a function of temperature.

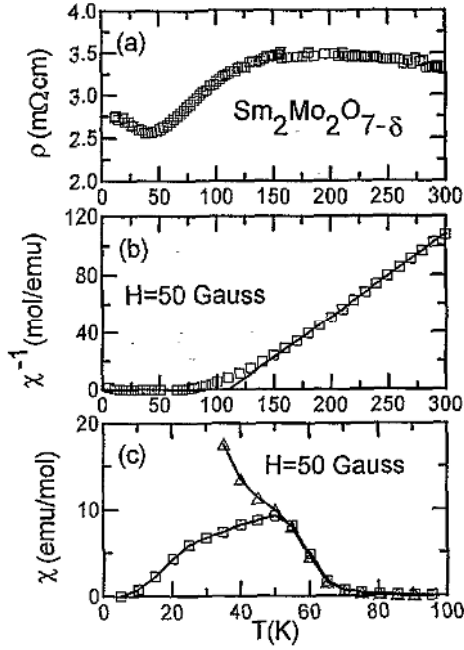


FIG. 9 Properties of an oxygen deficient single crystal of $\text{Sm}_2\text{Mo}_2\text{O}_{7-x}$ (a) Metallic behavior. (b) Inverse susceptibility showing a positive (FM) Curie-Weiss temperature. (c) Susceptibility showing $T_c = 65$ K and a zero field cooled (squares) field cooled (triangles) divergence at 50 K (Cao *et al.*, 1995).

Part III

Experimental Results

VIII. LONG-RANGE ORDERED PHASES

Many magnetic oxide pyrochlores enter a long range ordered state. These ordered phases are often promoted by single-ion anisotropy, anisotropic spin-spin interactions and/or further neighbor exchange interactions. Despite the fact that they develop long range order, these systems are still of significant interest, providing magnetic systems with axial and planar symmetry, quantum order by disorder transition, polarised moments and partially ordered systems, for example.

A. $\text{Gd}_2\text{Ti}_2\text{O}_7$ and $\text{Gd}_2\text{Sn}_2\text{O}_7$

Antiferromagnetically coupled Heisenberg spins on a pyrochlore lattice are expected to be highly frustrated because the exchange energy can be minimised in an infinite number of ways. Classical (Canals and Lacroix, 1998; Moessner and Chalker, 1998) and quantum calculations (Canals and Lacroix, 1998, 2000) show that the system should remain in a collective paramagnetic state with short-range spin-spin correlations at any non-zero temperature. As discussed in Section IV, Raju *et al.* (1999)

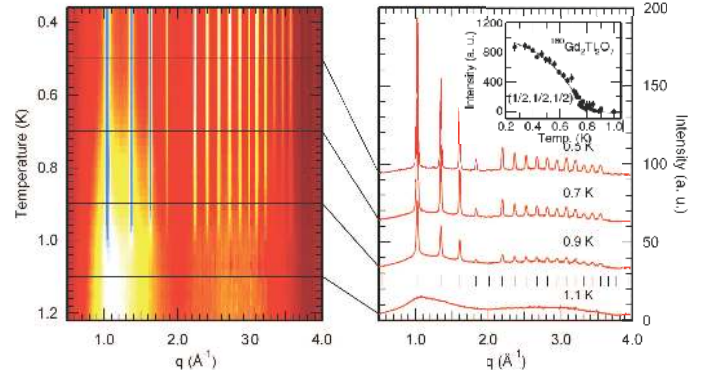


FIG. 10 Left: False colour map of the temperature dependence of the magnetic diffraction from $\text{Gd}_2\text{Ti}_2\text{O}_7$. As the temperature is lowered the broad diffuse scattering centered at 1.2 \AA^{-1} sharpens into peaks. Right: Diffraction patterns at specific temperatures are shown along with tic marks indicating where Bragg reflections should be for the proposed ground state. At the lowest temperatures the $\frac{1}{2} \frac{1}{2} \frac{1}{2}$ reflection has some intensity and this is highlighted in the inset (Stewart *et al.*, 2004a).

reported an infinite number of degenerate spin configurations near the mean field transition temperature when dipolar interactions are considered. However, Palmer and Chalker (2000) showed that a four-sublattice state with the ordering vector $\mathbf{k}_{\text{ord}}=000$ could be stabilized. More recent mean field theory calculations (Cépas and Shastry, 2004; Enjalran and Gingras, 2003) found a higher temperature second order transition to a phase with three ordered sublattices and 1 disordered one. At a slightly lower temperature another transition was found to the Palmer-Chalker state. In contrast, Monte Carlo simulations by Cépas *et al.* (2005) find a single strongly first order transition to the Palmer-Chalker state. As we shall see below, the experimental situation is even more complex.

The $S = 7/2$ Gd^{3+} ion, with its half-filled 4f-shell and zero orbital momentum is the best example of a Heisenberg spin amongst the rare earths. The bulk susceptibility for both $\text{Gd}_2\text{Ti}_2\text{O}_7$ and $\text{Gd}_2\text{Sn}_2\text{O}_7$ follows the Curie-Weiss law with an effective moment close to the theoretical limit of $7.94 \mu_B$ for the free ion (Bondah-Jagalu and Bramwell, 2001; Raju *et al.*, 1999) and a Curie-Weiss temperature of $\theta_{\text{CW}} \sim -10$ K. Both compounds however enter a magnetically ordered state at ≈ 1 K, resulting in a frustration index of about 10.

Early specific heat and AC susceptibility measurements showed that $\text{Gd}_2\text{Ti}_2\text{O}_7$ entered an ordered phase at 0.97 K (Raju *et al.*, 1999). A subsequent specific heat study showed two transitions in zero applied field, at 0.97 and 0.7 K (Ramirez *et al.*, 2002) and additional phase transitions, induced in applied fields. These phases were later confirmed by single crystal magnetisation work by Petrenko *et al.* (2004).

The nature of these ordered states is hard to deter-

mine by neutron diffraction due to the high absorption cross section of gadolinium. However a small, enriched, sample of $^{160}\text{Gd}_2\text{Ti}_2\text{O}_7$ has been studied. In the initial work at 50 mK, a partially ordered noncollinear antiferromagnetic structure, was proposed (Champion *et al.*, 2001). This unusual spin configuration had 3/4 of the Gd^{3+} spins ordered within kagome planes, separated by the triangular plane of Gd ions (see Fig. 4), which remain disordered down to the lowest temperature. This model was later modified when the diffuse scattering and a new magnetic reflection at $\frac{1}{2}\frac{1}{2}\frac{1}{2}$, was observed and studied (Stewart *et al.*, 2004). The magnetic scattering from $^{160}\text{Gd}_2\text{Ti}_2\text{O}_7$ is shown in Fig. 10. Very broad diffuse scattering is seen above 1 K. Below this temperature, Bragg peaks occur at the reciprocal lattice positions indicated by the tic marks (vertical bars) in the right panel. The lowest angle magnetic reflection, the very weak $\frac{1}{2}\frac{1}{2}\frac{1}{2}$ peak at $|\mathbf{Q}| = 0.6 \text{ \AA}^{-1}$ only gains intensity below the second transition. At all temperatures, diffuse magnetic scattering is observed which diminishes as the temperature decreases and the Bragg peaks grow. The diffuse magnetic scattering, centred at $|\mathbf{Q}| \approx 1.2 \text{ \AA}^{-1}$ indicates that the correlation length of the disordered spins is $\approx 3.5 \text{ \AA}$, the nearest-neighbor distance and not 7 \AA appropriate for the model proposed earlier by Champion *et al.* (2001). This picture of two different Gd moments is consistent with ^{155}Gd Mössbauer experiments (Bonville *et al.*, 2003). Most interestingly, this is not the state proposed by Palmer and Chalker (2000).

The isostructural stannate, $\text{Gd}_2\text{Sn}_2\text{O}_7$, has received comparatively less attention. As mentioned above, the paramagnetic properties are similar to $\text{Gd}_2\text{Ti}_2\text{O}_7$ (Matsuhira *et al.*, 2002). However, only one transition, at 1.0 K, and only one Gd moment has been observed in $\text{Gd}_2\text{Sn}_2\text{O}_7$ (Bonville *et al.*, 2003). Recent neutron diffraction measurements by Wills *et al.* (2006), shown in Fig. 11, have confirmed that $\text{Gd}_2\text{Sn}_2\text{O}_7$ undergoes only one transition down to the lowest temperatures and that the ground state is the one predicted theoretically for a Heisenberg pyrochlore antiferromagnet with dipolar interactions by Palmer and Chalker (2000).

The difference in these two materials highlights the extreme sensitivity of the ground state to small changes in composition and of the consequential details in the spin-spin interactions in these highly frustrated materials. Wills *et al.* (2006) proposed that a different relative magnitude in the two types of third-neighbour superexchange interaction may be responsible for the different ground states in these otherwise very similar Gd compounds (Del Maestro and Gingras, 2007).

To understand the magnetic ground states further and the true cause of the differences between $\text{Gd}_2\text{Ti}_2\text{O}_7$ and $\text{Gd}_2\text{Sn}_2\text{O}_7$ one has to investigate the excitation spectrum. Specific heat is a bulk probe that often provides a reliable insight into the low lying excitations. The specific heat, C_v , of these two compounds just below the transition temperature is described well by an anomalous power law, $C_v \propto T^2$, that had been presumed to be asso-

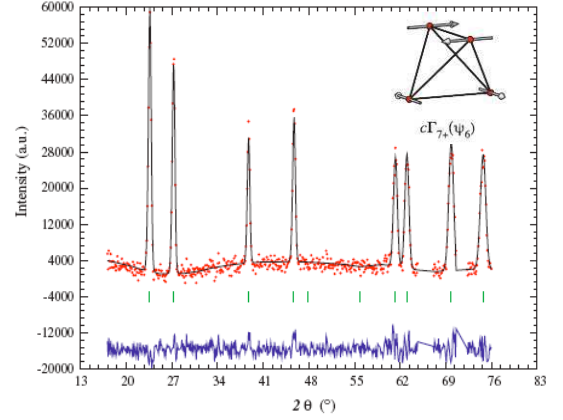


FIG. 11 Neutron powder diffraction pattern from $\text{Gd}_2\text{Sn}_2\text{O}_7$ at 0.1 K, after a nuclear background (1.4 K) data set was subtracted (Wills *et al.*, 2006). Inset: One of the 3 Γ_{7+} basis vectors that describe the data (see fit), consistent with the Palmer-Chalker model (Palmer and Chalker, 2000).

ciated with an unusual energy-dependence of the density of states (Bonville *et al.*, 2003,a; Ramirez *et al.*, 2002; Raju *et al.*, 1999). Electron spin resonance (ESR) (Hassan *et al.*, 2003; Sosin *et al.*, 2006,a), Mössbauer (Bertin *et al.*, 2002), muon spin relaxation (Bonville *et al.*, 2003a; Dunsiger *et al.*, 2006; Yaouanc, *et al.*, 2005) and neutron spin echo (Ehlers, 2006) have provided many interesting results. In all these measurements, spin fluctuations were observed much below the ordering temperature of the compound, seemingly consistent with the unusual energy-dependence of the density of states invoked to interpret the specific heat measurements. Sosin *et al.* (2006, 2007) failed to confirm the unusually large planar anisotropy measured by Hassan *et al.* (2003), however they found a small gap $\approx 1 \text{ K}$ that coexists with a paramagnetic signal in $\text{Gd}_2\text{Ti}_2\text{O}_7$, however no paramagnetic spins were observed at low temperatures in $\text{Gd}_2\text{Sn}_2\text{O}_7$. Recently Quilliam *et al.* (2007), remeasured the specific heat of $\text{Gd}_2\text{Sn}_2\text{O}_7$ and found that the $C_v \propto T^2$ behavior does not hold below 400 mK (see Fig. 12) and that C_v decreases exponentially below 350 mK, providing evidence for a gapped spin-wave spectrum due to anisotropy resulting from single-ion effects and long-range dipolar interactions (Del Maestro and Gingras, 2007).

The current experimental understanding of these Heisenberg antiferromagnets is at this time incomplete. $\text{Gd}_2\text{Sn}_2\text{O}_7$ appears to be a good example of the model considered by Palmer and Chalker (2000), and $\text{Gd}_2\text{Ti}_2\text{O}_7$ is perhaps a small perturbation from this. However, an explanation for the low lying excitations as probed by muon spin relaxation in both compounds still eludes theorists (Del Maestro and Gingras, 2007). Understanding these ubiquitous, low temperature spin dynamics in a relatively simple model magnet, like the Gd-based Heisenberg-like antiferromagnet on the pyrochlore lattice, would likely help elucidate the nature of the low tem-

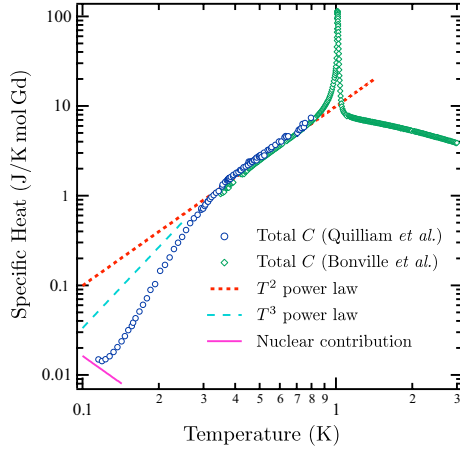


FIG. 12 Specific heat of $\text{Gd}_2\text{Sn}_2\text{O}_7$ from Quilliam *et al.* (2007) (circles) and Bonville *et al.* (2003) (diamonds). The T^2 power law (dotted line) and a conventional T^3 power law (dashed line) for a three dimensional antiferromagnet are plotted. The upturn seen below 150 mK results from the nuclear electric quadrupole interaction (Quilliam *et al.*, 2007).

perature spin dynamics in other frustrated magnets. We discuss in Section XII.A some recent work on $\text{Gd}_2\text{Ti}_2\text{O}_7$ in a magnetic field.

B. $\text{Er}_2\text{Ti}_2\text{O}_7$

The Er^{3+} single ion crystal field ground state in $\text{Er}_2\text{Ti}_2\text{O}_7$ is a Kramers doublet with a magnetic moment of $3.8 \mu_B$ and $0.12 \mu_B$ perpendicular and parallel to the local $\langle 111 \rangle$ axis, respectively. $\text{Er}_2\text{Ti}_2\text{O}_7$, like $\text{Yb}_2\text{Ti}_2\text{O}_7$, is a realization of an XY-like system on the pyrochlore lattice. However, while $\text{Yb}_2\text{Ti}_2\text{O}_7$ has a small ferromagnetic Curie-Weiss temperature ($\theta_{\text{CW}} \sim +0.75$ K) (Hodges *et al.*, 2002), $\text{Er}_2\text{Ti}_2\text{O}_7$ has a large negative Curie-Weiss temperature ($\theta_{\text{CW}} \sim -22$ K) (Champion *et al.*, 2003), and is therefore a pyrochlore XY antiferromagnet. The lowest-lying crystal field states of $\text{Er}_2\text{Ti}_2\text{O}_7$ are at 6.38 meV (74.1 K) and 7.39 meV (85.8 K) above the ground states (Champion *et al.*, 2003).

Specific heat measurements show a sharp feature at approximately $T_N \sim 1.2$ K (Blöte *et al.*, 1969; Champion *et al.*, 2003; Siddharthan *et al.*, 1999). Neutron scattering below T_N confirms the existence of a Néel long-range ordered state with propagation vector $\mathbf{k}_{\text{ord}} = 000$. The neutron scattering data strongly suggest a second order phase transition at T_N , with the scattered intensity I vanishing at T_N as $I(T) \propto (T_N - T)^{2\beta}$ with critical exponent $\beta \approx 0.33$, characteristic of the three-dimensional XY model.

As the transition is continuous, the system is expected to order in only one of the irreducible representations of the Er^{3+} site representation. A refinement of the magnetic structure finds that only the two basis vectors ψ_2 or ψ_3 of Γ_5 , or a superposition of both, is consistent with



FIG. 13 Ground state spin configuration determined for $\text{Er}_2\text{Ti}_2\text{O}_7$ (Poole *et al.*, 2007). In a macroscopic sample six symmetry equivalent spin configurations will co-exist.

the observed magnetic intensities of the Bragg peaks. Results from a spherical neutron polarimetry study find that the zero magnetic field ordered state is described almost entirely by ψ_2 with very little admixing from ψ_3 . The spin configuration corresponding to ψ_2 is shown in Fig. 13 (Poole *et al.*, 2007). The experimental observations of (i) an ordering into the noncoplanar ψ_2 structure via (ii) a second order phase transition are both surprising.

As discussed in Sections IV and VIII.A, isotropic exchange plus dipolar interactions select by themselves a state with spins perpendicular to the local $\langle 111 \rangle$ axes. Hence, easy plane (XY) anisotropy should further enhance the stability of this state. This was explicitly shown in calculations (Del Maestro and Gingras, 2007) pertaining to $\text{Gd}_2\text{Sn}_2\text{O}_7$ which does display a Palmer-Chalker ground state (Wills *et al.*, 2006). However a Palmer-Chalker ground state for $\text{Er}_2\text{Ti}_2\text{O}_7$ is seemingly robustly rejected by recent neutron polarimetry experiments (Poole *et al.*, 2007). Since nearest-neighbor antiferromagnetic exchange, dipolar interactions and the XY nature of the magnetic moments should conspire together to produce a Palmer-Chalker ground state in $\text{Er}_2\text{Ti}_2\text{O}_7$, other interactions or effects must be at play to stabilize the experimentally observed ψ_2 ground state (Poole *et al.*, 2007).

An early numerical study of the classical XY antiferromagnet on the pyrochlore lattice had found a strongly first order transition into a long-range ordered state with propagation vector $\mathbf{k}_{\text{ord}} = 000$ (Bramwell *et al.*, 1994). This finding was subsequently confirmed by another study (Champion *et al.*, 2003; Champion and Holdsworth, 2004). In an earlier study, Bramwell *et al.* (1994) had only identified a macroscopic degeneracy of discrete ground states, while there is in fact a continuous degree of freedom for antiferromagnetically coupled XY spins on a single tetrahedron, resulting in a continuous ground state degeneracy for a macroscopic sample (Champion *et al.*, 2003; Champion and Holdsworth, 2004). Monte Carlo simulations of a classical $\langle 111 \rangle$ pyrochlore XY antiferromagnet find that the degeneracy is lifted by an order-by-disorder transition driven by thermal fluctuations with, most interestingly, the system de-

veloping long range order in the same ψ_2 state as found experimentally in $\text{Er}_2\text{Ti}_2\text{O}_7$. The Monte Carlo results can be rationalized on the basis of a classical spin wave calculation (Champion and Holdsworth, 2004). There, it is found that there are zero energy spin wave modes over planes in the Brillouin zone for which the spin wave wavevector \mathbf{q} obeys $\mathbf{q} \cdot \mathbf{a} = 0$ and $\mathbf{q} \cdot (\mathbf{b} - \mathbf{c}) = 0$, where \mathbf{a} , \mathbf{b} and \mathbf{c} are the basis vectors of the primitive rhombohedral unit cell of the pyrochlore lattice.

On the basis of the results from Monte Carlo and classical spin wave calculations, Champion and Holdsworth (2004) proposed that the ψ_2 in $\text{Er}_2\text{Ti}_2\text{O}_7$ is perhaps stabilized by zero-point quantum fluctuations, arguing that their effects are captured by the classical spin wave argument. However, problems remain with this interpretation. As mentioned above, the transition at $T_N \sim 1.2$ K is second order in the experiment while simulations show a strong first order transition (Champion and Holdsworth, 2004). Also, the density of zero energy classical spin wave states is a constant, a result that is incompatible with the experimental specific heat data which shows a T^3 temperature dependence below 1 K. Inelastic neutron scattering reveals no evidence for such low lying excitations required to generate the T^3 temperature dependence of the specific heat. The experimental results and models presented above suggest a well established long-range ordered ground state for $\text{Er}_2\text{Ti}_2\text{O}_7$. Yet, muon spin relaxation data reveal that below T_N , the muon polarization relaxation rate remains large ($2 \times 10^6 \mu\text{s}^{-1}$) and essentially temperature independent down to 20 mK, indicative of a dynamic ground state (Lago *et al.*, 2005). This behavior reminds one of low-temperature muon data in several pyrochlores including the “ordered” Gd-pyrochlores and the “dynamic” $\text{Tb}_2\text{Ti}_2\text{O}_7$.

Unlike $\text{Er}_2\text{Ti}_2\text{O}_7$, $\text{Er}_2(\text{GaSb})\text{O}_7$ does not appear to order down to 50 mK (Blöte *et al.*, 1969). It is not clear at this stage whether the randomness on the B-sites leads to a disordered and glassy phase, i.e. an XY-like spin glass. Results on $\text{Er}_2\text{Sn}_2\text{O}_7$ will be discussed in Section XI.C.

C. $\text{Tb}_2\text{Sn}_2\text{O}_7$

Until recently the magnetic and electrical properties of the stannates had received little attention. This is probably due to the slightly more problematic synthesis and the lack of large, high quality, single crystals.

Like many frustrated magnets, the high temperature ($T > 40$ K) inverse susceptibility is very linear. In $\text{Tb}_2\text{Sn}_2\text{O}_7$, this yields a Curie-Weiss temperature of approximately $\theta_{\text{CW}} \sim -12$ K and an effective moment of $9.8 \mu_B$, which agrees well with the value of $9.72 \mu_B$ for the $^7\text{F}_6$ ground state of Tb^{3+} (Bondah-Jagalu and Bramwell, 2001). Reminiscent of the cooperative paramagnet $\text{Tb}_2\text{Ti}_2\text{O}_7$ (see Section XI), the inverse susceptibility deviates downwards at ≈ 30 K upon cooling. However, on cooling further, the system enters a frozen ferro-

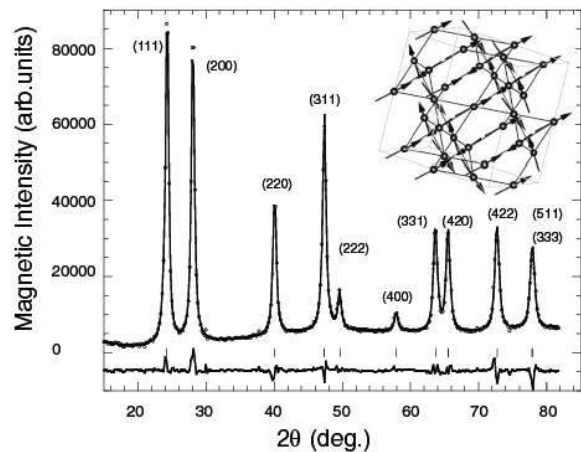


FIG. 14 Magnetic scattering from $\text{Tb}_2\text{Sn}_2\text{O}_7$ at 100 mK. Inset: the proposed “ordered” spin ice structure with spins canted off the $\langle 111 \rangle$ by 13° (Mirebeau *et al.*, 2005). The broad scattering at the base of the Bragg reflections is indicative of spin clusters which reach ≈ 200 Å at base temperature.

magnetic state at 0.87 K. This was first reported by Matsuhiro *et al.* (2002) from low temperature susceptibility measurements and then by Mirebeau *et al.* (2005) who determined the magnetic structure from neutron diffraction measurements. In this work by Mirebeau *et al.* (2005), a crossover from antiferromagnetic correlations to ferromagnetic correlations was observed at 2 K. This was followed, at a lower temperature, by a transition into an ordered state and the appearance of Bragg peaks, see Fig. 14. Rietveld analysis determined that the spins are canted by 13.3° off the local $\langle 111 \rangle$ directions with an ordered moment of $5.9 \mu_B$, significantly reduced from the free ion moment of $9 \mu_B$, presumably due to crystalline electric field effects.

Ferromagnetically coupled spins on the pyrochlore lattice fixed along the local $\langle 111 \rangle$ directions gives rise to a highly degenerate state that has become known as the spin ice state (see Section X). By comparing the Tb^{3+} moment value deduced from neutron diffraction ($5.9 \mu_B$) to the smaller value deduced from the nuclear specific heat ($4.5 \mu_B$) Mirebeau *et al.* (2006) suggested that slow collective fluctuations, on the time scale of 10^{-4} - 10^{-8} s, coexist with the ordered state at the lowest temperatures (Mirebeau *et al.*, 2006).

Subsequently, two groups led by Dalmas de Réotier, *et al.* (2006) and Bert *et al.* (2006) have suggested that the ground state is not static. They claim that the absence of any oscillations, even at the shortest times, in the muon spin relaxation spectrum precludes the existence of a static moment. Dalmas de Réotier, *et al.* (2006) argue that both neutron and muon data are consistent with a characteristic spin relaxation time of $\approx 10^{-10}$ s whilst Bert *et al.* (2006) suggest that the dynamics result from fluctuations of clusters of correlated spins with the ordered spin ice structure. On the other hand, the results

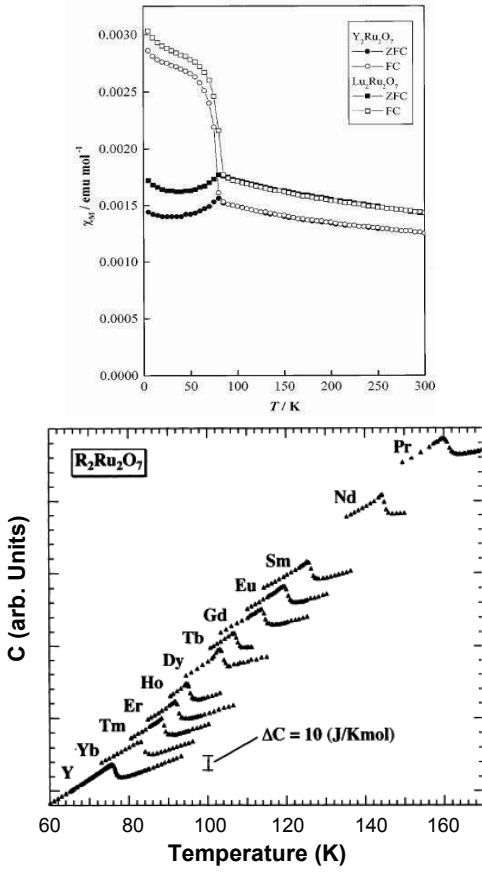


FIG. 15 Top: The temperature dependence of the susceptibility for Y and Lu ruthenate. Both data sets show the Ru^{4+} moments ordering at ≈ 75 K. Bottom: Heat capacity measurements over the entire rare earth ruthenate series showing how the Ru^{4+} ordering temperature increases as the size of the rare earth ion decreases (Ito *et al.*, 2001).

from the neutron spin echo study of Chapuis, *et al.* (2007) suggest no spin dynamics below 0.8 K.

Mirebeau *et al.* (2006) have suggested that the $\approx 3\%$ expansion in the lattice constant between $\text{Tb}_2\text{Sn}_2\text{O}_7$ and $\text{Tb}_2\text{Ti}_2\text{O}_7$ results in the dipolar interaction overcoming the weakened exchange interaction allowing $\text{Tb}_2\text{Sn}_2\text{O}_7$ to freeze. Clearly more experimental work is needed on this compound to determine the exact nature of the ground state. Recently, from inelastic neutron scattering studies, Mirebeau *et al.* (2007) found that the composition of the first two crystal field levels of $\text{Tb}_2\text{Sn}_2\text{O}_7$ are inverted when compared to those of $\text{Tb}_2\text{Ti}_2\text{O}_7$. This cannot be explained by simple calculations of the local crystal field environment and more work is needed.

D. $A_2\text{Ru}_2\text{O}_7$ ($A = \text{Y, Gd, Dy, Ho, Er and Tl}$)

All but the largest, $A = \text{La}$ and Ce , rare-earth ruthenates as well as $A = \text{Bi}$ and $A = \text{Tl}$ form as cubic py-

rochlores (Bertaut *et al.*, 1959; Subramanian *et al.*, 1983; Yoshii and Sato, 1999). The lattice parameters vary from 10.07 to 10.355 Å across the rare earth series with the $A = \text{Bi}$ and Tl compounds at the high end of this range. Crystals of several ruthenates have been made by hydrothermal, vapour transport and floating zone methods (Sleight and Bouchard, 1972; Zhou *et al.*, 2007). Historically, the ruthenium pyrochlore oxides have been extensively studied for their novel conductivity (Carcia *et al.*, 1982; Pike and Seager, 1977) and catalytic activity (Horowitz *et al.*, 1983), but until recently, very little was known about their magnetic properties. Most of the ruthenates are semiconductors at room temperature with hopping energies of ~ 0.1 eV, but the Bi based sample is metallic with Pauli paramagnetism. Ru^{4+} (low spin $4d^4$) has an $S = 1$ moment and the Ru sublattice appears to order between 70 and 160 K, depending on the rare earth (see Fig. 15). However, θ_{CW} for $\text{Y}_2\text{Ru}_2\text{O}_7$ is reported to be -1250 K although it is not clear that this was obtained in the paramagnetic regime (Gurgul *et al.*, 2007). Studies of diamagnetic $A = \text{Y}$ and Lu provide evidence of the magnetic nature of the Ru^{4+} ion. These indicate a magnetic transition at ≈ 75 K, leading to a high frustration index, $f \approx 17$. The magnetic susceptibilities measured under zero field cooled (ZFC) and under field cooled (FC) conditions show a different temperature dependence (see Fig. 15). This is consistent with the observation of a canted antiferromagnetic structure from neutron diffraction (Ito *et al.*, 2001; Kmiec *et al.*, 2006). Inelastic neutron scattering measurements by van Duijn *et al.* (2007) reveals the development of a large gap in the excitation spectrum below the ordering temperature.

$\text{Er}_2\text{Ru}_2\text{O}_7$ and $\text{Gd}_2\text{Ru}_2\text{O}_7$ have been studied by powder neutron diffraction (Taira *et al.*, 2003) and Mössbauer (Gurgul *et al.*, 2007). In both cases, the Ru sublattice orders at the temperature indicated by the peak in the specific heat plotted in Fig. 15. This long range ordered state is a $\mathbf{k}_{\text{ord}} = 000$ type. This is also true for $\text{Y}_2\text{Ru}_2\text{O}_7$ (Ito *et al.*, 2001). In the Er and Gd ruthenates, the rare earth moment is polarised by the ordered Ru-sublattice, via the rare earth - Ru^{4+} exchange interactions. This reveals itself in a small but finite moment on the A-site as soon as the ruthenium orders. This moment grows with decreasing temperature before the rare earth ion orders in its own right at 10 K (Er) and 40 K (Gd). A refinement of the low temperature (3 K) neutron diffraction data from $\text{Er}_2\text{Ru}_2\text{O}_7$ suggests that the magnetic moments, both Er and Ru, are in a plane oriented towards the same [100] direction, but antiparallel to each other. The refined moments for Ru^{4+} saturate at the theoretical limit for the $S=1$ ion ($2 \mu_B$) at 90 K, but at 3 K the moment on the Er site is only $4.5 \mu_B$, 50% of the predicted value, and is probably reduced by crystalline electric field effects, although the signal has not yet saturated at the lowest temperature studied (see Fig. 16).

Since Bansal *et al.* (2002) reported a possible spin-ice ground state (see Section X) in $\text{Ho}_2\text{Ru}_2\text{O}_7$ and

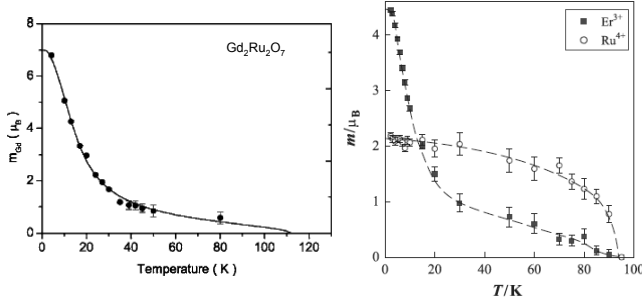


FIG. 16 Left: The temperature dependence of the Gd moment from Gd-Mössbauer (Gurgul *et al.*, 2007) on $\text{Gd}_2\text{Ru}_2\text{O}_7$. Right: The temperature dependence of the Ru^{4+} and Er^{3+} moments in $\text{Er}_2\text{Ru}_2\text{O}_7$ as measured by neutron diffraction (Taira *et al.*, 2003).

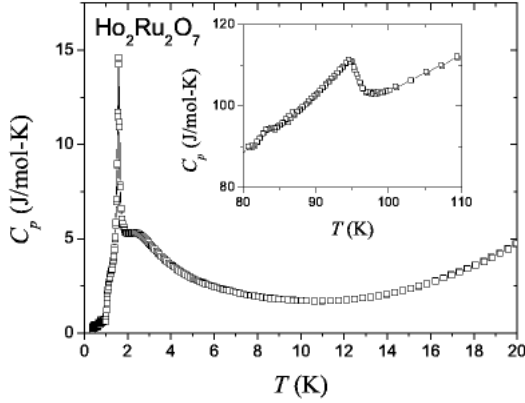


FIG. 17 Specific heat of polycrystalline $\text{Ho}_2\text{Ru}_2\text{O}_7$ as a function of temperature around the Ru^{4+} (inset) and Ho^{3+} (main) ordering temperatures (Gardner *et al.*, 2005).

$\text{Dy}_2\text{Ru}_2\text{O}_7$, there have been several studies of the magnetic behaviour of $\text{Ho}_2\text{Ru}_2\text{O}_7$ (Bansal *et al.*, 2003; Gardner *et al.*, 2005; Wiebe *et al.*, 2004). In this compound, unlike the other heavy rare earth ruthenates, a small difference is seen between FC and ZFC when the rare earth ion orders. This happens at 1.4 K when the Ho^{3+} sublattice enters a long-range ordered state, unlike a true spin ice material. Lower temperature ($T < 20$ K) specific heat (see Fig. 17) also highlights this transition. As seen in a number of geometrically frustrated systems, a broad feature (centered here at ≈ 3 K) precedes the sharp lambda-like transition at a slightly lower temperature. These features are related to the build-up of short- and long-range correlations between Ho spins, respectively. The ‘ordered’ spin ice has the holmium moments canted off the local $\langle 111 \rangle$ axes presumably due to the local fields generated by the ordered Ru^{4+} sublattice. The ordered structure of $\text{Gd}_2\text{Ru}_2\text{O}_7$ is similar to $\text{Ho}_2\text{Ru}_2\text{O}_7$. In both cases the full moment of the rare earth ion was not measured at the lowest temperatures investigated (Gurgul

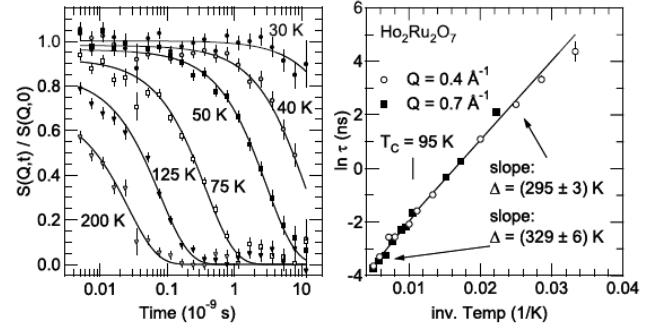


FIG. 18 Neutron spin echo spectra from $\text{Ho}_2\text{Ru}_2\text{O}_7$ at $|\mathbf{Q}| = 0.4 \text{ \AA}^{-1}$ as measured on NG5NSE (left) and the dependence of the relaxation time on temperature (right) from two different positions in reciprocal space. The lines through the spectra on the left are a simple exponential, where the characteristic relaxation time is used in the Arrhenius plot on the right (Gardner *et al.*, 2005).

et al., 2007; Wiebe *et al.*, 2004).

The magnetic entropy associated with $\text{Ho}_2\text{Ru}_2\text{O}_7$ at these low temperatures reaches neither $R \ln 2$ (expected for a completely ordered doublet system) nor $R(\ln 2 - \frac{1}{2} \ln \frac{3}{2})$ (expected for spin ice). In fact, the magnetic entropy of $\text{Ho}_2\text{Ru}_2\text{O}_7$ (Gardner *et al.*, 2005) resembles that of the dipolar spin ices in an applied field of 1 T. Several neutron scattering (Gardner *et al.*, 2005; Wiebe *et al.*, 2004) and AC susceptibility (Gardner *et al.*, 2005) experiments have investigated the spin dynamics in $\text{Ho}_2\text{Ru}_2\text{O}_7$. The nature of the Ho-moments is governed by the crystalline electric field levels which are slightly perturbed from those measured in $\text{Ho}_2\text{Ti}_2\text{O}_7$ (Rosenkranz *et al.*, 2000) especially after the ordering of the Ru^{4+} sublattice (Gardner *et al.*, 2005). This is most apparent in neutron spin echo measurements where a 35 K change in the gap to the first excited state is observed once the Ru^{4+} -ions order (Gardner *et al.*, 2005) (see Fig. 18).

While $\text{Tl}_2\text{Ru}_2\text{O}_7$ is cubic with a room temperature lattice parameter of 10.18 \AA , when it is cooled below 120 K, the structure transforms to an orthorhombic structure. Concomitantly, a metal-insulator transition occurs and the resistivity changes by 5 orders of magnitude. A sudden drop in the susceptibility also occurs at this temperature (Lee *et al.*, 2006). These data have been interpreted as the three-dimensional analogue to the more commonly known one-dimensional $S = 1$ Haldane gap system (Haldane, 1983). Specifically, it is believed that the structural phase transition creates effective $S = 1$, chains of Ru-ions which do not dimerize. These chains are arguably created due to the orbital ordering of the Ru 4d electrons.

Three $(2+, 5+)$ pyrochlores of interest are $\text{Cd}_2\text{Ru}_2\text{O}_7$ (Wang and Sleight, 1998), $\text{Ca}_2\text{Ru}_2\text{O}_7$ (Munakata and Sato, 2006) and $\text{Hg}_2\text{Ru}_2\text{O}_7$ (Yamamoto *et al.*, 2007), with an $S = 3/2$ Ru^{5+} ion and non-metallic transport properties. $\text{Hg}_2\text{Ru}_2\text{O}_7$, like $\text{Tl}_2\text{Ru}_2\text{O}_7$, has a metal-insulator transition that is concomitant with a

A	a_0 (Å)	T_c (K)	θ_{CW} (K)	θ_{CW}/T_c	Reference
Sc	9.586(3)	15	-	-	(Troyanchuk <i>et al.</i> , 1988)
Sc	9.5965(4)	20(1)	77(3)	3.9	(Greedan <i>et al.</i> , 1996a)
Y	9.912(3)	-	-	-	(Fujinaka <i>et al.</i> , 1979)
Y	9.912(3)	-	-	-	(Troyanchuk <i>et al.</i> , 1988)
Y	9.901	20(5)	50(10)	2.5	(Subramanian <i>et al.</i> , 1988)
Y	9.919(2)	15(1)	42(2)	2.8	(Reimers <i>et al.</i> , 1991)
Y	9.91268(3)	15	50	3.3	(Shimakawa <i>et al.</i> , 1999)
Lu	9.814(3)	9	-	-	(Troyanchuk <i>et al.</i> , 1988)
Lu	9.815	23(5)	70(10)	3.0	(Subramanian <i>et al.</i> , 1988)
Lu	9.82684(3)	15	60	4.0	(Shimakawa <i>et al.</i> , 1999)
In	9.717(3)	132	-	-	(Troyanchuk <i>et al.</i> , 1988)
In	9.727(1)	120	150	1.25	(Raju <i>et al.</i> , 1994)
In	9.70786(9)	120	155	1.29	(Shimakawa <i>et al.</i> , 1999)
Tl	9.890(3)	120	-	-	(Fujinaka <i>et al.</i> , 1979)
Tl	9.892(1)	121(1)	155	1.28	(Raju <i>et al.</i> , 1994)
Tl	9.89093(7)	122	175	1.43	(Shimakawa <i>et al.</i> , 1999)

TABLE II Collected values for unit cell constants, a_0 , measured Curie temperatures, T_c , and Curie-Weiss temperatures, θ_{CW} , for $A_2Mn_2O_7$ phases with $A = \text{Sc, Y, Lu, In and Tl}$.

structural phase transition. Single crystals of $\text{Ca}_2\text{Ru}_2\text{O}_7$ have been grown by the hydrothermal method (Munekata and Sato, 2006) and the effective paramagnetic moment is only $0.36 \mu_B$, about one order of magnitude smaller than the theoretical value for the $S = 3/2$ ion. At 23 K, there is clear irreversibility between FC and ZFC susceptibilities indicative of a spin glass transition and reminiscent of $\text{Y}_2\text{Mo}_2\text{O}_7$ (Greedan *et al.*, 1986).

E. $A_2Mn_2O_7$ ($A = \text{Sc, Y, Tb - Lu and Tl}$)

The rare earth manganese (IV) pyrochlores are not stable at ambient pressure at any temperature and must be prepared using high pressure methods. The earliest published report is by Fujinaka *et al.* (1979) who synthesized the pyrochlores $A_2B_2O_7$ with $A = \text{Y, Tl}$ and $B = \text{Cr, Mn}$ using temperatures in the range 1000 - 1100°C and pressures from 3 - 6 GPa. Reports of the high pressure synthesis of several $A_2Mn_2O_7$ phases appeared from the groups of Troyanchuk *et al.* (1988) and Subramanian *et al.* (1988) about ten years later. Troyanchuk *et al.*

(1988) prepared the phases $A = \text{Sc, Y, In, Tl}$ and Tb-Lu with pressures between 5 - 8 GPa and temperatures 1000 - 1500°C. Subramanian *et al.* (1988) were able to prepare $A = \text{Y}$ and Dy-Lu using much lower pressures and temperatures with a hydrothermal method in sealed gold tubes including NaClO_3 , NaOH and H_2O at 3 kbar (0.3 GPa) and 500°C. Greedan *et al.* (1996a) synthesized $A = \text{Sc}$ using a tetrahedral anvil press at 850°C and 60 kbar (6 GPa). Subsequently, Shimakawa *et al.* (1999) used a hot isostatic press apparatus at 1000°C - 1300°C and only 0.4 kbar (0.04 GPa) for the series $A = \text{In, Y}$ and Lu while the $A = \text{Tl}$ material required 2.5 GPa and 1000°C in a piston-cylinder apparatus (Shimakawa *et al.*, 1999).

The unit cell constants from all known preparations of Mn_2O_7 phases along with preliminary magnetic characterization data are collected in Table II for $A = \text{Sc, Y, Lu, In and Tl}$, i.e., where only the Mn-sublattice is magnetic. Given the variety of preparative conditions, the agreement among the various groups for these key parameters is excellent, suggesting that sample to sample compositional variation is small. As seen in the case of the molybdate pyrochlores (Section VII), both the unit cell constant, a_0 , and T_c are very sensitive to composition. All of these materials appear to be ferromagnets, consistent with the observation of a positive Curie-Weiss temperature and an apparent Curie temperature as shown for example in Fig. 19 for $\text{Tl}_2\text{Mn}_2\text{O}_7$ (Raju *et al.*, 1994). Note, however, that there appear to be two separate classes of ferromagnetic materials, if sorting is done by the ratio θ_{CW}/T_c . The compounds $A = \text{Tl}$ and In have T_c values of 120 K and θ_{CW}/T_c ratios of about 1.25 - 1.3. Of course mean field theory gives $T_c = \theta_{CW}$ for a ferromagnet. Empirically, for most ferromagnets this ratio is larger than 1, with typical values between 1.1 and 1.2 as shown in Table III for some selected ferromagnetic insulators. As well, one can estimate a theoretical ratio calculated using the Rushbrooke-Wood relationship for T_c and the mean field theory for θ_{CW} , assuming the same exchange constant J (nearest-neighbors only) and $S = 3/2$, appropriate for Mn^{4+} , which gives $T_c/\theta_{CW} = 1.4$ (Rushbrooke and Wood, 1958). On the other hand the $A = \text{Sc, Y}$ and Lu compounds show corresponding ratios within the range 3 - 4, values well outside those seen for typical ferromagnets and well outside the expected theoretical limits. This suggests that these phases present a much more complex situation than that of a simple ferromagnet. Interestingly, when the A element has a magnetic moment ($A = \text{Tb - Yb}$), the properties, especially the θ_{CW}/T_c ratio, return to typical simple ferromagnetic levels just above 1 as shown in Table IV.

	θ_{CW} (K)	T_c (K)	θ_{CW} / T_c
EuO	80	69	1.2
EuS	19	16.6	1.2
$\text{Lu}_2\text{V}_2\text{O}_7$	83	74	1.1
YTlO_3	33	29	1.1

TABLE III Comparison of the Curie-Weiss and ordering temperatures for selected ferromagnetic insulators.

1. $\text{Tl}_2\text{Mn}_2\text{O}_7$

$\text{Tl}_2\text{Mn}_2\text{O}_7$ has attracted considerable attention following the discovery of giant magneto-resistance (GMR) (Cheong *et al.*, 1996; Shimakawa *et al.*, 1996;

A	a_0 (Å)	T_c (K)	θ_{CW} (K)	θ_{CW}/T_c	Reference
Tb	9.972(3)	38	-	-	(Troyanchuk <i>et al.</i> , 1988)
Dy	9.929	40(5)	43(2)	1.08	(Subramanian <i>et al.</i> , 1988)
Ho	9.906(3)	24	-	-	(Troyanchuk <i>et al.</i> , 1988)
Ho	9.905	37(5)	33(5)	1	(Subramanian <i>et al.</i> , 1988)
Ho	9.907(1)	37(1)	37(1)	1.0	(Greedan <i>et al.</i> , 1996)
Er	9.888(3)	24	-	-	(Troyanchuk <i>et al.</i> , 1988)
Er	9.869	35(5)	40(5)	1.15	(Subramanian <i>et al.</i> , 1988)
Tm	9.852(3)	14	-	-	(Troyanchuk <i>et al.</i> , 1988)
Tm	9.847	30(5)	56(8)	1.8	(Subramanian <i>et al.</i> , 1988)
Yb	9.830(3)	22	-	-	(Troyanchuk <i>et al.</i> , 1988)
Yb	9.830	35(5)	41(3)	1.17	(Subramanian <i>et al.</i> , 1988)
Yb	9.838(1)	37(1)	44(1)	1.19	(Greedan <i>et al.</i> , 1996)

TABLE IV Collected values for unit cell constants, a_0 Curie temperatures, T_c , and Curie-Weiss temperatures, θ_{CW} , for $A_2Mn_2O_7$ phases with $A = Tb - Yb$.

Subramanian *et al.*, 1996). While this topic is outside the main area of this review, having little to do with geometric frustration, some comments are in order. Figure 19 shows the evidence for this effect (Shimakawa *et al.*, 1996). It was soon realized that the mechanism for this GMR must be different from that for the well-studied perovskite manganates (Schiffer *et al.*, 1995). In the latter, double exchange between Mn^{3+} and Mn^{4+} is in part involved in both the metallic behavior and the ferromagnetism. From a combination of accurate measurements of Mn - O1 distances and core level spectroscopies, it was determined that only Mn^{4+} is present in $Tl_2Mn_2O_7$ (Kwei *et al.*, 1997; Rosenfeld and Subramanian, 1996; Subramanian *et al.*, 1996). The ferromagnetism arises from superexchange, not double exchange, and the metallic properties are due to accidental overlap between the Tl 6s band and the Mn 3d band. The coupling between magnetic and transport properties results from abnormally strong incoherent scattering of the conduction electrons due to spin fluctuations which accompany the FM order in GMR thus arises from the large field dependence of T_c . Interestingly, doping of the Tl site with In or Sc, the parent compounds of which are both insulating, greatly enhances the GMR effect as does doping with Tl-vacancies or even Cd (Alonso *et al.*, 2000; Cheong *et al.*, 1996; Ramirez and Subramanian, 1997; Velasco *et al.*, 2002).

Neutron diffraction confirmed the ferromagnetic long range order for this material, finding an ordered moment of $2.91(4) \mu_B$ per Mn^{4+} ion, in excellent agreement with the $3.0 \mu_B$ expected for an $S = 3/2$ state. Small angle neutron scattering is fully consistent with the formation of domain walls and spin waves below $T_c = 123.2(3) K$ (Lynn *et al.*, 1998; Raju *et al.*, 1994). These results are of interest when compared to data from the insulating materials $A = Y, Ho$ and Yb , below.

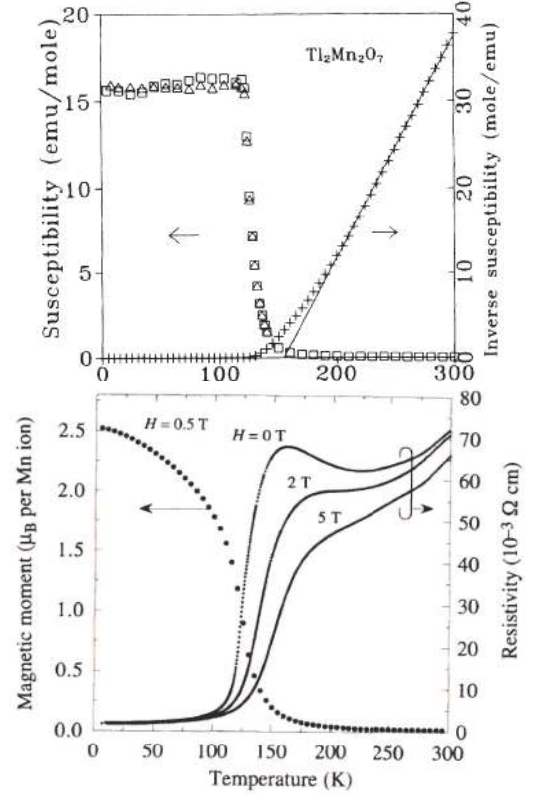


FIG. 19 Top: Magnetic properties of $Tl_2Mn_2O_7$ showing evidence for ferromagnetic order in 0.005 T (Raju *et al.*, 1994). Bottom: Evidence for a giant magneto resistance effect in $Tl_2Mn_2O_7$ (Shimakawa *et al.*, 1996).

2. $Y_2Mn_2O_7$

As shown by Reimers *et al.* (1991), this material exhibits many of the features of a ferromagnet, including an apparent $T_c \approx 16(1) K$ from DC magnetization studies and saturation with applied magnetic field at low temperatures (see Fig. 20). Note that saturation is not reached even at $\mu_0 H = 4 T$ and that the moment is close to $2 \mu_B$ rather than the $3 \mu_B$ expected for an $S = 3/2$ ion.

Behavior quite atypical of ferromagnetism is found in the AC susceptibility and the heat capacity is shown in Figs. 20 and 21. First, while χ' does indeed show a sharp increase below 16 K, the dominant feature is a broad maximum centered at about 7 K which shows a strong frequency dependence, typical of spin glassiness. Controversy exists concerning measurements of the specific heat. Reimers *et al.* (1991) report no lambda-type anomaly near 16 K and a linear temperature dependence below 7 K, behavior again typical of spin glasses. They also reported that about 60 percent of the total entropy of $R \ln 4$ (attained by 100 K) is removed above 16 K. On the other hand Shimakawa *et al.* (1999) find a lambda anomaly at 15 K which they have interpreted as evidence for long range ferromagnetic order. Figure

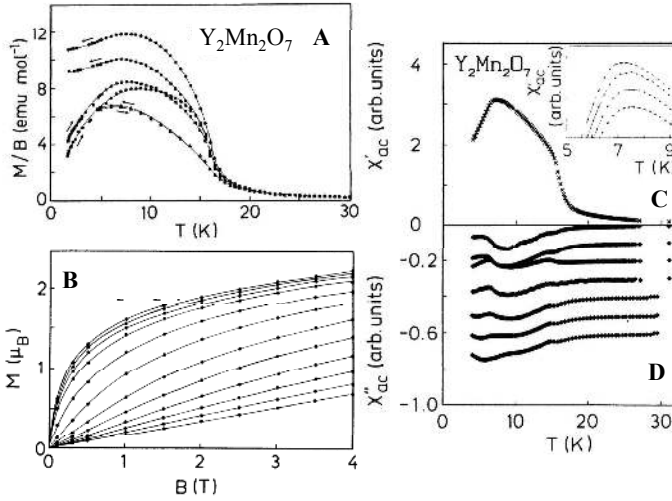


FIG. 20 Bulk properties of $\text{Y}_2\text{Mn}_2\text{O}_7$. Top left: DC susceptibility showing $T_c = 16$ K in 0.15 mT (circle), 0.56 mT (square) and 10 mT (triangle). Bottom left: Magnetization versus applied field at various temperatures (K) from top to bottom: 1.8, 5, 7.5, 10, 15, 20, 25, 30, 35, 40, 45 and 50 K. Right: AC susceptibility. (C) $\chi' = 20$ Hz. The inset shows the χ' maximum for various frequencies, top to bottom: 20, 100, 200 and 1000 Hz. (D) χ'' at various frequencies, from top to bottom: 20, 40, 80, 100, 200, 500 and 1000 Hz. The curves are each shifted by -0.1 from the preceding one (Reimers *et al.*, 1991).

21 compares both results and those for a non-magnetic, lattice matched material, $\text{Y}_2\text{Sn}_2\text{O}_7$. Although the agreement in the data between the two groups is good, apart from the weak lambda anomaly, Fig. 21 shows considerable magnetic heat capacity both above and below the lambda feature when compared to $\text{Y}_2\text{Sn}_2\text{O}_7$. Clearly, this is not consistent with a simple ferromagnetic transition. As well, even the observation of a lambda anomaly in the specific heat is no guarantee of a phase transition to a conventional long-range ordered state as has been demonstrated for other pyrochlores like $\text{Yb}_2\text{Ti}_2\text{O}_7$ and the garnet, $\text{Yb}_3\text{Ga}_5\text{O}_{12}$ (Blöte *et al.*, 1969; Dalmas de Réotier, *et al.*, 2003; Hodges *et al.*, 2002). While the results of Fig. 21 cannot be easily reconciled, the claim by Shimakawa *et al.* (1999) that the heat capacity demonstrates, unequivocally, an ordered state is not substantiated and should be investigated further.

Neutron scattering data from Reimers *et al.* (1991) and Greedan *et al.* (1991) also provide evidence for a quite complex ground state. Elastic scattering data show mainly broad features below 50 K (see Fig. 22). Enhanced magnetic scattering forms below 15 K at nuclear Bragg positions corresponding to the 111 and 222 at 13.9° and 28.0° respectively. These data were further analyzed via Fourier transformation to give the real space spin-spin correlation function which suggested that the nearest-neighbor exchange was weakly antiferromagnetic while further neighbor exchange is strongly ferromagnetic. This is consistent with the observed positive

Curie-Weiss temperatures and the apparent failure to order in a simple ferromagnetic ground state.

Small angle neutron scattering (SANS) data from Greedan *et al.* (1991, 1996) are also unusual and in fact unprecedented. These are compared with corresponding data for ferromagnetic $\text{Ti}_2\text{Mn}_2\text{O}_7$ in Fig. 23 (Lynn *et al.*, 1998; Raju *et al.*, 1994). At $|\mathbf{Q}| = 0.030 \text{ \AA}^{-1}$ the ferromagnet ($\text{Ti}_2\text{Mn}_2\text{O}_7$) shows a decrease in scattering intensity with decreasing temperature below T_c which is ascribed to scattering from spin waves which diminish in intensity as the long range order is established and the cluster size moves out of the SANS window. On the other hand, the behavior of $\text{Y}_2\text{Mn}_2\text{O}_7$ is the opposite, showing an increase below the apparent ordering temperature of 15 K, indicating that the population of subcritical clusters does not diminish significantly to low temperatures. In addition the full range of data could not be fitted to a simple Lorentzian as is normally the rule for ferromagnets, as for example in $\text{Ti}_2\text{Mn}_2\text{O}_7$ (Lynn *et al.*, 1998), but only to a Lorentzian plus Lorentzian-squared ($L+L^2$) law which involves two correlation lengths, ξ_1 and ξ_2 ,

$$S(Q) = \frac{A}{(Q + 1/\xi_1)} + \frac{B}{(Q + 1/\xi_2)^2}. \quad (5)$$

The $L + L^2$ law is often found for systems in which there is competition between ferromagnetic order and random-field disorder and where ξ_1 is associated with the ferromagnetic correlations and ξ_2 with the random fields (Aharony and Pytte, 1983; Arai *et al.*, 1985; Rhyne, 1985). As shown in Fig. 24, for $\text{Y}_2\text{Mn}_2\text{O}_7$ the two correlation lengths differ by nearly an order of magnitude over the temperature range investigated. ξ_1 shows a buildup through a rounded maximum to a value near 20 Å. Similar broad maxima are found in nearly ferromagnetic, metallic glasses (Rhyne, 1985; Rhyne and Fish, 1985). ξ_2 quickly diverges to a resolution limited value below 15 K. The most straightforward interpretation is that ξ_1 measures the temperature evolution of ferromagnetic correlations that never realize a long-range ordered state due

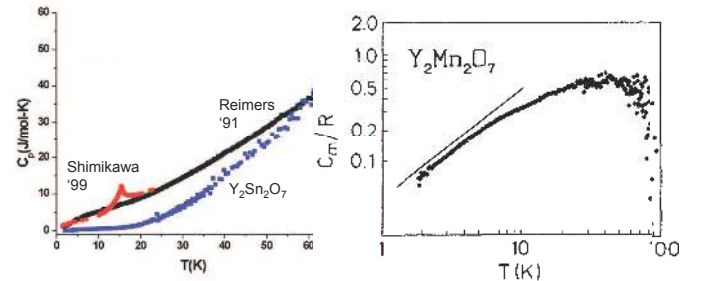


FIG. 21 Left: Comparison of the total heat capacity for $\text{Y}_2\text{Mn}_2\text{O}_7$ reported by Reimers *et al.* (1991) (black) and Shimakawa *et al.* (1996) (red) and the diamagnetic material, $\text{Y}_2\text{Sn}_2\text{O}_7$ (blue). Right: The magnetic component of the heat capacity. Note the absence of a sharp peak and the linear dependence at low temperatures (Reimers *et al.*, 1991).

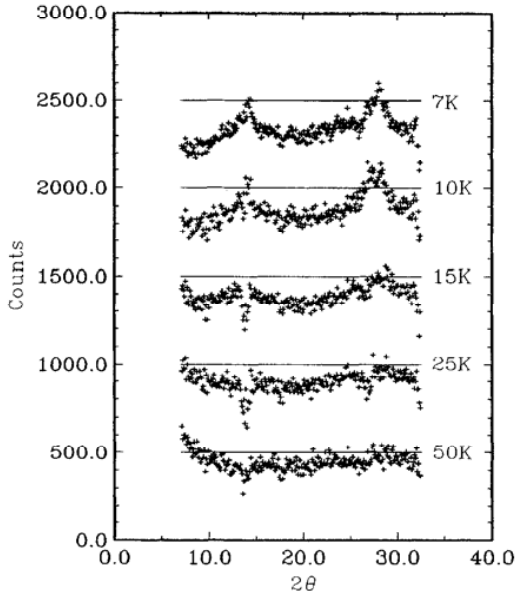


FIG. 22 Neutron diffraction data for $\text{Y}_2\text{Mn}_2\text{O}_7$ showing difference plots (data at 200K subtracted) at various temperatures. Note the buildup of broad peaks at the 111 and 222 Bragg positions (Reimers *et al.*, 1991).

to the intervention of random fields as monitored by ξ_2 . In this case, both tendencies have onsets near the same temperature. Note that there is no anomaly near 7 K, the maximum in the real part of the AC susceptibility. While a detailed understanding of the SANS results for this material is not yet available, there is little in these data to indicate that $\text{Y}_2\text{Mn}_2\text{O}_7$ behaves as a conventional ferromagnet.

3. $\text{Ho}_2\text{Mn}_2\text{O}_7$ and $\text{Yb}_2\text{Mn}_2\text{O}_7$

Among the remaining $A_2\text{Mn}_2\text{O}_7$ pyrochlores only those with $A = \text{Ho}$ and Yb have been studied in detail (Greedan *et al.*, 1996). As seen from Table III, the θ_{CW}/T_c ratio is within the range typically seen for ferromagnets and both show positive Curie-Weiss temperatures which indicates ferromagnetic rather than ferrimagnetic correlations between the two sublattices. The apparent T_c values are significantly higher than those for $A = \text{Y}$, Lu or Sc indicating that the A - Mn exchange has a strong influence on the ordering temperature. Unlike $\text{Y}_2\text{Mn}_2\text{O}_7$, both materials show magnetic saturation at 5 K for modest applied fields $\mu_0 H > 2$ T with values of $12.4 \mu_B$ and $9.2 \mu_B$ per formula unit for $A = \text{Ho}$ and Yb , respectively. Assuming ferromagnetic A - Mn coupling and that the Mn sublattice moment saturates with the full spin-only value of $3.0 \mu_B$ per Mn^{4+} , the A sublattice saturation moments are $3.2 \mu_B$ and $1.6 \mu_B$ per Ho^{3+} and Yb^{3+} ion, respectively. These are considerably smaller than the full saturation moments, $g_L J$, for free Ho^{3+}

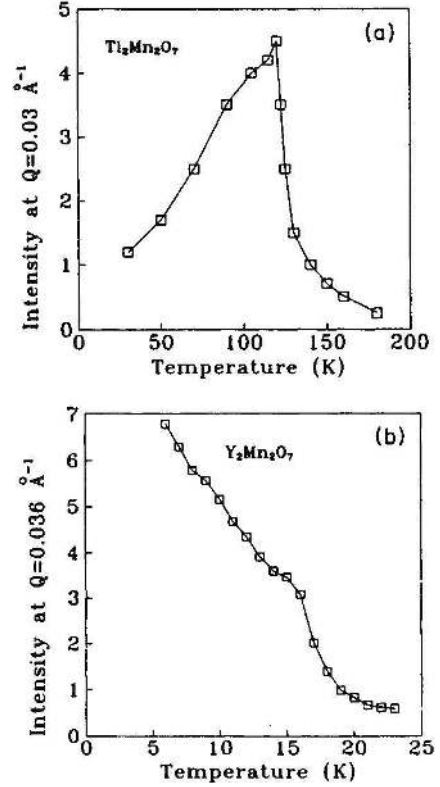


FIG. 23 Comparison of the temperature dependence of the total small angle neutron scattering (SANS) intensity data for the ferromagnet $\text{Tl}_2\text{Mn}_2\text{O}_7$ and $\text{Y}_2\text{Mn}_2\text{O}_7$ at $|\mathbf{Q}| = 0.03 \text{ \AA}^{-1}$ (Greedan *et al.*, 1996; Raju *et al.*, 1994). Similar results for $\text{Tl}_2\text{Mn}_2\text{O}_7$ were obtained by Lynn *et al.* (1998).

($10.0 \mu_B$) and Yb^{3+} ($4.0 \mu_B$), and indicate the strong influence of crystal fields on the ground state. A similar Yb moment is found in the isostructural compound, $\text{Yb}_2\text{V}_2\text{O}_7$ (Soderholm *et al.*, 1980).

In addition to DC susceptibility and magnetization, AC susceptibility, heat capacity and neutron scattering data are available but these do not lead straightforwardly to a consistent interpretation. For example, the real part of the AC susceptibility data shown in Fig. 25 indicates divergent behavior for the two materials. While there is an apparent T_c at 38(1) K with a broad maximum just above at 30 K for both materials, the data for $\text{Ho}_2\text{Mn}_2\text{O}_7$ show a strong frequency dependence while those for $\text{Yb}_2\text{Mn}_2\text{O}_7$ do not. Thus, the $\text{Ho}_2\text{Mn}_2\text{O}_7$ phase appears to show a so-called re-entrant spin glass state where glassy behavior develops at a temperature below T_c .

Heat capacity (see Fig. 25), and neutron scattering (see Fig. 26), data seem to suggest a very complex magnetic ground state for both materials. No lambda anomaly consistent with true long range order has been observed but resolution limited magnetic Bragg peaks are seen for both materials, the temperature dependence of which is order parameter like and consistent with $T_c = 38(1) \text{ K}$

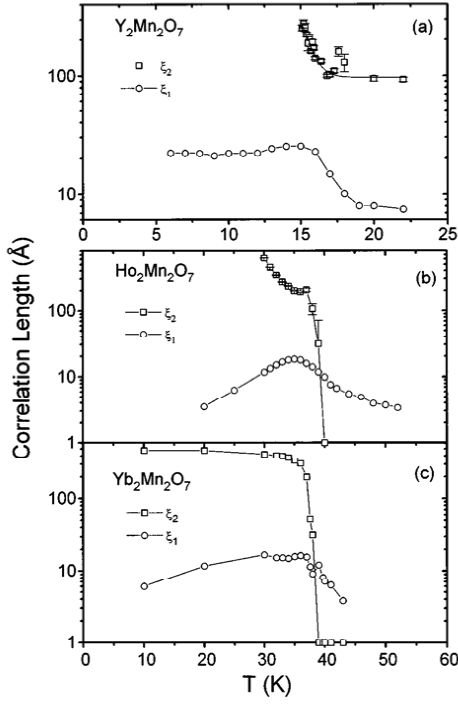


FIG. 24 Temperature dependence of the correlation lengths ξ_1 and ξ_2 for $\text{Y}_2\text{Mn}_2\text{O}_7$, $\text{Ho}_2\text{Mn}_2\text{O}_7$ and $\text{Yb}_2\text{Mn}_2\text{O}_7$ (Greedan *et al.*, 1996).

for both compounds. However, the magnetic structure for $\text{Yb}_2\text{Mn}_2\text{O}_7$ and $\text{Ho}_2\text{Mn}_2\text{O}_7$ is still unknown. SANS data are similar to those for $\text{Y}_2\text{Mn}_2\text{O}_7$ in that the $L + L^2$ law holds and the two correlation lengths have different temperature dependences (see Fig. 24). Interestingly, the B coefficient in Equ. 5, which measures the contribution

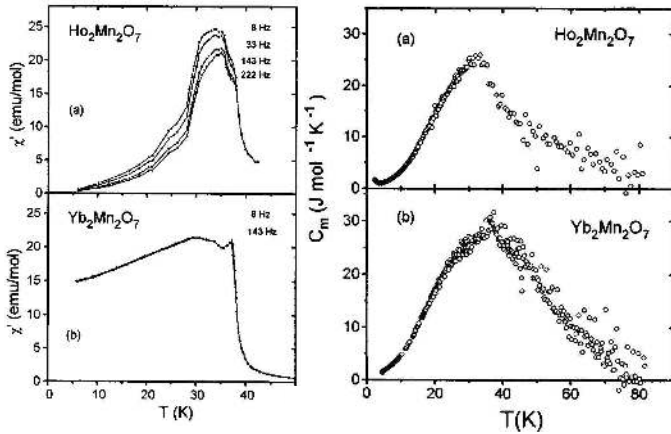


FIG. 25 Bulk properties of $\text{Yb}_2\text{Mn}_2\text{O}_7$ and $\text{Ho}_2\text{Mn}_2\text{O}_7$. Left column is the real part of the AC susceptibility for and right column is the magnetic component of the heat capacity (Greedan *et al.*, 1996).

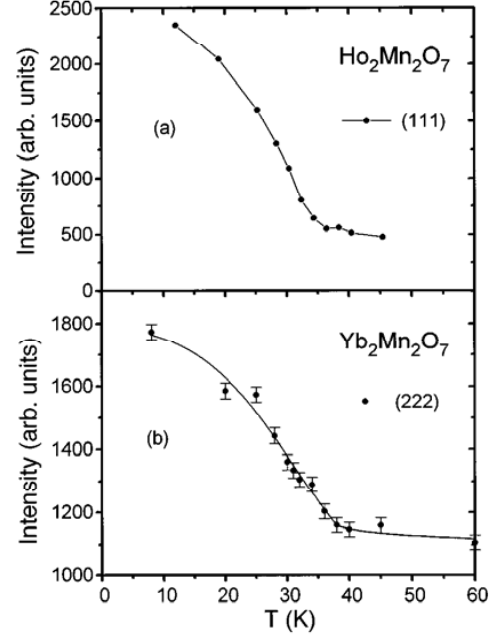


FIG. 26 Temperature dependence of magnetic Bragg peaks for $\text{Yb}_2\text{Mn}_2\text{O}_7$ and $\text{Ho}_2\text{Mn}_2\text{O}_7$ showing order parameter like behavior and an apparent T_c of 38(1) K for both (Greedan *et al.*, 1996).

from the L^2 term associated with the ξ_2 correlation length shows a temperature dependence akin to that of an order parameter for all three materials.

More work on the ordered manganese pyrochlores is needed to understand fully their magnetic ground states. The role of random fields arising from the geometrically frustrated Mn sublattice, but whose microscopic origin is not understood, play an important role in the determination of the magnetic ground state which appears to be rather inhomogeneous. The $A = \text{Y}, \text{Ho}$ and Yb compounds do not behave like simple ferromagnets and studies of their spin dynamics are warranted. In addition, diffraction studies using modern instruments should be performed on $A = \text{Ho}$ and Yb to determine the ordered component of the ground state.

F. $A_2\text{Ir}_2\text{O}_7$ ($A = \text{Nd} - \text{Yb}$)

In the rare earth iridium(IV) pyrochlores, iridium has an electronic configuration $5d^5$ which is expected to be low spin, resulting in an $S = 1/2$ system and this series is thus of considerable interest. The pyrochlore structure is reported to be stable for $A = \text{Pr} - \text{Lu}$, one of the widest stability ranges for any pyrochlore system (Subramanian and Sleight, 1993). This series of compounds not only shows a metal-insulator (MI) transition across the rare earth series at room temperature, like that discussed in Section VII for the molybdates, but several individual

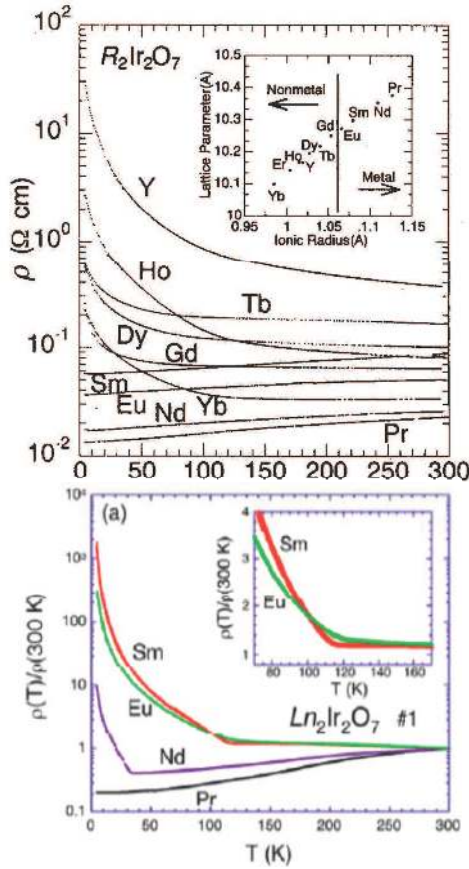


FIG. 27 Top: Resistivity data for the $A_2\text{Ir}_2\text{O}_7$ series showing the metal-insulator crossover between $A = \text{Eu}$ and $A = \text{Gd}$ (Yanagishima and Maeno, 2001). Bottom: Evidence for metal/insulator transitions with decreasing temperature for $A = \text{Eu}$, Sm and Nd but not for Pr (Matsuhira *et al.*, 2007).

compounds do show a MI transition as a function of temperature. These materials were first studied in the early 70's by Sleight and Bouchard (1972), but have not been studied systematically until fairly recently. Early reports on the electrical transport behavior were contradictory. One group, Lazarev and Shaplygin (1978), reported room temperature resistivities in the range of poor metals while Subramanian and Sleight (1993) argued that the entire series of compounds were low activation energy semiconductors. Also, among the earliest measurements were specific heat studies for $A = \text{Er}$ and Lu which showed no magnetic anomalies up to 20 K but a rather large gamma coefficient which is not expected for materials reported to be insulating (Blacklock and White, 1980). Interest in these materials was re-kindled in 2001 with the report of magnetic anomalies above 100 K for the $A = \text{Y}$, Lu , Sm and Eu series members by Taira *et al.* (2001) and the study of Yanagishima and Maeno (2001) who found a crossover from metallic to insulating behavior with decreasing A radius and with the metal-insulator boundary between $A = \text{Eu}$ and Gd . Representative results are

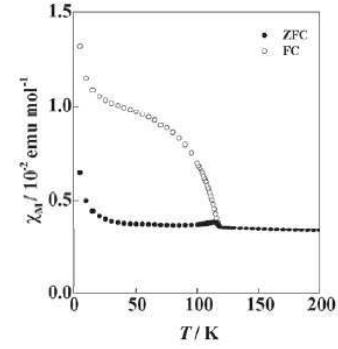


FIG. 28 Magnetic susceptibility for $\text{Sm}_2\text{Ir}_2\text{O}_7$ showing evidence for a magnetic anomaly near 120 K (Taira *et al.*, 2001).

shown in Fig. 27.

There exists a controversy concerning the connection between the magnetic and metallic properties of these materials. Initial reports by Yanagishima and Maeno (2001) indicated that the metallic series members, $A = \text{Pr}$, Nd , Sm and Eu were not magnetic. This is contradicted by Taira *et al.* (2001), as can be seen in Fig. 28, where the metallic $\text{Sm}_2\text{Ir}_2\text{O}_7$ also clearly shows a magnetic transition.

In subsequent work, it was found that hole doping of $\text{Y}_2\text{Ir}_2\text{O}_7$ by substitution of Ca^{2+} for Y^{3+} induces an insulator to metal transition at doping levels of about 15 atomic percent (Fukazawa and Maeno, 2002). The magnetic transition disappears with the onset of metallic behavior. One other important issue addressed here is the apparent large gamma coefficient of the specific heat which persists at low temperatures, first noted by Blacklock and White (1980). Fukazawa and Maeno (2002) found gamma to tend toward zero, $0.0(5) \text{ mJ/K}^2 \text{ mol Ir}$, at 0.4 K and thus concluded that $\text{Y}_2\text{Ir}_2\text{O}_7$ is indeed a Mott insulator.

Nonetheless, the issue of the persistence of magnetic order into the metallic samples remains an important question. Another attempt to address this problem has appeared very recently by Matsuhira *et al.* (2007). These authors have investigated the correlation between sample quality and their transport and magnetic properties. These studies have revealed MI transitions as the temperature is lowered for $A = \text{Eu}$, Sm and Nd . However, $\text{Pr}_2\text{Ir}_2\text{O}_7$ appears to remain metallic down to the lowest temperatures investigated (see Fig. 27). We return to $\text{Pr}_2\text{Ir}_2\text{O}_7$ in Section XI.D. For one sample, $\text{Sm}_2\text{Ir}_2\text{O}_7$, the onset temperatures for both the MI and magnetic transition were shown to be identical, suggesting that the two phenomena are intimately connected. The samples showing these effects were prepared by a different route than those from Yanagishima and Maeno (2001) and Fukazawa and Maeno (2002) which involved firing of the starting materials in air. Matsuhira *et al.* (2007) used Pt tubes in evacuated silica with a 10 percent excess of IrO_2 and many regrinding sequences. X-ray powder

diffraction showed single phase samples with well resolved $K\alpha_1/K\alpha_2$ splittings at high angles, indicative of good crystallinity. No evidence for changes in the diffraction pattern were observed below the apparent MI transitions from which the authors suggest that these are continuous rather than first order. As well, the nature of the magnetic transition is still unclear. The observation of a lambda-type anomaly in the specific heat at T_m indicated by the susceptibility is evidence for a long range ordered antiferromagnetic ground state but more work is needed. For $S = 1/2$ systems, neutron diffraction can be a challenge but studies on a single crystal should be definitive. Clearly, studies of this very interesting pyrochlore series are at an early stage and more work is needed to resolve the discrepancies among the various groups.

Related 5d Pyrochlores.

Very little has been reported about other pyrochlore oxides based on 5d transition elements. The synthesis of $B = \text{Os}$ ($5d^4$) and Pt ($5d^6$) pyrochlores with $A = \text{Pr} - \text{Lu}$ (including Sc and In for $B = \text{Pt}$) have been reported (Hoekstra and Gallagher, 1968; Lazarev and Shaplygin, 1978). The $B = \text{Pt}$ series can only be prepared using high pressures, 4 GPa, and high temperatures, 1200°C (Hoekstra and Gallagher, 1968). Room temperature electrical resistivity values are reported for the $B = \text{Os}$ series and all are in the range for poor metals, very similar to the initial reports for the $B = \text{Ir}$ compounds described above. $\text{Cd}_2\text{Os}_2\text{O}_7$ was first studied by Sleight *et al.* (1974) and later by others for its unusual MI transition at 226 K (Mandrus *et al.*, 2001). This suggests that a closer study of this series could be very interesting.

G. $A_2\text{Mo}_2\text{O}_7$ ($A = \text{Gd}, \text{Nd}$ and Sm)

The earliest report of the existence of rare earth molybdenum pyrochlores appears to be that of McCarthy (1971) from a study of the $\text{Eu} - \text{Mo} - \text{O}$ and $\text{Sm} - \text{Mo} - \text{O}$ phase diagrams in which the pyrochlore compounds were observed. Hubert (1974) was the first to report magnetic susceptibility for $\text{Y}_2\text{Mo}_2\text{O}_7$ in the range 300 to 1000 K. Ranganathan *et al.* (1983) synthesized the series $A = \text{Gd} - \text{Lu}$ along with solid solutions in which the A-site contained various ratios of Nd/Yb and Nd/Er and reported magnetic susceptibility and limited electrical transport data for 77 K - 300 K. The observation of positive Curie-Weiss (θ_{CW}) temperatures led the authors to suggest that some of these materials might be ferromagnets, for example $\text{Sm}_2\text{Mo}_2\text{O}_7$ (Mandirani and Gopalakrishnan, 1980). As well, samples rich in Nd appeared to be metallic (Ranganathan *et al.*, 1983). This situation was clarified by Greedan *et al.* (1987) who showed that Mo(IV) pyrochlores for $A = \text{Nd}, \text{Sm}$ and Gd were indeed ferromagnets with $T_c = 97, 93$ and 83 K, respectively, which was attributed to the ordering of the Mo(IV) moments, an unprecedented observation. As mentioned in Section VII, there is a link between the ionic radius of

the A-ion and the electrical transport properties of the molybdenum pyrochlores which in turn are strongly correlated to the magnetic properties.

The existing evidence appears to support the view that the properties of ferromagnetism and metallic behavior are fundamentally linked in these materials. A proposal for the origin of the ferromagnetism (and antiferromagnetism for $\text{Y}_2\text{Mo}_2\text{O}_7$) has been advanced by Solovyev (2003). While the argument is complex and has a number of elements, the key idea is that the $\text{Mo } t_{2g}$ states are split by the axial crystal field component into a_{1g} and e_g states. These states are effected differently by systematic changes in crystal structure in proceeding from $A = \text{Nd}$ to Y . For $A = \text{Nd}$ and Gd , the e_g band is found to be relatively broad and can support itinerant spin up electrons, rather in analogy to the double exchange mechanism in the manganate perovskites which selects a ferromagnetic ground state. However, for $\text{Y}_2\text{Mo}_2\text{O}_7$, the e_g states become more localized, while the a_{1g} band broadens. This is found to favor an antiferromagnetic ground state. The marked differences in magnetism and transport properties are very surprising given that the structural changes in moving from $A = \text{Nd} \rightarrow \text{Gd} \rightarrow \text{Y}$ are very subtle. For example the $\text{Mo} - \text{O} - \text{Mo}$ bond angle changes from $131.4^\circ[\text{Nd}]$ to $130.4^\circ[\text{Gd}]$ to $127.0^\circ[\text{Y}]$ (Moritomo *et al.*, 2001; Reimers *et al.*, 1988).

1. $\text{Gd}_2\text{Mo}_2\text{O}_7$

$\text{Gd}_2\text{Mo}_2\text{O}_7$ has attracted much interest due to its position near the metal/insulator (MI) boundary (see Fig. 7) in this molybdate series. As already mentioned, the electrical transport properties are dependent on the stoichiometry of the sample (see Fig. 8). Stoichiometric samples are ferromagnetic and metallic with T_c near 80 K. These show a giant negative magneto-resistance exceeding 40 percent below 15 K (Troyanchuk *et al.*, 1998). Insulating samples are oxygen deficient and electron doped. It has been shown by Hanasaki *et al.* (2006) that insulating samples of $\text{Gd}_2\text{Mo}_2\text{O}_7$ can be driven metallic by application of high pressure with the MI boundary occurring between 3 and 4 GPa (see Section XII.B). Extensive specific heat studies have been carried out on polycrystalline samples for both $A = \text{Sm}$ and Gd by Schnelle and Kremer (2004). Unlike previous studies by Raju *et al.* (1992), clear maxima were observed for both materials near 75 K, indicative of long range magnetic order on the Mo sublattice. For $\text{Gd}_2\text{Mo}_2\text{O}_7$, a step-like anomaly at 11.3 K superimposed on a dominant Schottky peak suggests partial ordering of the Gd spins, which was supported by measurement of the entropy.

Until quite recently, there has been little information regarding the magnetic structure of either the $A = \text{Sm}$ or Gd molybdate pyrochlores, due to the high neutron absorption cross sections for both elements. Mirebeau *et al.* (2006a) have solved this problem with the use of ^{160}Gd substituted materials. The room temperature unit

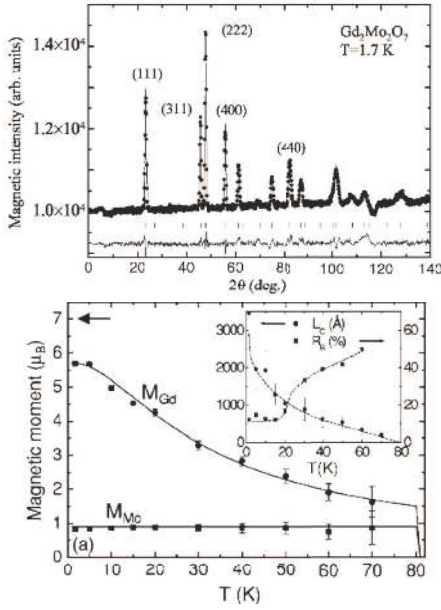


FIG. 29 Neutron powder diffraction results for $\text{Gd}_2\text{Mo}_2\text{O}_7$ by Mirebeau *et al.* (2006a). Top: The magnetic scattering at 1.7 K after a 90 K data set has been subtracted. The solid line is a fit to a model with collinear ferromagnetic coupling between Gd and Mo moments. Bottom: The temperature dependence of the ordered moments for the Gd and Mo sublattices. The inset shows the temperature development of the correlation lengths (L) obtained from the widths of the Bragg peaks and the Bragg R for the magnetic structure.

cell constant for this sample is $10.3481(2) \text{ \AA}$, which indicates only a very slight oxygen doping. The magnetic diffraction pattern at 1.7 K is shown in Fig. 29 along with the temperature dependence of the sublattice moments and correlation lengths. The absence of a (200) reflection is consistent with a collinear magnetic structure and the best fit occurs for a ferromagnetic coupling of the Gd and Mo sublattices. This agrees with the earliest magnetization studies of Sato *et al.* (1986) who found that the bulk saturation moment could only be understood in terms of a ferromagnetic Gd - Mo coupling.

From the right panel of Fig. 29 it is clear that the Mo sublattice orders above 80 K and that the Gd moments are polarized due to the Gd-Mo coupling. The ordered moments on both sublattices are significantly smaller than the spin only values of $2.0 \mu_B$ and $7.0 \mu_B$ for Mo^{4+} and Gd^{3+} , respectively, although the Mo moments are similar to those found for the $A = \text{Nd}$ phase. Muon spin relaxation data (Apetrei *et al.*, 2007), which are most sensitive to the Gd spins, indicate that strong spin fluctuations persist below T_c and as low as 6.6 K. This is consistent with the ^{155}Gd Mössbauer data of Hodges *et al.* (2003) and also, perhaps, with the specific heat data of Schnelle and Kremer (2004). The conclusion is that $\text{Gd}_2\text{Mo}_2\text{O}_7$ is perhaps an unconventional ferromagnet with strong spin fluctuations. This maybe analogous

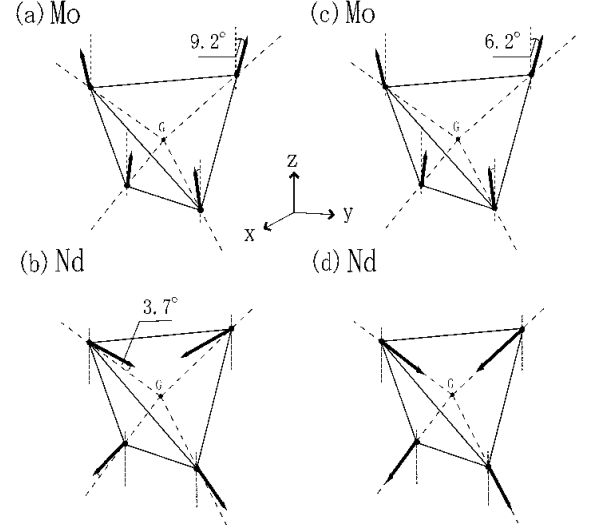


FIG. 30 Proposed spin configurations [(a),(b) and (c),(d)] for the Mo and Nd moments from neutron diffraction on a single crystal of $\text{Nd}_2\text{Mo}_2\text{O}_7$ at 4 K (Yasui *et al.*, 2001).

to the situation encountered for manganate pyrochlores in Section VIII.E. The remarkable properties of this material under applied pressure will be described in Section XII.B.2

2. $\text{Nd}_2\text{Mo}_2\text{O}_7$

Magnetism. It is well established that the $\text{Nd}_2\text{Mo}_2\text{O}_7$ phase is a metallic ferromagnet with $T_c = 95 \text{ K}$ for stoichiometric, polycrystalline samples. That the ferromagnetism is due to the Mo sublattice was first demonstrated by Greedan *et al.* (1991) from powder neutron diffraction studies. A canted ferromagnetic structure on the Mo sites with an ordered moment of $1.1 \mu_B$ was proposed from analysis of data at 53 K which are dominated by magnetic scattering from the Mo. Subsequent studies by Yasui *et al.* (2001) using a single crystal with $T_c = 93 \text{ K}$ have provided a better defined magnetic structure for both the Nd and Mo sublattices. The magnetic structure at 4 K is shown in Fig. 30. The Mo spins are non-collinear making an angle of 9° with the local z axis which is parallel to a four fold axis of the crystal. The Mo moment is $1.2 \mu_B$, very close to that found earlier and slightly greater than half the value expected for a spin only $S = 1$ ion. The Nd moments are aligned nearly along the principal 3-fold rotation axes of the tetrahedra, in a 2-in/2-out pattern. Nd moments at 4 K are $1.5 \mu_B$ and the relative orientations of the Nd and Mo sublattice moment directions are antiferromagnetic.

Anomalous Hall Effect. Much attention has been focussed on $\text{Nd}_2\text{Mo}_2\text{O}_7$ since the observation of the un-

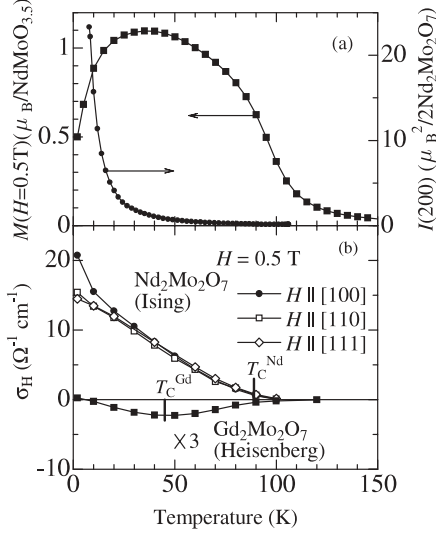


FIG. 31 (a) Temperature dependence of the bulk magnetic moment and the (200) magnetic reflection which tracks the development of the chiral order on the Nd sites in $\text{Nd}_2\text{Mo}_2\text{O}_7$. (b) Temperature dependence of Hall conductivities for $\text{Nd}_2\text{Mo}_2\text{O}_7$ and $\text{Gd}_2\text{Mo}_2\text{O}_7$. Note the conventional behavior for $A = \text{Gd}$ while the conductivity remains large and finite at low temperature for $A = \text{Nd}$ (Taguchi *et al.*, 2004).

precedented behavior of the so-called anomalous Hall effect (AHE) independently by Katsufuji *et al.* (2000) and Taguchi *et al.* (2001). In ferromagnets, the transverse or Hall resistivity has two contributions, the “ordinary” Hall coefficient, R_o , which is proportional to the applied magnetic field B and the “anomalous” coefficient, R_s which is proportional to the sample magnetization, M , as in Eq. (6).

$$\rho_H = R_o B + 4\pi R_s M. \quad (6)$$

The usual behavior is for the AHE contribution to vanish at low temperatures in ferromagnetic metals with collinear spin configurations. However, in the case of $\text{Nd}_2\text{Mo}_2\text{O}_7$, the AHE actually increases and remains large and finite at $T = 0$ (see Fig. 31). In one interpretation, this behavior has been attributed to the spin chirality (the two-in, two-out state is 6-fold degenerate) of the Nd^{3+} moment configuration which acts as an effective magnetic field and effects the carrier dynamics in the same way as a real magnetic field (Taguchi *et al.*, 2001, 2004). A strong point of this argument is the contrast between this AHE and that in the Heisenberg, $A = \text{Gd}$ phase where spin chirality is not present. For the $A = \text{Gd}$ material the AHE vanishes at low temperatures as with a normal ferromagnetic metal. However, this interpretation has been questioned by Yasui *et al.* (2003a) and Kageyama *et al.* (2001) who argue, based on extensive neutron scattering and specific heat studies, that the

origins of the AHE for $\text{Nd}_2\text{Mo}_2\text{O}_7$ are much more complex than thought originally and that the spin chirality mechanism alone cannot provide a quantitative explanation and may at best play only a minor role (Kageyama *et al.*, 2001; Yasui *et al.*, 2003, 2006). On the other hand, Kézsmárki *et al.* (2005) interpret magneto-optical data on both $\text{Nd}_2\text{Mo}_2\text{O}_7$ and $\text{Gd}_2\text{Mo}_2\text{O}_7$ in favor of an important contribution from spin chirality. At present this controversy appears to be unresolved. Further comment on this problem is presented in Section VIII.G.4 below.

3. $\text{Sm}_2\text{Mo}_2\text{O}_7$

Stoichiometric samples of this material generally show $T_c = 93\text{ K}$, although as already mentioned in Section VII, for oxygen deficient samples this value can be significantly reduced (see Fig. 9). A crystal of $\text{Sm}_2\text{Mo}_2\text{O}_7$ with a $T_c = 73\text{ K}$ was reported by Taguchi and Tokura (1999) to show also a finite anomalous Hall Effect coefficient at $T = 0\text{ K}$. A giant negative magnetoresistance of 13 percent near T_c and 18 percent at 4 K has been reported (Taguchi and Tokura, 2000), but little more is known about $\text{Sm}_2\text{Mo}_2\text{O}_7$.

4. $A_2(\text{MoB})_2\text{O}_7$

Studies of B -site substituted compounds are very sparse. Troyanchuk *et al.* (1998) have reported the preparation of V - doped $\text{Gd}_2\text{Mo}_2\text{O}_7$ with B -site composition $\text{Mo}_{1.2}\text{V}_{0.8}$. $\text{Gd}_2\text{Mo}_2\text{O}_7$ is a ferromagnetic metal while the corresponding Gd - V pyrochlore does not exist even under high pressures. Nonetheless, the $A_2\text{V}_2\text{O}_7$ series members, which include only $A = \text{Lu}$, Yb and Tm at ambient pressure are all ferromagnetic semiconductors with T_c in the range 70 K - 75 K (Bazuev *et al.*, 1976; Shin-ike *et al.*, 1977; Soderholm *et al.*, 1980). At this particular composition, the solid solution is insulating with resistivities in the range of $\Omega\text{-cm}$ but remains ferromagnetic with a slightly enhanced T_c relative to the undoped material and a GMR effect of about 40 percent seen for the pure material has been destroyed (Troyanchuk *et al.*, 1998).

In another case, the AHE has been studied for $\text{Nd}_2\text{Mo}_2\text{O}_7$ with Ti substitutions for Mo up to the B -site composition $\text{Mo}_{1.7}\text{Ti}_{0.3}$ (Kageyama *et al.*, 2001). At this doping level the compound is still metallic. This group had shown earlier that the AHE has two contributions, proportional to the magnetizations of Mo and Nd separately, that is, (Iikubo *et al.*, 2001; Yoshii *et al.*, 2000)

$$\rho_H = R_o B + 4\pi R_s M(\text{Mo}) + 4\pi R'_s M(\text{Nd}) \quad (7)$$

Of these two components, the doping experiments showed that R_s changes sign from positive to negative with increasing Ti content while R'_s does not. This observation was taken as evidence that the mechanism for

AHE in these materials is more complex than the pure chirality model advanced initially (Taguchi *et al.*, 2001).

IX. SPIN GLASS PHASES

The spin glass state is one where the combination of (i) randomness and (ii) frustration prevents the development of conventional long range magnetic order characterized by delta-function magnetic Bragg peaks (Binder and Young, 1986). There are a number of experimental pathways to the spin glass state. The classic case involves dilute concentrations of magnetic atoms in a metallic, diamagnetic host such as $\text{Au}_{1-x}\text{Fe}_x$ where $x \sim 0.05$, already mentioned in Section I. Here the effective coupling between Fe moments is mediated by the Au conduction electrons, giving rise to an RKKY interaction whose sign depends on the distance between two Fe moments. This leads to competing random ferro- and antiferromagnetic constraints at each magnetic site. Another approach is to introduce disorder into a magnetically ordered but geometrically frustrated material by dilution of the magnetic sites with diamagnetic ions to levels near the percolation threshold for the particular lattice. An example is $\text{Eu}_{1-x}\text{Sr}_x\text{S}$ where Sr^{2+} dilution of the face centered cubic Eu^{2+} sites destroys the ferromagnetic ground state and a spin glass state emerges near $x = 0.5$. Similar to the latter example is $\text{LiHo}_x\text{Y}_{1-x}\text{F}_4$, where Ho^{3+} is an effective Ising spin and where the predominant interactions are dipolar. Dipolar interactions are intrinsically frustrated since they can be either ferromagnetic or antiferromagnetic depending on the orientation of the vector $\mathbf{r}_j - \mathbf{r}_i$ between spins at positions \mathbf{r}_i and \mathbf{r}_j . As a result, substitution of Ho by Y generates random frustration. Indeed, $\text{LiHo}_x\text{Y}_{1-x}\text{F}_4$ is an Ising ferromagnet for x down to about $x \sim 0.2$. For $x \lesssim 0.2$, a dipolar spin glass state develops (Reich *et al.*, 1990; Wu *et al.*, 1993), although this conclusion has recently been questioned (Jönsson *et al.*, 2007).

One question that has attracted much attention in the field of spin glasses is whether or not a thermodynamic spin freezing transition occurs at nonzero temperature for physical dimensions. While it was determined some time ago that there is no spin glass transition in two dimensions, a seemingly definite conclusion for three-dimensional (3D) systems has only recently become available, thanks to the work of Ballesteros *et al.* (2000) who pioneered the use of the scaled correlation length method in finite-size scaling analysis of spin glass models. A large majority of real magnetic systems are better described by Heisenberg spins rather than Ising spins and it was believed that the 3D XY and Heisenberg spin glass models do not have a transition. The explanation for the experimentally observed transition in real systems therefore had to invoke random anisotropy as the mechanism responsible for driving the system into the Ising spin glass universality class (Binder and Young, 1986). However, recent extensive Monte Carlo simulations on

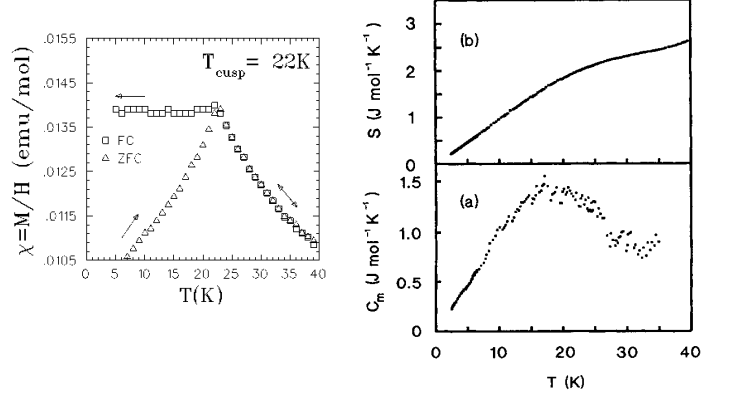


FIG. 32 Left: DC magnetic susceptibility for $\text{Y}_2\text{Mo}_2\text{O}_7$ at an applied field of 100 Oe (Gingras *et al.*, 1997). Right: Heat capacity (a) and entropy (b) for $\text{Y}_2\text{Mo}_2\text{O}_7$. Note the broad maximum below 20 K and the linear dependence on temperature below 7 K (Raju *et al.*, 1992).

the 3D XY and Heisenberg models employing the Ballesteros *et al.* (2000) method find some compelling evidence for a phase transition at nonzero temperature in these two systems (Lee and Young, 2003), although the lower-critical dimension for these models for a nonzero transition temperature seems to be very close to three (Lee and Young, 2007).

From a theoretical perspective, models with couplings of random signs, such as the so-called Edwards-Anderson model, have attracted by far the most attention. One generally believes that as long as there is a transition at nonzero temperature, the universality class should be the same irrespective of the details of the model, i.e., either continuous or discrete distributions of random bonds or a randomly diluted frustration.

Experimentally, a number of signatures are taken as indicative of the spin glass state, such as the frequency dependence of χ' in the AC susceptibility, the linear temperature dependence of the low temperature heat capacity or the μSR line shape, but the definitive approach is the measurement of the temperature dependence of the nonlinear magnetic susceptibility, χ_3 (Binder and Young, 1986). The DC magnetization, $M_z(T, B_z)$, can be expanded as a Taylor series of the applied magnetic field B_z as

$$M_z(T, B_z) \approx \chi_1(T)B_z - \chi_3(T)B_z^3, \quad (8)$$

where T is the temperature. At a second order spin glass transition, one expects $\chi_3(T)$ to show a power-law divergence as $\chi_3(T) \sim (T - T_f)^{-\gamma}$, with γ a critical exponent characterizing the spin glass transition at the freezing temperature T_f (Binder and Young, 1986; Gingras *et al.*, 1997). Other critical exponents can also be determined by measuring the full nonlinear magnetic field

dependence of $M_z(B_z, T)$ (Binder and Young, 1986; Gingras *et al.*, 1997).

With this very minimal background material in hand, we can now discuss the spin glass behaviors observed in some of the pyrochlore oxides.

A. $\text{Y}_2\text{Mo}_2\text{O}_7$ and $\text{Tb}_2\text{Mo}_2\text{O}_7$

1. $\text{Y}_2\text{Mo}_2\text{O}_7$

The initial report by Greedan *et al.* (1986), showing a canonical spin glass behavior, (see Fig. 32a) for $\text{Y}_2\text{Mo}_2\text{O}_7$ has sparked considerable interest which continues to the present time. Neutron powder diffraction data, albeit of moderate resolution, could be analyzed in terms of a fully ordered pyrochlore model (Reimers *et al.*, 1988). Specific heat studies by Raju *et al.* (1992) showed only a broad maximum near the apparent $T_f = 22$ K and a linear dependence on temperature at low T , another feature typical of spin glasses (see Fig. 32b). AC susceptibility (Miyoshi *et al.*, 2000), thermo-remnant magnetization by Dupuis *et al.* (2002) and Ladiou *et al.* (2004) provide more evidence for the canonical spin glass behavior of this material. The AC susceptibility in nearly zero field shows the classic frequency dependence (see Fig. 33).

The best evidence for the nearly canonical spin glass character came from measurements of the non-linear susceptibility, χ_3 , by Gingras *et al.* (1996, 1997). The non-linear magnetization could be analyzed, (see Fig. 34) according to a scaling model for phase transitions, yielding critical exponents γ , β and δ which satisfied the scaling relationship

$$\delta = 1 + \gamma/\beta \quad (9)$$

with values $T_f = 22$ K, $\gamma = 2.9(5)$, $\beta = 0.8(2)$ and $\delta \approx 4.7$. These agree well with those found for conventional spin glasses with dilute magnetic centers and positional

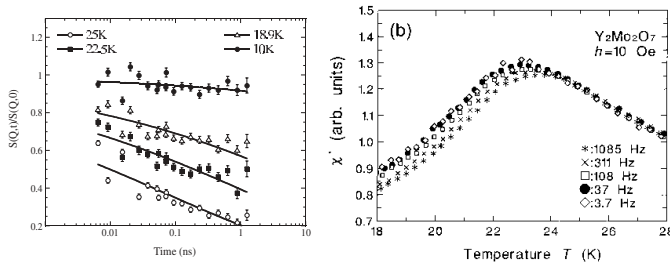


FIG. 33 Left: Neutron spin echo results for $\text{Y}_2\text{Mo}_2\text{O}_7$ at temperatures spanning $T_f = 22.5$ K determined from static magnetization data. Note that within this time window, spin freezing is not fully established until 10 K (Gardner *et al.*, 2001, 2004). Right: Frequency dependent AC susceptibility, χ' , for $\text{Y}_2\text{Mo}_2\text{O}_7$ showing classical spin glass behavior (Miyoshi *et al.*, 2000).

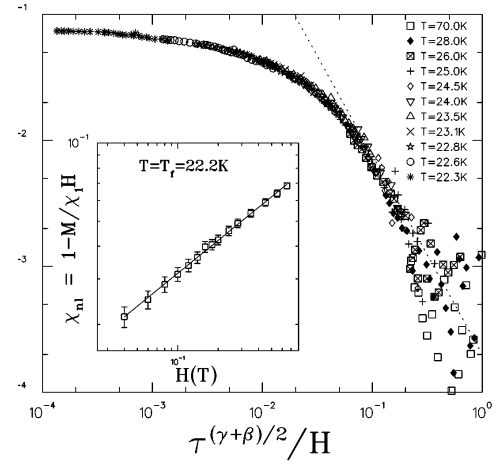


FIG. 34 Nonlinear magnetization analyzed according to a scaling model for a $T_f = 22$ K and $\gamma = 2.8$ and $\beta = 0.75$. Inset shows a log-log plot which allows determination of the critical parameters with $\delta = 4.73$ which follows from the scaling law with the above γ and β values (Gingras *et al.*, 1997).

disorder (Binder and Young, 1986), making $\text{Y}_2\text{Mo}_2\text{O}_7$ indistinguishable from such systems.

Strong evidence for spin freezing comes also from studies of spin dynamics by muon spin relaxation (Dunsiger *et al.*, 1996). Fig. 35 shows $1/T_1$, the muon spin relaxation rate, as a function of temperature. These data show features typical of disordered spin-frozen systems such as a critical slowing down as T_f is approached from above followed by a sharp decrease. A finite $1/T_1$ persists down to the lowest temperatures studied, but this is at the resolution limit of this technique and more needs to be done to conclusively determine if the spins are still dynamic in the mK temperature range.

Neutron scattering experiments, Gardner *et al.* (1999a), provide more insight into the possible local ordering and the spin dynamics over a wide temperature range. Figure 36 shows the $|\mathbf{Q}|$ dependence of the magnetic elastic scattering at 1.8 K. The obvious feature is a broad peak centered at $|\mathbf{Q}| = 0.44 \text{ \AA}^{-1}$. In terms of unit cell dimensions, this value of $|\mathbf{Q}|$ corresponds to $2\pi/d(110)$, which involves the cubic face diagonal. From the half-width at half maximum (HWHM) a correlation length can be estimated as $\xi = 1/\text{HWHM} = 5 \text{ \AA}$. These two observations are consistent with a four sublattice structure as depicted in the inset of Fig. 36.

Inelastic scattering data give a detailed picture of the evolution of the spin dynamics in terms of four distinct regimes: (1) For $T > 200$ K there are no discernable correlations in either space or time. (2) Between 200 K and $T = 2T_f$ spatial correlations build up, peaking at $|\mathbf{Q}| = 0.44 \text{ \AA}^{-1}$, but the energy distribution is broad. (3) Within the interval $T_f < T < 2T_f$, the spatial correlations are no longer evolving but the spin fluctuation rate decreases proportionally to $(T - T_f)$ in a manner appropriate to the approach to a phase transition. (4)

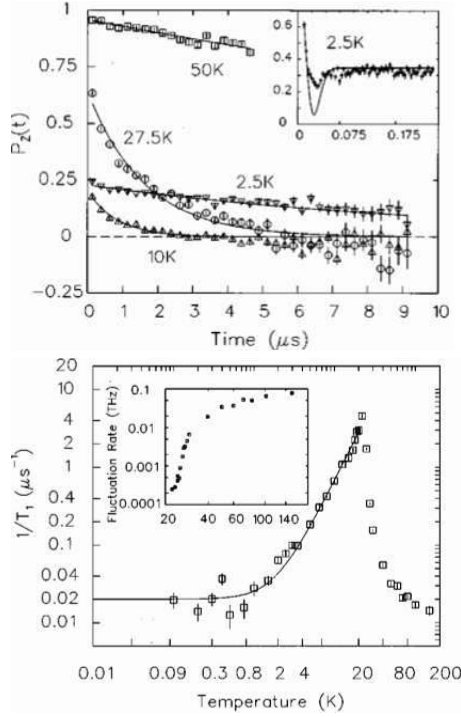


FIG. 35 The muon spin relaxation rate, $1/T_1$ versus temperature. Note the critical slowing down near T_f and the presence of a small but finite relaxation rate persisting to very low temperatures (Dunsiger *et al.*, 1996).

Below T_f the spin fluctuation rate is small and changes very little, consistent with a highly spin frozen state.

The neutron spin echo technique provides information on spin dynamics over a shorter time scale than μ SR, from about 1 to 10^{-2} ns. Within this time window, a different view of the spin dynamics emerges (Gardner *et al.*, 2001, 2004). The left panel of Fig. 33 shows the time dependence of the normalized intermediate scattering function, $S(Q, t)/S(Q, 0)$ for temperatures spanning T_f (22.5 K) determined from static magnetization studies. While the data for 10 K show spin-frozen behavior, there are still significant spin dynamics below T_f . Fits to these data indicate that spin relaxation times increase by a factor of 10^7 between 25 K and 10 K, from 0.07 ns to 8×10^5 ns.

The evidence presented above raises a fundamental question: why is $\text{Y}_2\text{Mo}_2\text{O}_7$ such a typical spin glass? In general, insulating antiferromagnetic spin glasses involve dilution of the magnetic centers by diamagnetic ions at a concentration below the percolation limit which introduces both positional disorder and frustration simultaneously, two conditions considered necessary for the establishment of the spin glass ground state. In $\text{Y}_2\text{Mo}_2\text{O}_7$ the magnetic frustration is provided by the magnetic lattice topology but is there also disorder of some subtle type? While powder neutron diffraction data show that the average structure is well described by the fully ordered py-

rochlore model (Lozano *et al.*, 2007; Reimers *et al.*, 1988), local structure probes such as EXAFS, and NMR have suggested the presence of disorder at some level in this material. Mo K edge EXAFS data were interpreted by Booth *et al.* (2000) to show that the variance in the Mo - Mo nearest-neighbor distance was about ten times larger than that for the Mo - O and Mo - Y distances. From this and a number of assumptions it was estimated that the level of disorder introduced in a pair-wise exchange constant would be of the order of 5 percent. This was judged to be about a factor of five too small when compared with predictions from the Sherrington and Southern (1975) mean field theory for spin glasses. Keren and Gardner (2001) carried out ^{89}Y NMR experiments over a limited temperature range. Data obtained above 200 K (the Curie-Weiss temperature) showed a smooth and broad resonance but at 200 K and 92.4 K, a large number of peaks of small amplitude become superimposed on the broad feature (see Fig. 37). This was interpreted in terms of a distribution of ^{89}Y environments due to localized “lattice” distortions and led to speculation that these distortions are frustration driven. A similar experiment was performed using muon spin relaxation by Sagi *et al.* (2005) down to 20 K. The width of the internal field distribution as detected by the muon grows upon cooling at a rate which cannot be explained by the increasing susceptibility alone. Therefore, they conclude that the width of the distribution of coupling constants also grows upon cooling, or in other words, the lattice and spin degrees of freedom are involved in the freezing process in $\text{Y}_2\text{Mo}_2\text{O}_7$.

A model of Heisenberg spins with magnetoelastic coupling was invoked to account for the high freezing temperature. The derivative of the exchange strength relative to bond length was found to be $0.01 \text{ eV}/\text{\AA}$ and the elas-

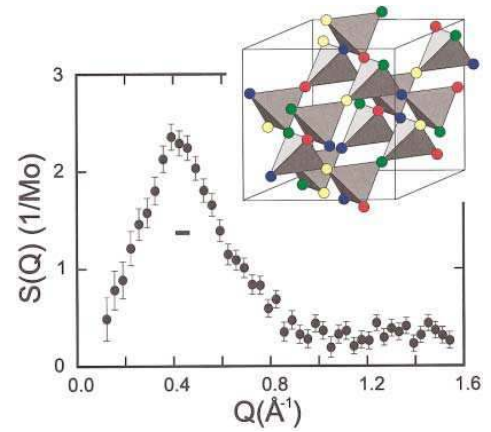


FIG. 36 Elastic neutron scattering for $\text{Y}_2\text{Mo}_2\text{O}_7$ shown as the difference between data at 1.8 K and 50 K. The broad peak suggests the short range order model shown in the inset (Gardner *et al.*, 1999a).

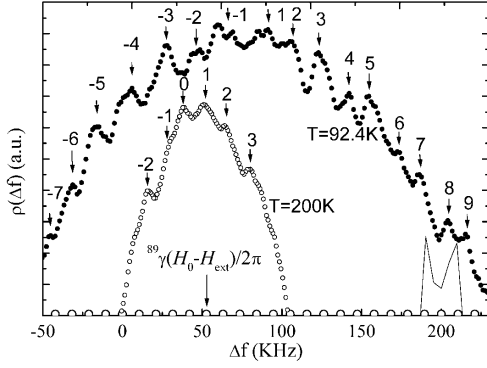


FIG. 37 Y-NMR data for $\text{Y}_2\text{Mo}_2\text{O}_7$ showing multiple peaks arising below 200K, indicating the presence of multiple Y sites (Keren and Gardner, 2001)

tic constant to be $0.1\text{ eV}/\text{\AA}^2$. In ZnCr_2O_4 , where magnetoelastic coupling appears to be important, these values are $0.04\text{ eV}/\text{\AA}$ and $6.5\text{ eV}/\text{\AA}^2$ respectively (Sushkov *et al.*, 2006). Other theoretical studies that have considered classical pyrochlore Heisenberg antiferromagnets with random variations of the exchange couplings include Bellier-Castella *et al.* (2001) and Saunders and Chalker (2007).

At the time of writing, the microscopic mechanism behind the spin glass transition in $\text{Y}_2\text{Mo}_2\text{O}_7$ is unresolved. Ideally, one would like to find a means to reconcile the diffraction studies with the local probe results. One possibility is the application of the neutron pair distribution function method (Billinge, 2004; Proffen *et al.*, 2003). Studies using this approach are currently ongoing (Lozano *et al.*, 2007).

Dunsiger *et al.* (1996a) showed that a 20% dilution of the magnetic Mo^{4+} site with nonmagnetic Ti^{4+} reduces the freezing temperature but increases the residual muon relaxation rate, indicating an increased density of states for magnetic excitations near zero energy. While there are no other published reports on B-site substitution in $\text{Y}_2\text{Mo}_2\text{O}_7$, there may be much to learn from such efforts. As already noted, the microscopic origin of the spin glass behavior in this material is not understood. What is known suggests that $\text{Y}_2\text{Mo}_2\text{O}_7$ falls into the category of a bond disordered spin glass rather than a site disordered glass such as $\text{Eu}_{1-x}\text{Sr}_x\text{S}$, for example. In the context of a picture in which $\text{Y}_2\text{Mo}_2\text{O}_7$ is an “intrinsic” random bond spin glass, it would be of interest to track T_f as a function of the doping of the Mo site with a non-magnetic ion such as Ti^{4+} . Interesting physics may emerge at low temperature close to the percolation limit which is 39 percent of magnetic site occupancy for the pyrochlore lattice.

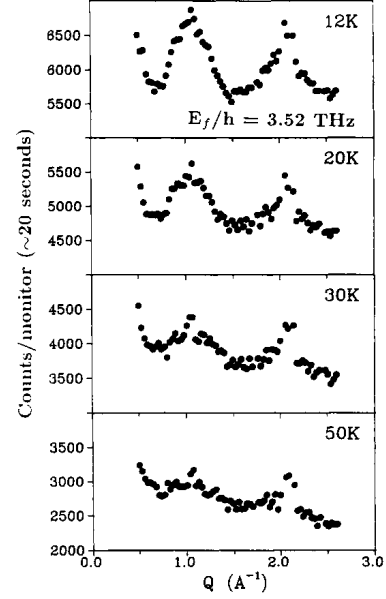


FIG. 38 Diffuse magnetic elastic scattering for $\text{Tb}_2\text{Mo}_2\text{O}_7$ at various temperatures (Gaulin *et al.*, 1992).

2. $\text{Tb}_2\text{Mo}_2\text{O}_7$

Although this material has received much less attention than the Y-based pyrochlore, there are strong similarities. $\text{Tb}_2\text{Mo}_2\text{O}_7$ is an inherently more complex system with two geometrically frustrated magnetic sublattices. Also, the $A = \text{Tb}$ phase is just on the insulating side of the MI boundary for this series and is not a bulk ferromagnet although the Curie-Weiss temperature is reported to be $\theta_{\text{CW}} = +17\text{K}$ (Sato *et al.*, 1986). Among the few detailed studies of transport properties, the material is shown to exhibit an unusual magnetoresistance with both positive (10 percent) and negative (30 percent) MR at low and high fields, respectively (Troyanchuk *et al.*, 1988). This behavior lacks an explanation to date.

Magnetization and neutron scattering studies indicated spin glass like behavior with $T_f = 25\text{K}$ and intense diffuse magnetic scattering (Gaulin *et al.*, 1992; Greedan *et al.*, 1990). The diffuse magnetic scattering sets in below 50 K (see Fig. 38), showing two very broad peaks near $|\mathbf{Q}| = 1.0\text{ \AA}^{-1}$ and 2.0 \AA^{-1} . This pattern is quite different from that for $\text{Y}_2\text{Mo}_2\text{O}_7$ (see Section IX.A.1) and indicates that the Tb sublattice scattering is dominant here. Note also the upturn at low Q .

SANS data were also reported over the Q -range 0.019 \AA^{-1} to 0.140 \AA^{-1} . Subtraction of the 300 K data from low temperature data shows that non-zero SANS appeared only above $|\mathbf{Q}| = 0.14\text{ \AA}^{-1}$, so it is unlikely that this SANS tail is of ferromagnetic origin (Greedan *et al.*, 1990). However, these results might be in conflict with a recent report from Apetrei *et al.* (2007) who observe SANS above $|\mathbf{Q}| = 0.25\text{ \AA}^{-1}$. This issue should be clar-

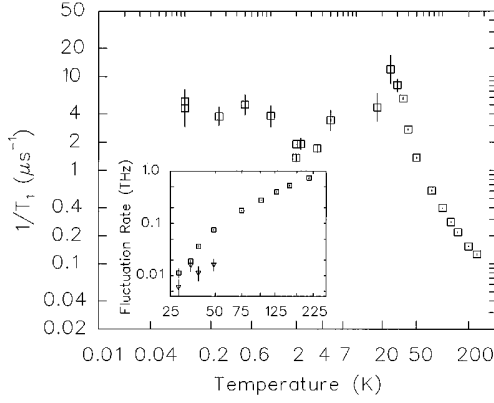


FIG. 39 The muon spin relaxation rate vs temperature for $\text{Tb}_2\text{Mo}_2\text{O}_7$ in an applied field of 5 mT. The inset shows the Tb moment fluctuation rate above the spin freezing point compared with neutron data indicated by the inverted triangles (Dunsiger *et al.*, 1996).

ified. From inelastic neutron scattering, the Tb spins have been shown to be fluctuating at about 0.02 THz above T_f , but spin freezing within the experimental time window was seen below 25 K (Gaulin *et al.*, 1992). Spin relaxation studies were extended into the μSR time window (see Fig. 39). Comparing with Fig. 35, which shows corresponding data for $\text{Y}_2\text{Mo}_2\text{O}_7$, one notes some similarities and differences. First, the data above T_f are very similar, indicating a critical slowing down behavior, followed by a clear maximum and a subsequent decrease. Note, however, that the relaxation time below about 1 K remains very large (5 μs), relative to that for $A = \text{Y}$ (0.02 μs). This difference is attributed to the larger moment of Tb^{3+} relative to Mo^{4+} being roughly proportional to the ratio of the squares of the moments. These results show that the Tb spins are involved in the freezing and that there exists an appreciable density of states for low energy magnetic excitations for these materials which are accessible even at very low temperatures.

3. Other $A_2\text{Mo}_2\text{O}_7$

In fact there is relatively little published information on other members of this series for $A = \text{Dy}$, Ho , Er , Tm , Yb or Lu . Most show DC and AC susceptibility anomalies near $T = 22$ K, as in the $A = \text{Y}$ material (Raju and Gougeon, 1995). Miyoshi *et al.* (2000) show AC susceptibility data for $A = \text{Ho}$ and Tb . The $A = \text{Yb}$ material has been studied using ^{170}Yb Mössbauer measurements. The major results are that evidence was found for a lower than axial symmetry at the Yb site, suggesting some local disorder and that the local magnetic fields acting on the Yb nucleus show a random distribution, consistent with the bulk spin glass properties (Hodges *et al.*, 2003).

There have been a few studies involving mixed occu-

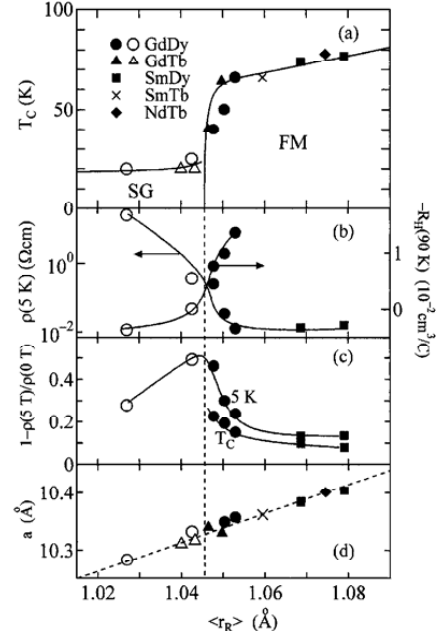


FIG. 40 A phase diagram for $(A_{1-x}A'_x)\text{Mo}_2\text{O}_7$ pyrochlores. (a) T_c or T_f . (b) Resistivity at 5K. (c) Magneto-resistance at 5K and T_c (d) Unit cell constant (Katsufuji *et al.*, 2000).

pation of the A site. Katsufuji *et al.* (2000) investigated materials of the type $A_{1-x}A'_x\text{Mo}_2\text{O}_7$ with $A = \text{Nd}$, Sm and Gd and $A' = \text{Tb}$ and Dy . That is, solid solutions between the ferromagnetic phases, $A = \text{Nd}$, Sm and Gd and the spin glass materials $A' = \text{Tb}$ and Dy . The results are summarized in Fig. 40 where the FM metal to spin glass insulator transition occurs at an average A-site radius between that for Gd^{3+} [1.053 Å] and Tb^{3+} [1.04 Å]. This is fully consistent with the results from the pure samples. Two studies have been reported in which the A-site is substituted with non magnetic ions and the results are markedly different. In some very early work by Sato and Greedan (1987), solid solutions of the type $A = \text{Y}_{1-x}\text{La}_x$ were investigated. Compositions were chosen to span the average A site radius from Nd to Y, intending to cover the ferromagnet to spin glass transition range. Surprisingly, perhaps, all samples showed only spin glass behavior with T_f values not far from that for $A = \text{Y}$, $T_f \sim 22$ K. Even the compositions $A = \text{Y}_{0.5}\text{La}_{0.5}$ and $\text{Y}_{0.6}\text{La}_{0.4}$, which have an average A site radius equivalent to Nd and Sm, respectively, showed no ferromagnetic transition, although the Curie temperatures were positive, +41 K and +31 K respectively. Unfortunately, no electrical transport data have been reported.

Hanasaki *et al.* (2007) chose solid solutions with $A = \text{Eu}$ (Eu^{3+} is, technically, a non-magnetic ion as $J = 0$) and $A' = \text{Y}$ or La . The pure $A = \text{Eu}$ is reported to be metallic and ferromagnetic with $T = 50$ K or so (Kézmárki *et al.*, 2006). The data are from an image furnace grown crystal and unfortunately no unit cell

constant is reported, so some electron doping is likely. Hanasaki *et al.* (2007) report ferromagnetic behavior for the La-doped materials but with a re-entrant spin glass transition at 22 K. T_c for the $\text{Eu}_{0.85}\text{La}_{0.15}$ material appears to be about 65 K. For this A -site composition the average A -site radius is equivalent to that of Sm^{3+} and one might expect a higher value. Perhaps, electron doping is playing a role again. The phases with $A = (\text{Eu}, \text{Y})$ are spin glasses. These results are quite new and interesting but the system should be investigated further. Finally, the discrepancy between the results of Sato and Greedan (1987) where the A -site involves La and Y and those of Hanasaki *et al.* (2007), just described, is difficult to understand. One obvious difference is that the variance of the average radius is of course greater for the $A = \text{La}, \text{Y}$ combination than for Eu, La or Eu, Y . Thus, the influence of the A -site composition on the magnetic and transport properties is apparently subtle and merits closer investigation.

X. SPIN ICE PHASES

The spin ice phenomenology in the pyrochlore oxides was discovered in 1997 in $\text{Ho}_2\text{Ti}_2\text{O}_7$ (Harris *et al.*, 1997, 1998a). This system possesses a ferromagnetic Curie-Weiss temperature $\theta_{\text{CW}} \sim +2$ K. It was thus quite surprising that this material does not develop long range order down to 50 mK, with neutron scattering revealing only broad diffuse scattering features for temperatures much lower than θ_{CW} .

In $\text{Ho}_2\text{Ti}_2\text{O}_7$ the strong axial crystal electric field acting on Ho^{3+} gives rise to an almost ideal, classical Ising spin. Because of symmetry, the local Ising (quantization) axis is along the local cubic $\langle 111 \rangle$ directions, such that on a tetrahedron, a spin can only point “in”, towards the middle of the opposing triangular face, or oppositely, hence “out” of the tetrahedron. While geometric frustration is generally associated with antiferromagnetic interactions, here frustration arises for ferromagnetic ones. Indeed, there are six “two in/two out” spin configurations that minimize the ferromagnetic exchange energy on an individual tetrahedron, and thus six ground states. There is an infinity of such ground states for a macroscopically large sample, and there is therefore an extensive ground state entropy. This entropy, S_0 , can be estimated by borrowing the argument used by Pauling for estimating the residual proton configuration disorder in common hexagonal water ice (Pauling, 1935). The main point is to consider the difference between the number of constraints necessary to determine a ground state and the number of degrees of freedom that the system possesses. Consider Anderson’s Ising pyrochlore antiferromagnet, onto which the local $\langle 111 \rangle$ pyrochlore Ising model maps, as discussed above (Anderson, 1956). The ground state condition is “underconstrained”, demanding only that the total magnetization of the four Ising spins on each tetrahedron be zero. Six of the $2^4 = 16$ pos-

sible spin configurations satisfy this condition. Counting 2^4 configurations for each tetrahedron gives, for a system of N spins and $N/2$ tetrahedra, a total number of microstates, $\tilde{\Omega} = (2^4)^{N/2} = 4^N$. This number drastically overestimates the exact total, $\Omega = 2^N$. The reason is that each spin is shared between two tetrahedra, hence the above 16 configurations on each tetrahedron are not independent. Following Pauling’s argument, we allocate $2^2 = 4$ states per tetrahedron and, assuming that 6/16 of them satisfy the constraint, this leads to a ground state degeneracy $\Omega_0 = \{2^2(6/16)\}^{N/2} = (3/2)^{N/2}$. The corresponding entropy $S_0 = k_B \log(\Omega_0) = (Nk_B)/2 \log(3/2)$ is of course just Pauling’s original result.

Not only is the residual entropy of ferromagnetic $\langle 111 \rangle$ spins on the pyrochlore lattice the same as Pauling’s entropy for water ice but, as shown in Fig. 41, there is also a rather direct connection between the spin configurations in the pyrochlore problem and that of the proton positions in water ice. For this reason, the term *spin ice* was coined. In anticipation of the forthcoming discussion of the physics at play in $\text{Tb}_2\text{Ti}_2\text{O}_7$, it is worthwhile to comment on a case where the nearest-neighbor exchange interactions are antiferromagnetic for a situation with local $\langle 111 \rangle$ spins. In that case, the ground state consists of all spins pointing in or out of a reference tetrahedron. Hence, there are in that case only two ground states related by a global spin inversion symmetry, and a second order transition in the universality class of the (unfrustrated) three-dimensional Ising model is expected. Earlier, Anderson had noticed the connection between the statistical mechanics of antiferromagnetically coupled Ising spins on the pyrochlore lattice and Pauling’s model of proton disorder in water ice. However, in Anderson’s model, the Ising spins share a common (global) z -axis direction, and frustration arises as usual for antiferromagnetic interactions with spins on triangu-

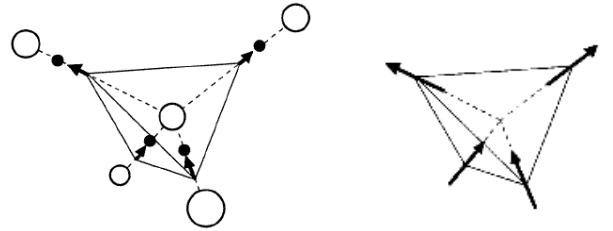


FIG. 41 Illustration of the equivalence of the water ice rule “two protons near, two protons far” and the spin ice rule “two spins in, two spins out”. The diagram (left) illustrates a water molecule in the tetrahedral coordination of the ice structure with proton positions located by displacement vectors that occupy a lattice of linked tetrahedra. In spin ice (right) the displacement vectors are replaced by rare earth moments (“spins”) occupying the pyrochlore lattice, which is the dual lattice (i.e. the lattice formed by the mid-points of the bonds) of the oxide lattice in cubic ice.

lar or tetrahedral units. However, since the pyrochlore lattice has cubic symmetry, the x , y and z directions are equivalent, and this renders Anderson's global antiferromagnetic Ising model unrealistic. It is the local nature of the quantization direction that is crucial, and which is the origin of the frustration for ferromagnetic interactions and for the "elimination" of the frustration for antiferromagnetic exchange. To see this, consider the following toy-model Hamiltonian

$$H = -J \sum_{\langle i,j \rangle} \mathbf{S}_i \cdot \mathbf{S}_j - \Delta \sum_i (\hat{z}_i \cdot \mathbf{S}_i)^2, \quad (10)$$

with classical Heisenberg spins \mathbf{S}_i on the sites i of the pyrochlore lattice, interacting via nearest-neighbor exchange coupling J . The second term is a single ion anisotropy interaction with Δ the anisotropy parameter and \hat{z}_i a unit vector in the local $\langle 111 \rangle$ direction at site i . For $J = 0$ and $\Delta > 0$, the energy is lower if \mathbf{S}_i points along \hat{z}_i , and one refers to this as an Ising anisotropy. The case $\Delta < 0$ would be referred to as an XY model (Bramwell *et al.*, 1994; Champion and Holdsworth, 2004). However, as discussed in Section V.B, the real microscopic crystal field Hamiltonian is more complicated than that considered by Bramwell *et al.* (1994) and Champion and Holdsworth (2004) where the limit $\Delta \rightarrow \infty$ was taken.

Hence, we assume an extreme Ising limit, $\Delta/J \rightarrow \infty$. \mathbf{S}_i is then confined to be either parallel or antiparallel to \hat{z}_i . To implement this energetic single-ion constraint, we write $\mathbf{S}_i = \sigma_i^{z_i} \hat{z}_i$. Injecting this back into H above, we obtain

$$\begin{aligned} H &= -J \sum_{\langle i,j \rangle} (\hat{z}_i \cdot \hat{z}_j) \sigma_i^{z_i} \sigma_j^{z_j} \\ &= +J/3 \sum_{\langle i,j \rangle} \sigma_i^{z_i} \sigma_j^{z_j}, \end{aligned} \quad (11)$$

where we have taken $\hat{z}_i \cdot \hat{z}_j = -1/3$ for two distinct cubic $[111]$ directions. One sees that for ferromagnetic J ($J > 0$), the now "global" $\sigma_i^{z_i}$ Ising variables map onto an equivalent Ising antiferromagnet (Anderson's model, Anderson (1956)) with coupling $J/3$, and is therefore frustrated. Conversely, for antiferromagnetic J ($J < 0$), the minimum energy state consists of all spins pointing in (say $\sigma_i^{z_i} = +1 \forall i$) or all out ($\sigma_i^{z_i} = -1 \forall i$).

As will be discussed in Section X.A, $\text{Dy}_2\text{Ti}_2\text{O}_7$ is also identified as a spin ice material. It turns out that both Ho^{3+} and Dy^{3+} carry a sizeable magnetic moment, μ , of approximately $10\mu_B$ in the crystal field ground state of $\text{Ho}_2\text{Ti}_2\text{O}_7$ and $\text{Dy}_2\text{Ti}_2\text{O}_7$. Thus, these systems have a magnetostatic dipole-dipole interaction $D = \mu_0\mu^2/(4\pi r_{\text{nn}}^3)$ of approximately $D \sim 1.4$ K at the nearest-neighbor distance r_{nn} . Since D is approximately the same as θ_{CW} , it is surprising that the long-range and complex nature of the dipolar interactions do not lift the spin ice degeneracy and drive the system to

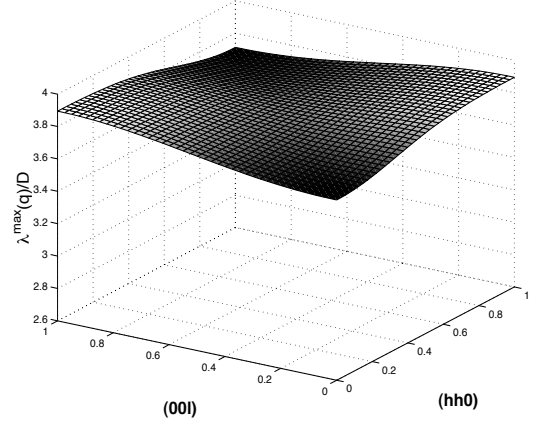


FIG. 42 Dipolar spin ice model: the scaled maximum eigenvalues, $\lambda^{\text{max}}(\mathbf{q})/D$, in the (hhl) plane. The dipole-dipole interactions are treated with the Ewald approach. Here, the exchange coupling \mathcal{J}_{nn} was set to zero. While the spectrum is very flat, suggesting a weak propensity towards long-range order, a maximum at a unique ordering wavevector $\mathbf{q}_{\text{max}} = 001$.

long range order at a critical temperature $T_c \sim D$. In fact, numerical and theoretical studies have compellingly demonstrated that it is *precisely* the mathematical form of the dipole-dipole interactions that is at the origin of the spin ice phenomenology in rare-earth pyrochlores. In particular, it is the ferromagnetic character of the dipolar interactions at the nearest-neighbor distance, and not a ferromagnetic nearest-neighbor exchange (which turns out to be antiferromagnetic, as analysis of experimental data on $\text{Ho}_2\text{Ti}_2\text{O}_7$ and $\text{Dy}_2\text{Ti}_2\text{O}_7$ have revealed) that is primarily the source of frustration. Indeed, as discussed above, if it were not for the dipolar interactions, the nearest-neighbor antiferromagnetic interactions alone in $\text{Ho}_2\text{Ti}_2\text{O}_7$ and $\text{Dy}_2\text{Ti}_2\text{O}_7$ would drive the system into a long-range ordered phase.

The minimal model, called the dipolar spin ice model (DSM), that is needed to investigate these questions includes nearest-neighbor exchange (first term) and long range magnetic dipole interactions (second term) in.

$$\begin{aligned} H &= -J \sum_{\langle ij \rangle} \mathbf{S}_i^{\hat{z}_i} \cdot \mathbf{S}_j^{\hat{z}_j} \\ &+ D r_{\text{nn}}^3 \sum_{i>j} \frac{\mathbf{S}_i^{\hat{z}_i} \cdot \mathbf{S}_j^{\hat{z}_j}}{|\mathbf{r}_{ij}|^3} - \frac{3(\mathbf{S}_i^{\hat{z}_i} \cdot \mathbf{r}_{ij})(\mathbf{S}_j^{\hat{z}_j} \cdot \mathbf{r}_{ij})}{|\mathbf{r}_{ij}|^5} \end{aligned} \quad (12)$$

For the open pyrochlore lattice structure, we expect further neighbor exchange to be very small, so these can be neglected as a first approximation. Recent Monte Carlo simulations seem to confirm this expectation (Ruff *et al.*, 2005; Yavors'kii *et al.*, 2007). Here the spin vector $\mathbf{S}_i^{\hat{z}_i}$ labels the Ising moment of magnitude $|\mathbf{S}_i^{\hat{z}_i}| = 1$ at lattice site i , oriented along the local Ising $\langle 111 \rangle$ axis \hat{z}_i . The distance $|\mathbf{r}_{ij}|$ is measured in units of the near-

est neighbor distance, r_{nn} . J represents the exchange energy and $D = (\mu_0 \mu^2 / (4\pi r_{nn}^3))$. Because of the local Ising axes, the effective nearest-neighbor energy scale is $J_{\text{eff}} = J_{nn} + D_{nn}$ where $J_{nn} \equiv J/3$ and $D_{nn} \equiv 5D/3$, since $\hat{z}_i \cdot \hat{z}_j = -1/3$ and $(\hat{z}_i \cdot \mathbf{r}_{ij})(\mathbf{r}_{ij} \cdot \hat{z}_j) = -2/3$. If $D_{nn} = 0$ and $J > 0$ one obtains the spin ice model originally proposed by Harris *et al.* (1997, 1998) henceforth referred to as the “nearest-neighbour spin ice model”.

The condition $J_{\text{eff}} > 0$ is a simple criterion to assess whether a system displays a spin ice state. Mean field theory (Gingras and den Hertog, 2001) and Monte Carlo simulations (Melko *et al.*, 2004) find a critical value for the transition between “all-in/all-out” Néel order and spin ice at $J_{nn}/D_{nn} \approx -0.901$, hence quite close to the naive nearest-neighbor estimate $J_{nn}/D_{nn} = -1$. The dipolar interactions beyond nearest-neighbors provide a weak, extra stabilization of the Néel phase over the spin ice state.

The success of the nearest-neighbor criterion in assessing whether a system should display spin ice phenomenology or not indicates that, to a large extent, dipolar interactions beyond nearest-neighbors are *self-screened*, as originally suggested by a mean field calculation (Gingras and den Hertog, 2001) and Monte Carlo simulations (den Hertog and Gingras, 2000). The reason why dipolar spin ice systems obey the ice rules is not immediately apparent. Isakov *et al.* (2005) have proposed that the ice rules result from the fact that the dipolar interactions are, up to a perturbatively small and rapidly decaying function, a real-space projector onto the manifold of ice-rule obeying states. A possibly simpler explanation has recently been proposed which involves separating each point dipole into its constituent magnetic (monopole) charges and requiring that each tetrahedron is, magnetic charge wise, neutral, which automatically leads to the conclusion that all ice-rule obeying states are, again up to a small correction, ground states of the dipolar interactions (Castelnovo *et al.*, 2007). Such a real-space argument is possibly not unrelated to the Ewald energy calculations in which the dipolar lattice sums are regularized by effective Gaussian charges either in reciprocal space (Enjalran and Gingras, 2003) or in direct space (Melko *et al.*, 2004).

A. $\text{Dy}_2\text{Ti}_2\text{O}_7$ and $\text{Ho}_2\text{Ti}_2\text{O}_7$

The Dy^{3+} ion in $\text{Dy}_2\text{Ti}_2\text{O}_7$ was first identified as having strongly anisotropic properties from the maximum in the DC susceptibility (Blöte *et al.*, 1969) at $T \sim 0.9$ K followed by a precipitous drop to essentially 0 at $T \sim 0.4$ K. This suggested a strongly anisotropic effective g tensor with a $g_{\perp} \approx 0$ component perpendicular to the local $\langle 111 \rangle$ axis, making Dy^{3+} in effect a $\langle 111 \rangle$ Ising model. This was confirmed by Flood (1974) from direct measurement of the magnetic moment and from analysis of inelastic neutron scattering data by Rosenkranz (Rosenkranz *et al.*, 2000). Calculations from crystal field theory, complemented by fitting crystal field parameters (CFPs) to

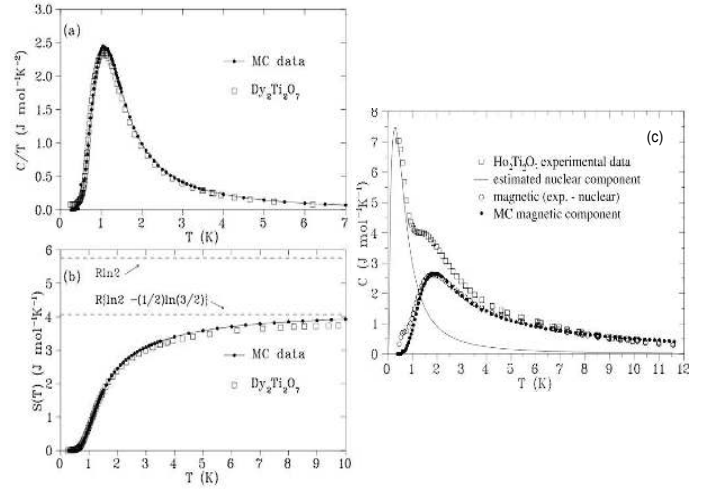


FIG. 43 $\text{Dy}_2\text{Ti}_2\text{O}_7$: (a) Specific heat and (b) entropy versus temperature, measured by Ramirez *et al.* (1999). The recovered entropy at 10 K agrees reasonably well with Pauling’s entropy, $R/2 \ln(3/2)$. The data are compared to that calculated by Monte Carlo simulations of den Hertog and Gingras (2000) for the dipolar spin ice model with exchange $J_{nn} = -1.24$ K and dipolar coupling $D_{nn} = 2.35$ K. (c) $\text{Ho}_2\text{Ti}_2\text{O}_7$: The total specific heat is shown by the empty squares and the expected nuclear contribution by the solid line. The electronic contribution has been estimated by subtracting these two curves (open circles). Near to 0.7 K, this subtraction is prone to a large error (see text). Dipolar spin ice simulation results are indicated by the filled circles (from Bramwell *et al.* (2001a)).

susceptibility data also confirmed the strong Ising nature of Dy^{3+} in $\text{Dy}_2\text{Ti}_2\text{O}_7$ (Jana *et al.*, 2002). Specifically, the single ion electronic ground state of Dy^{3+} is a Kramers doublet of almost pure $|J = 15/2, m_J = \pm 15/2\rangle$ separated from the first excited state by a gap $\Delta \approx 33$ meV (~ 380 K) while the rescaled CFPs of Rosenkranz *et al.* (2000) and Jana *et al.* (2002) finds a much smaller excitation gap $\Delta \approx 100 \text{ cm}^{-1}$ (~ 140 K).

Blöte *et al.* (1969) measured the specific heat $C(T)$ of $\text{Dy}_2\text{Ti}_2\text{O}_7$ between 0.37 K and 1.3 K and found only a broad maximum around 1.2 K and no sign of a sharp specific heat feature indicating a phase transition to long-range magnetic order. Most interestingly, a total magnetic entropy of only $\frac{3}{4}R \ln(2)$ was found. Hence, a noticeable fraction of $R \ln(2)$ expected for a Kramers doublet was missing.

Soon after the proposal of spin ice in $\text{Ho}_2\text{Ti}_2\text{O}_7$ (Harris *et al.*, 1997, 1998a), Ramirez *et al.* (1999) showed that the missing entropy in $\text{Dy}_2\text{Ti}_2\text{O}_7$ could be determined rather precisely by a measurement of the magnetic specific heat $C(T)$ between 0.4 K and 12 K. Figure 43 shows the temperature dependence of $C(T)/T$. The magnetic entropy change, $\Delta S_{1,2}$, between temperatures T_1 and T_2 can be found by integrating $C(T)/T$ between these two temperatures:

$$\Delta S_{1,2} \equiv S(T_2) - S(T_1) = \int_{T_1}^{T_2} \frac{C(T)}{T} dT. \quad (13)$$

Figure 43b shows that the magnetic entropy recovered is about $3.9 \text{ J mol}^{-1} \text{ K}^{-1}$, a value that falls considerably short of $R \ln(2) \approx 5.76 \text{ J mol}^{-1} \text{ K}^{-1}$. The difference, $1.86 \text{ J mol}^{-1} \text{ K}^{-1}$ is close to Pauling's estimate for the residual extensive entropy of water ice: $(R/2) \ln(3/2) \approx 1.68 \text{ J mol}^{-1} \text{ K}^{-1}$, thus providing compelling thermodynamic evidence for the existence of an ice-rules obeying state in $\text{Dy}_2\text{Ti}_2\text{O}_7$.

As mentioned above, the large $10\mu_B$ moments of both Dy^{3+} and Ho^{3+} lead to a critical role for magnetic dipole-dipole interactions in spin ices. This energy, D_{nn} , at nearest-neighbor distances can be estimated from the effective Curie constant or from the single-ion crystal field doublet wavefunctions. The earlier theoretical studies (den Hertog and Gingras, 2000; Siddharthan *et al.*, 1999) of the DSM estimated

$$D = \frac{5}{3} \left(\frac{\mu_0}{4\pi} \right) \frac{\mu^2}{r_{nn}^3} \approx +2.35 \text{ K} \quad (14)$$

for both $\text{Ho}_2\text{Ti}_2\text{O}_7$ and $\text{Dy}_2\text{Ti}_2\text{O}_7$. Here $r_{nn} = (a_0/4)\sqrt{2}$ is the nearest-neighbor distance and a is the size of the conventional cubic unit cell. As discussed above, the factor $5/3$ originates from the orientation of the Ising quantization axes relative to the vector direction \mathbf{r}_{nn} that connects nearest-neighbor magnetic moments. As we briefly discuss below, the current estimate on D_{nn} for $\text{Dy}_2\text{Ti}_2\text{O}_7$ is probably accurate to within 8%–10%. Hence, the nearest-neighbor exchange, J_{nn} , is the main unknown. It can be estimated from the high-temperature (paramagnetic) regime of the magnetic susceptibility, χ , (Siddharthan *et al.*, 1999) or of the specific heat, $C(T)$, (Jana *et al.*, 2002) data. A different approach, followed by den Hertog and Gingras (2000) and Bramwell *et al.* (2001a) has been to determine J_{nn} by fitting either the height of the specific heat, C_p , peaks near 1 K or the temperature at which the peaks occurs, T_p , against Monte Carlo simulations of the DSM. Interestingly, fits of T_p or C_p allow for a consistent determination of $J_{nn} \approx -1.24 \text{ K}$ for $\text{Dy}_2\text{Ti}_2\text{O}_7$. Figure 43 shows the good agreement between Monte Carlo results and experimental data (den Hertog and Gingras, 2000). Note here that the parameter D_{nn} sets the scale for the dipolar interactions, at $\mu_0\mu^2/(4\pi r_{nn}^3)$; the simulations themselves use true long-range dipole-dipole interactions implemented via the Ewald method (Melko *et al.*, 2004). These results show convincingly the spin ice phenomenology in $\text{Dy}_2\text{Ti}_2\text{O}_7$, and also in $\text{Ho}_2\text{Ti}_2\text{O}_7$, as we now discuss.

While $\text{Ho}_2\text{Ti}_2\text{O}_7$ was the first compound to be proposed as a spin ice, specific heat measurements proved initially less straightforward to interpret than in $\text{Dy}_2\text{Ti}_2\text{O}_7$, and this led to some confusion. Specifically,

the rapid increase of the specific heat below 1 K was originally interpreted as an indication of a phase transition to a partially ordered state around a temperature of 0.6 K (Siddharthan *et al.*, 1999). Instead, it turns out that the anomalous low-temperature behavior of the specific heat in $\text{Ho}_2\text{Ti}_2\text{O}_7$ is of nuclear origin. An anomalously large hyperfine interaction between the electronic and nuclear spins for Ho commonly leads to a nuclear specific heat Schottky anomaly at 0.3 K. A subtraction of the nuclear contribution from the total low-temperature specific heat reveals the purely electronic specific heat (Bramwell *et al.*, 2001a), $C(T)$. The integration of $C(T)/T$ from 300 mK up to 10 K gave a magnetic entropy deficit of an amount close to Pauling's $R/2 \ln(3/2)$ zero-point entropy, hence confirming, thermodynamically, that $\text{Ho}_2\text{Ti}_2\text{O}_7$ is indeed a spin ice (Cornelius and Gardner, 2001). Following the same procedure as the one used for $\text{Dy}_2\text{Ti}_2\text{O}_7$ (den Hertog and Gingras, 2000), a comparison of $C(T)$ with Monte Carlo simulations allows to estimate the exchange constant in $\text{Ho}_2\text{Ti}_2\text{O}_7$ as $J_{nn} \sim -0.55 \text{ K}$, an antiferromagnetic value (Bramwell *et al.*, 2001a).

While specific heat measurements on $\text{Ho}_2\text{Ti}_2\text{O}_7$ are problematic, this is emphatically not so for neutron scattering experiments. Unlike dysprosium, holmium has only one stable isotope whose neutron absorption cross section is negligible. A comparison of the experimental neutron scattering intensity with that calculated from Monte Carlo simulations of the dipolar spin ice model with an exchange constant $J_{nn} \sim -0.55 \text{ K}$ determined as above shows excellent agreement. Interestingly, both the experiment and Monte Carlo data differ substantially from that calculated for the nearest-neighbor spin ice model (see Fig. 44). This clearly shows that non-trivial spin correlations develop in the material as it progressively freezes within the low-temperature spin ice regime. Indeed, those correlations are the precursors of those that would ultimately lead to long-range order, if not precluded by spin freezing (Melko *et al.*, 2001, 2004).

A puzzling question raised by the good agreement between Monte Carlo simulations of the DSM and the experimental results illustrated in Fig. 43 is: why don't the dipolar interactions drive a transition to long-range order at a critical temperature $T_c \sim D_{nn} \sim 2 \text{ K}$? A partial answer can be found in the mean field theory calculations of Gingras and den Hertog (2001). It was found there that the \mathbf{q} dependence of the softest branch of critical modes in the dipolar spin ice model is very weakly dispersive, reaching a global maximum eigenvalue $\lambda(\mathbf{q}_{\max})$ at $\mathbf{q}_{\max} = 001$. At the mean field level, this indicates that a transition to long range order should occur at a critical temperature $T_c = \lambda(\mathbf{q}_{\max})$, with the development of delta-function Bragg peaks below T_c .

First of all, this transition does not occur at $T_c \sim D_{nn}$ because the soft (critical) mode at \mathbf{q}_{\max} is in "entropic" competition with all the other quasi-soft modes at $\mathbf{q} \neq \mathbf{q}_{\max}$. The correlated spin ice regime, which one may dub a "collective paramagnet" in Villain's sense (Vil-

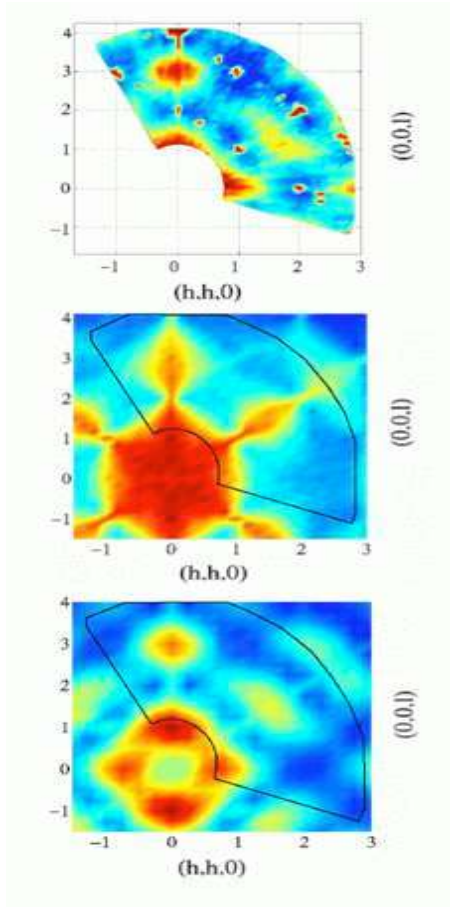


FIG. 44 $\text{Ho}_2\text{Ti}_2\text{O}_7$: Neutron scattering in the hhl plane showing experimental data (upper panel; the sharp spots are nuclear Bragg scattering with no magnetic component), compared with Monte Carlo simulations of the near neighbour spin ice model (middle panel) and the dipolar spin ice model (lower panel) (Bramwell *et al.*, 2001a). Blue indicates the weakest and red-brown the strongest intensity.

lain, 1979), albeit with utterly sluggish spin dynamics for $T \lesssim 1$ K in $\text{Dy}_2\text{Ti}_2\text{O}_7$, has so much entropic disorder that it is not energetically favorable to localize the system in phase space to a long-range ordered state. In the standard single spin-flip Monte Carlo simulations, this transition is not observed because the probability to flip a spin once the system enters a state where each tetrahedron obeys on average the “two-in/two-out” ice rule is very small and decreases experimentally very fast with decreasing temperature (Melko *et al.*, 2004). The low-energy excitations deep in the spin ice state correspond to nonlocal closed loops of spins flipping from “in” to “out” and vice versa so that the system, as it experiences those excitations, remains in a spin ice state (Barkema and Newman, 1998). Using such loop excitations, Monte Carlo simulations (Melko *et al.*, 2001, 2004) found a transition to the long-range order predicted by mean field theory (Gingras and den Hertog, 2001). In Monte Carlo

simulations of the DSM, a strongly first order transition occurs at a critical temperature $T_c \sim 0.07D_{\text{nn}}$ where all the residual Pauling entropy is recovered through the pre-translational build-up of correlations and, mostly, via a large latent heat (Melko *et al.*, 2001, 2004). For $D_{\text{nn}} \sim 2.35$ K believed appropriate for $\text{Dy}_2\text{Ti}_2\text{O}_7$ (and $\text{Ho}_2\text{Ti}_2\text{O}_7$), this T_c amounts to 160 mK. However, to this date, no experimental work has observed a transition to long-range order in spin ice materials down to 60 mK (see for example, Fukazawa *et al.* (2002a)). A common explanation for this absence of a transition in real spin ice materials is that equilibration is lost in the spin ice state (e.g. $T \lesssim 0.4$ K in $\text{Dy}_2\text{Ti}_2\text{O}_7$ and $T \lesssim 0.6$ K in $\text{Ho}_2\text{Ti}_2\text{O}_7$), with the real materials not “benefitting” from nonlocal dynamics as employed in the simulations (Melko *et al.*, 2001, 2004). However, this explanation is certainly somewhat incomplete since, as we discuss further below, a number of experiments report spin dynamics down to 20 mK. However, before we discuss experiments investigating the dynamics of spin ices, we briefly comment on the spin-spin correlations in the spin ice regime of $\text{Dy}_2\text{Ti}_2\text{O}_7$.

Since the original work of Ramirez *et al.* (1999), other measurements of the magnetic specific heat data of $\text{Dy}_2\text{Ti}_2\text{O}_7$ have been reported (Higashinaka *et al.*, 2002, 2003; Hiroi *et al.*, 2003; Ke *et al.*, 2007). Measurements of the magnetic specific heat of magnetic insulators are notoriously difficult experiments owing to the poor sample thermal conductivity. It is perhaps for this reason that specific heat data of $\text{Dy}_2\text{Ti}_2\text{O}_7$ from different measurements show some disparity. For example, the height of the magnetic specific heat at its maximum, C_p , for a

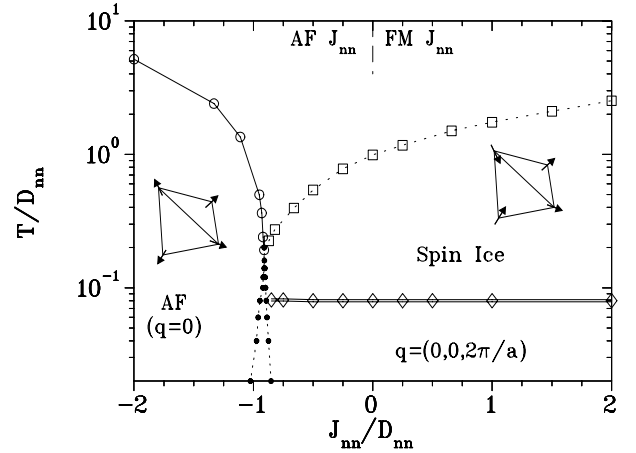


FIG. 45 Dipolar spin ice model: the phase diagram. The antiferromagnetic ground state is an all-spins-in or all-spins-out configuration for each tetrahedron. The spin ice configuration, which includes the $\mathbf{q} = 001$ ground state, is a two spins in-two spins out configuration for each tetrahedron. The region encompassed between the quasi vertical dotted lines displays hysteresis in the long-range ordered state selected ($\mathbf{q} = 000$ vs. $\mathbf{q} = 001$) as $J_{\text{nn}}/D_{\text{nn}}$ is varied at fixed temperature T (Melko *et al.* (2004)).

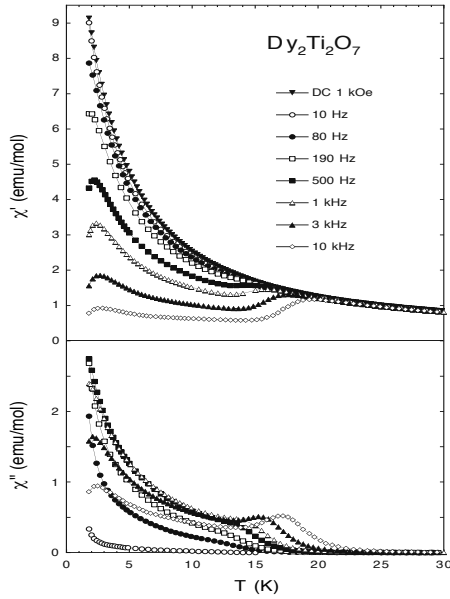


FIG. 46 $\text{Dy}_2\text{Ti}_2\text{O}_7$: ac-susceptibility (upper panel: χ' , lower panel χ'') as a function of temperature at several frequencies, illustrating the “15 K peak” from Matsuhira *et al.* (2001).

powder sample (Ramirez *et al.*, 1999) differs by as much as 10% compared to that reported in Higashinaka *et al.* (2003) for a single crystal. Ultimately, precise measurements of $C(T)$ are needed if one wants to make an accurate determination of the residual entropy in the system (Ke *et al.*, 2007).

The Monte Carlo prediction of long range order developing at low temperature in the dipolar spin ice model and the experimentally observed collapse of the magnetic specific heat below 0.4 in $\text{Dy}_2\text{Ti}_2\text{O}_7$ raise the question of low temperature spin dynamics in spin ice materials. In fact experimental studies of this question have led to the observation of a much richer phenomenology than that which would have been naively expected.

Measurements of the AC magnetic susceptibility $\chi(\omega)$ of $\text{Dy}_2\text{Ti}_2\text{O}_7$ down to 60 mK (Fukazawa *et al.*, 2002a) and 100 mK (Matsuhira *et al.*, 2001) find that the real part of χ , χ' , drops precipitously below a temperature of roughly 1 K for a frequency of the order of 10 Hz (see Fig. 46). At the same time, the imaginary part, χ'' , shows a rounded maximum. Both χ' and χ'' remain essentially zero below 0.5 K down to the lowest temperature considered, hence signalling an essentially complete spin freezing of the system. Thus, no signature of the transition to long range order predicted by numerical simulations (Melko *et al.*, 2001, 2004) is observed.

The behavior of χ' and χ'' near 1 K signals a spin freezing process analogous to what is observed in spin glasses. Indeed, measurements of the magnetization of $\text{Dy}_2\text{Ti}_2\text{O}_7$ show irreversibilities between zero field cooling (ZFC) and field cooling (FC) below 0.7 K (Matsuhira *et al.*, 2001; Snyder *et al.*, 2004). Similar FC-ZFC irre-

versibilities occur in the $\text{Ho}_2\text{Sn}_2\text{O}_7$ spin ice (Matsuhira *et al.*, 2000). An analysis of the temperature dependence of the frequency f_m at which χ'' displays a peak reveals a sort of thermally activated freezing behavior which was originally parametrized by an Arrhenius form with an activation energy of approximately 10 K. However, Snyder *et al.* (2004) questioned the application of the Arrhenius law to these data. On the other hand, Monte Carlo simulations that employ a standard single spin-flip Metropolis algorithm find that the fraction of accepted spin flips decreases with decreasing temperature according to a Vogel-Fulcher form $\exp[-A/(T-T^*)]$ with $T^* \sim 0.3$ K (Melko *et al.*, 2004). The dynamical freezing behavior seen in $\text{Dy}_2\text{Ti}_2\text{O}_7$ differs from the critical slowing down observed in conventional disordered spin glass materials (Binder and Young, 1986). Interestingly, for the lowest temperature considered, χ'' is cut-off on the low-frequency regime (Snyder *et al.*, 2004), reminding one of what is observed in the $\text{LiHo}_x\text{Y}_{1-x}\text{F}_4$ Ising system – a phenomenon that has been referred to as “antiglass” behavior (Ghosh *et al.*, 2002; Reich *et al.*, 1987). Another difference between the spin freezing in $\text{Dy}_2\text{Ti}_2\text{O}_7$ and that in conventional disordered spin glasses is the magnetic field dependence of T_f . In spin glasses, T_f decreases with increasing magnetic field strength, while in $\text{Dy}_2\text{Ti}_2\text{O}_7$, the opposite is seen for applied magnetic fields up to 5 kOe (Snyder *et al.*, 2004). Measurements on single crystals (Shi *et al.*, 2007) find that the spin freezing has a stronger frequency and magnetic field dependence for a field along the [111] axis compared to [100], and the starting freezing frequency of the single crystal is higher than that of the powder sample (Snyder *et al.*, 2001). While a quantitative understanding does not exist, the behavior at $T \lesssim 4$ K is qualitatively interpreted as a signature of the collective freezing as the system enters the low-temperature state where the “two-in/two-out” ice rules become fulfilled.

In addition to the low-temperature freezing in the ice-rule obeying state, two experimental studies coincidentally reported results from AC susceptibility $\chi(\omega)$ measurements in $\text{Dy}_2\text{Ti}_2\text{O}_7$ above 4 K (Matsuhira *et al.*, 2001; Snyder *et al.*, 2001), finding another freezing process in a temperature range around 15 K, referred to as the ‘15 K feature’. The signature of this freezing is only seen in the AC susceptibility at finite frequency and not in the DC susceptibility data (see Fig. 46). The maximum in the imaginary part, χ'' , is at 12 K for a frequency of 10 Hz increasing to 17 K for a frequency of 10 kHz. While the raw data of Snyder *et al.* (2001) and Matsuhira *et al.* (2001) are similar, they were analyzed somewhat differently. Snyder *et al.* (2001) characterized the freezing via a single exponential relaxation while Matsuhira *et al.* (2001) characterized the AC susceptibility using the so-called Davidson-Cole framework, based on an underlying distribution of time scales. Notwithstanding these differences, both analyses agreed that there exists a typical time scale, $\tau(T)$, for this freezing phenomenon that is parametrized by an Arrhenius form, $\tau \sim \exp(E_a/T)$,

with an activation barrier energy E_a of the order of 200 K. A recent μ SR study also finds that the relaxation rate of the muon spin polarization in a temperature range of 70 K to 280 K can be described by a typical relaxation rate $\lambda(T) \sim \exp(-E_a/T)$ with $E_a \sim 220$ K (Lago *et al.*, 2007). The $\exp(E_a/T)$ dependence of the typical time scale characterizing the dynamics around 15 K and the energy scale $E_a \sim 220$ K indicates that the relaxation involves transitions to and from the first excited doublet which constitute the main contribution to the spin dynamics in the temperature range above 20 K or so. While this freezing phenomenon and energy scales characterizing it suggest an Orbach process (Finn *et al.*, 1961; Orbach, 1961) that involves both the lattice degrees of freedom and the excited crystal field states, a concrete microscopic calculation has not yet been done.

One interesting aspect of the 15 K feature is its behavior when Dy^{3+} is substituted by diamagnetic Y^{3+} in $\text{Dy}_{2-x}\text{Y}_x\text{Ti}_2\text{O}_7$. In particular, initial studies found that the 15 K peak in $\chi''(\omega)$ disappears by $x = 0.4$ (Snyder *et al.*, 2001). This was originally interpreted as a sign that the 15 K feature is of collective origin. However, in a subsequent study (Snyder *et al.*, 2004a), it was found to re-emerge as x is further increased and is almost as strong for $x = 1.98$ as it is for $x = 0$, but, interestingly, repositioned at a higher temperature of 22 K for a frequency of 1 kHz. This high temperature freezing feature is essentially a single-ion phenomenon, akin to superparamagnetic spin blocking. While this is not seen in AC measurements on $\text{Ho}_2\text{Ti}_2\text{O}_7$, it can be revealed by the application of a magnetic field (Ehlers *et al.*, 2003). Neutron spin echo experiments on the same material confirms the single-ion nature of the 15 K feature (Ehlers *et al.*, 2003).

Another noteworthy aspect of the spin dynamics in $\text{Dy}_2\text{Ti}_2\text{O}_7$ is the temperature independence of the relaxation time τ between 5 K and 10 K (Snyder *et al.*, 2003). Below 5 K, the relaxation time becomes again sharply dependent on temperature upon approaching the spin ice freezing discussed above. This temperature independence of τ has been interpreted as a quantum tunneling effect between the up and down Ising spin states. This was first observed in $\text{Ho}_2\text{Ti}_2\text{O}_7$ using neutron spin echo (Ehlers *et al.*, 2003). Such temperature-independent relaxation in $\text{Dy}_2\text{Ti}_2\text{O}_7$ has also been seen in muon spin relaxation (μ SR) (Lago *et al.*, 2007). However, there is a three-orders of magnitude difference between the relaxation rate measured in μ SR and AC susceptibility. Perhaps this is because μ SR relies on a local measurement that probes all wavevectors of the spin susceptibility. At this time, this discrepancy is unresolved.

A further important topic pertaining to the dynamics of spin ice materials is that of the low-temperature spin dynamics deep in the frozen spin ice state. As discussed above, there is evidence that the electron spin flip dynamics are exponentially frozen out below 1 K in $\text{Dy}_2\text{Ti}_2\text{O}_7$, as well as in other spin ice materials. There is, however, some indication of residual spin dynamics in these sys-

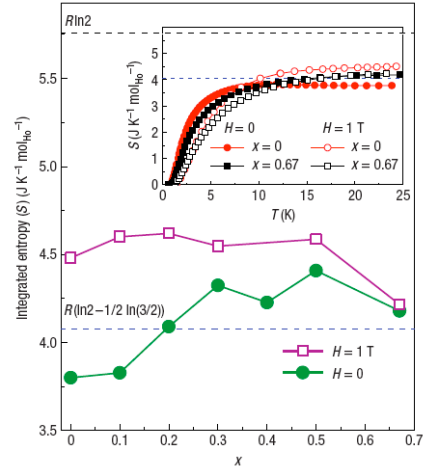


FIG. 47 The magnetic entropy for $\text{Ho}_{2+x}\text{Ti}_{2-x}\text{O}_{7-\delta}$ (integrated from below $T \approx 1$ to 22 K) as a function of stuffing at $H=0$ and 1 T. The dashed lines represent the predicted ice entropy and total spin entropy values. Inset: The temperature dependence of the integrated entropy for few compositions at $H=0$ and 1 T (Lau *et al.*, 2006).

tems that survives down to the lowest temperatures. For example, μ SR experiments find a relaxation rate of $0.2 \mu\text{s}^{-1}$ of the muon spin polarization at a temperature of 20 mK (Lago *et al.*, 2007). This relaxation has been ascribed to hyperfine coupling of the electronic and nuclear spins which induce a “wobble” around the local $\langle 111 \rangle$ Ising directions. Another work has suggested that the absence of a low-temperature nuclear specific heat anomaly in $\text{Dy}_2\text{Ti}_2\text{O}_7$ may indicate that the electron spin dynamics persist to the lowest temperature (Bertin *et al.*, 2002). This argument would suggest that $\text{Ho}_2\text{Ti}_2\text{O}_7$, which has a fully developed nuclear specific heat (Bramwell *et al.*, 2001a), is completely static. More experimental and theoretical work is required to fully understand the low-temperature dynamics of the spin ices.

Above, we touched on what role magnetic dilution plays on the spin dynamics and freezing phenomenon in $\text{Dy}_2\text{Ti}_2\text{O}_7$. A recent magnetocaloric study of $\text{Dy}_2\text{Ti}_2\text{O}_7$ has found a crossover at a temperature of about 0.3 K to a low-temperature regime characterized by extremely slow relaxation (Orendác *et al.*, 2007). In addition, a dilution of Dy by 50% of non-magnetic Y, giving DyYTi_2O_7 , leads to an increase of the relaxation time compared to pure $\text{Dy}_2\text{Ti}_2\text{O}_7$. This is in contrast with the behavior seen above in the formation of the ice state, say above 2 K, where a nontrivial dependence of the relaxation time as a function of Dy concentration is observed. In particular, a level of magnetic dilution less than 12% was found to accelerate the relaxation rate while a dilution level higher than 12% was found to slow it down again, such that the relaxation rates are nearly the same for DyYTi_2O_7 and $\text{Dy}_2\text{Ti}_2\text{O}_7$ (Snyder *et al.*, 2004a).

This discussion illustrates that the nature of the dy-

namics in spin ices and the role magnetic dilution is still poorly understood. In the context of magnetic dilution, we note that a recent paper reports a non-monotonic dependence of the residual entropy in $\text{Dy}_{2-x}\text{Y}_x\text{Ti}_2\text{O}_7$ and $\text{Ho}_{2-x}\text{Y}_x\text{Ti}_2\text{O}_7$. The data are qualitatively explained by a generalization of Pauling's theory for the entropy of ice that incorporates site-dilution (Ke *et al.*, 2007). The topic of residual entropy in spin ice when the magnetic species are diluted is an interesting problem. One would naively expect that the extensive degeneracy would ultimately be lifted by disorder (Villain, 1979). There are two obvious ways that one can envisage this happening. Perhaps the most interesting is where dilution would lead to conventional long range order. For example, in water ice, KOH doping (which effectively removes protons) leads to a long-range ordered phase of ice called ice XI. The proton vacancies created in the proton structure enhance the dynamics so that the system can develop long range order. Studies of diluted spin ice, such as $\text{Dy}_{2-x}\text{Y}_x\text{Ti}_2\text{O}_7$ (Ke *et al.*, 2007) and $\text{Ho}_{2-x}\text{Y}_x\text{Ti}_2\text{O}_7$ (Ehlers *et al.*, 2006a), have so far not reported any signs that diamagnetic dilution leads to long range order. Most likely, the extensive degeneracy is lifted at high x with the system leaving the ice regime to become a dipolar Ising spin glass akin to $\text{LiHo}_x\text{Y}_{1-x}\text{F}_4$ (Reich *et al.*, 1987). Indeed, the systematic study of the development of dipolar spin glass in both $\text{Dy}_{2-x}\text{Y}_x\text{Ti}_2\text{O}_7$ and $\text{Ho}_{2-x}\text{Y}_x\text{Ti}_2\text{O}_7$ might help shed light on the paradoxical antiglass phenomenon in $\text{LiHo}_x\text{Y}_{1-x}\text{F}_4$ (Ghosh *et al.*, 2002; Reich *et al.*, 1987), or even the possible absence of a spin glass phase altogether in that material (Jönsson *et al.*, 2007).

On the theoretical front, the DSM of Eq. (12) with nearest-neighbor exchange and long range dipole-dipole interactions has been fairly successful in describing semi-quantitatively the thermodynamic properties of $\text{Dy}_2\text{Ti}_2\text{O}_7$ both in zero (den Hertog and Gingras, 2000; Fennell *et al.*, 2004) and in nonzero magnetic field (Fukazawa *et al.*, 2002a; Ruff *et al.*, 2005; Tabata *et al.*, 2006). A detailed comparison between experimental results from measurements and Monte Carlo simulations (Ruff *et al.*, 2005) for a field along the [112] direction provides strong evidence that exchange interactions beyond nearest-neighbors are required to describe quantitatively the experimental data (see also Tabata *et al.* (2006)). This may come as a surprise given the already good agreement that was first reported between Monte Carlo simulations of the DSM (den Hertog and Gingras, 2000) and the specific heat measurements of Ramirez *et al.* (1999). However, since that work, as mentioned above, several other zero field specific heat data sets have been reported (Higashinaka *et al.*, 2002, 2003; Hiroi *et al.*, 2003; Ke *et al.*, 2007) and these are no longer so-well described by the original DSM. A systematic study of more recent specific heat measurements in zero and nonzero field and magnetization measurements for [110] and [111] fields have estimated first (J_1), second (J_2) and third (J_3) nearest-neighbor exchange parameters in $\text{Dy}_2\text{Ti}_2\text{O}_7$ (Ya-

vors'kii *et al.*, 2008). Perhaps most interestingly, such a refinement of the spin Hamiltonian seemingly allows one to explain from a microscopic basis the diffuse scattering on the Brillouin zone boundary (Fennell *et al.*, 2004), akin to the highly structured inelastic features found in the ZnCr_2O_4 spinel (Lee *et al.*, 2002).

B. $\text{A}_2\text{Sn}_2\text{O}_7$ ($A = \text{Pr, Dy and Ho}$)

Other pyrochlore oxides with similar properties include $\text{Ho}_2\text{Sn}_2\text{O}_7$, $\text{Dy}_2\text{Sn}_2\text{O}_7$ and $\text{Pr}_2\text{Sn}_2\text{O}_7$ (Matsuhira *et al.*, 2000, 2002, 2004). These have not been studied in single crystal form, as far as we know, but bulk magnetic properties would suggest they are ferromagnetic with large Ising anisotropy and very slow dynamics.

Of these three compounds, only $\text{Ho}_2\text{Sn}_2\text{O}_7$ has been investigated using neutron scattering techniques on powder samples (Kadowaki *et al.*, 2002). In the inelastic spectrum they found very slow dynamics below 40 K and crystal field levels at 22 and 26 meV, suggesting the local Ho environment is very similar to that of $\text{Ho}_2\text{Ti}_2\text{O}_7$. Analysis of the diffuse magnetic scattering also led the authors to conclude that $\text{Ho}_2\text{Sn}_2\text{O}_7$ was a dipolar-spin-ice material.

C. $\text{Ho}_{2+x}\text{Ti}_{2-x}\text{O}_{7-\delta}$: stuffed spin ice

Besides thermodynamic variables such as temperature and magnetic field, the chemical composition of the systems may be altered to study the relationship of structural and magnetic properties. To this end, 'stuffed' spin ices with general formula $\text{A}_{2+x}\text{B}_{2-x}\text{O}_{7-\delta}$ have recently been synthesized (Lau *et al.*, 2006; Ueland, 2008), in which additional magnetic ions replace the non-magnetic Ti^{4+} ions ($\delta > 0$, as the oxygen content needs to be adjusted for charge balance). The entire rare earth series of titanates have been formed (Lau *et al.*, 2006a) but to date, the only published data is on the 'stuffed' spin ice (SSI) compounds. Lau *et al.* (2007) have reported phase separation in these compounds, however the magnetic properties are very similar between samples. Single crystals have been produced by Zhou *et al.* (2007).

The additional magnetic exchange pathways represent a major disturbance of the system, introducing positional disorder and, naively, an increased level of energetic constraints to the formation of the spin ice manifold. Surprisingly, it has been found that the 'stuffed' spin ice systems do not freeze, have short range correlations down to the lowest temperatures and, most interestingly, have the same entropy per spin at low temperature as the 'un-stuffed' spin ice (Lau *et al.*, 2006; Zhou *et al.*, 2007). The origins of this residual entropy per spin in these systems is still debatable.

Another interesting feature of the residual entropy in the stuffed spin ice materials is its robustness to an applied field. As seen in Fig. 47 the entropy per spin with

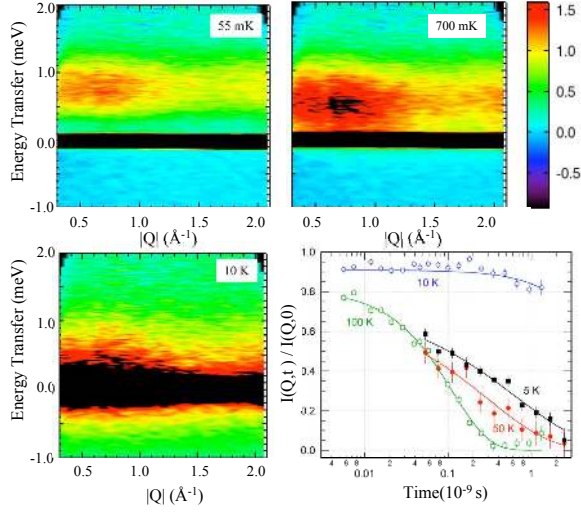


FIG. 48 Inelastic neutron scattering from $\text{Ho}_{2.3}\text{Ti}_{1.7}\text{O}_{7-\delta}$ (Zhou *et al.*, 2007). Data at 55 mK, 700 mK and 10 K, noting the appearance of a gapped spin excitation at low temperatures. Neutron spin echo results on stuffed (open symbols) and unstuffed (closed symbols) spin ice are depicted in the bottom right panel. Within the neutron time window, the spin ice appears static by 10 K (90% of the spin are static), but the stuffed spin ice has persistent dynamics.

$x = 0.67$ in 1 T and zero field are identical. This robust residual entropy in a very disordered sample like $\text{Ho}_{2.67}\text{Ti}_{1.33}\text{O}_{6.67}$ ($x = 0.67$) needs investigating further.

Inelastic and quasielastic neutron scattering on polycrystalline and single crystalline $\text{Ho}_{2.3}\text{Ti}_{1.7}\text{O}_{7-\delta}$ have revealed subtle changes vis à vis the parent compound. Diffuse scattering is centered at 0.9 \AA^{-1} , but it is broader than the diffuse scattering seen in $\text{Ho}_2\text{Ti}_2\text{O}_7$. Also, as seen in Fig. 48, the quasielastic scattering at temperatures above 10 K opens a gap resulting in a low lying excitation, centered at 0.8 meV (Zhou *et al.*, 2007).

More research is currently being done by several groups on ‘stuffed’ spin ice. It appears that the stuffed Dy-spin ices do not have residual entropy (Ueland, 2008).

XI. SPIN LIQUID PHASES

An array of Heisenberg spins forming a three-dimensional pyrochlore lattice that interact among themselves via nearest-neighbor antiferromagnetic exchange interactions is theoretically predicted to remain disordered at finite temperature for either classical (Moessner and Chalker, 1998,a; Moessner, 2001) or quantum spins (Canals and Lacroix, 1998, 2000). Ising spins that are coupled antiferromagnetically on a pyrochlore lattice also possess a large ground state degeneracy characteristic of the spin liquid or cooperative paramagnetic state (Anderson, 1956).

A. $\text{Tb}_2\text{Ti}_2\text{O}_7$

$\text{Tb}_2\text{Ti}_2\text{O}_7$ is a well studied system where Tb^{3+} ions are magnetic and the Ti^{4+} ions are nonmagnetic. The temperature dependence of the magnetic susceptibility of $\text{Tb}_2\text{Ti}_2\text{O}_7$ is described well by the Curie-Weiss law down to 50 K with $\theta_{\text{CW}} = -19 \text{ K}$ and $9.6 \mu_B/\text{Tb-ion}$. This effective moment is appropriate for the $^7\text{F}_6$ Tb^{3+} ion. By studying a magnetically dilute sample, $(\text{Tb}_{0.02}\text{Y}_{0.98})_2\text{Ti}_2\text{O}_7$, a value of -6 K was established as the crystal field contribution to θ_{CW} . Assuming a maximum of -2 K for the dipolar interactions, $\approx -11 \text{ K}$ was proposed as a good estimate for the contribution of the exchange interactions to θ_{CW} . Figure 49a shows the temperature dependence of the bulk susceptibility down to 0.5 K.

Han *et al.* (2004) found, using neutron powder diffraction and x-ray absorption fine-structure, that the chemical structure of $\text{Tb}_2\text{Ti}_2\text{O}_7$ is well ordered with no structural transitions between 4.5 and 600 K. More recently however, Ruff *et al.* (2007) found a broadening of structural peaks in a high resolution, single crystal, x-ray diffraction experiment below 20 K, as expected just above a cubic-to-tetragonal transition, however this transition never fully develops even at 300 mK.

Powder neutron diffraction measurements on $\text{Tb}_2\text{Ti}_2\text{O}_7$ clearly revealed two contributions to the scattering at 2.5 K (Gardner *et al.*, 1999). One of these consists of sharp nuclear Bragg peaks due to the crystalline order in the material and results in a cubic lattice parameter of 10.133 \AA . A second diffuse, liquid-like, background is also present and was attributed to magnetic short range correlations. Gardner *et al.* (1999) used an *isotropic* spin model, correlated over nearest spins only, to describe this scattering which captured the minimum in the forward direction, $|\mathbf{Q}| \sim 0 \text{ \AA}^{-1}$, as well as the approximate location of the peaks and valleys in the data.

Inelastic scattering experiments were also carried out on polycrystalline $\text{Tb}_2\text{Ti}_2\text{O}_7$ (Gardner *et al.*, 2001) and a typical scan at $|\mathbf{Q}| = 2 \text{ \AA}^{-1}$ is shown in Fig. 50. Three bands of excitations are clearly observed near 0.37, 2.53,

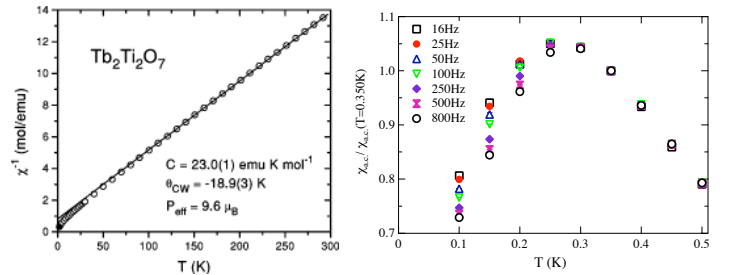


FIG. 49 Left: The temperature dependence of the inverse molar susceptibility and the resulting fit to the Curie-Weiss law at high temperature ($T > 250 \text{ K}$). Right: The low temperature ($T < 0.5 \text{ K}$) dependence of the magnetic susceptibility as a function of frequency (Gardner *et al.*, 2003).

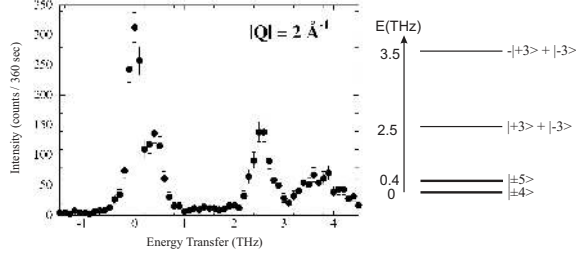


FIG. 50 Left: A typical constant $|Q|$ scan at 2 \AA^{-1} revealing low energy inelastic modes at 12 K on a powder sample of $\text{Tb}_2\text{Ti}_2\text{O}_7$. Right: A schematic of the crystalline electric field levels (Gingras *et al.*, 2000).

and 3.50 THz and these were shown to be dispersionless above 30 K, a characteristic of a single ion effect associated with the rare earth site. A weak, but very interesting dispersion develops in the lowest energy band at temperatures below ~ 20 K, which we will discuss later in this section.

A crystalline electric field (CEF) level scheme appropriate to the $^7\text{F}_6$ configuration of Tb^{3+} in the A -site environment of $\text{Tb}_2\text{Ti}_2\text{O}_7$ was determined on the basis of these neutron and other bulk property data (Gingras *et al.*, 2000). The ground state and first excited states are both doublets, with two singlets at much higher energies, as shown schematically in Fig. 50. The J^z eigenstates $|\pm 4\rangle$ and $|\pm 5\rangle$ are believed to make up most of the weight of the ground state doublet and of the first excited state, respectively. Such a CEF scheme means the moment can be considered extremely Ising in nature and pointing in the local $\langle 111 \rangle$ directions at temperatures $T \lesssim 20$ K. More recently Mirebeau *et al.* (2007) reported a series of neutron scattering measurements that “refined” the CEF scheme of $\text{Tb}_2\text{Ti}_2\text{O}_7$ and compared it to $\text{Tb}_2\text{Sn}_2\text{O}_7$, which orders just below 1 K, and which was discussed in Section VIII.C.

Large single crystals of $\text{Tb}_2\text{Ti}_2\text{O}_7$ were first grown using floating zone image furnace techniques by Gardner *et al.* (1998). The resulting single crystals enabled a series of experiments which could probe the four-dimensional dynamic structure factor $S(\mathbf{Q}, \hbar\omega)$. Figure 51 shows $S(\mathbf{Q}) = \int S(\mathbf{Q}, \hbar\omega) d\omega$ measured at $T=50$ mK and at 9 K within the (hhl) plane. Bragg peaks are clearly seen at the allowed positions for the $Fd\bar{3}m$ space group, that is (hhl) being all even, or all odd, integers. Also one clearly observes a “checkerboard” pattern to the magnetic diffuse scattering. This covers the entire Brillouin zone indicating the spins are correlated on a length scale much smaller than the unit cell $\sim 10.1 \text{ \AA}$. However, the single crystal data are clearly *not* isotropic in reciprocal space, explaining the quantitative failure of the simple isotropic model used to analyze the earlier powder data (Gardner *et al.*, 2001). Also, the scattering does not

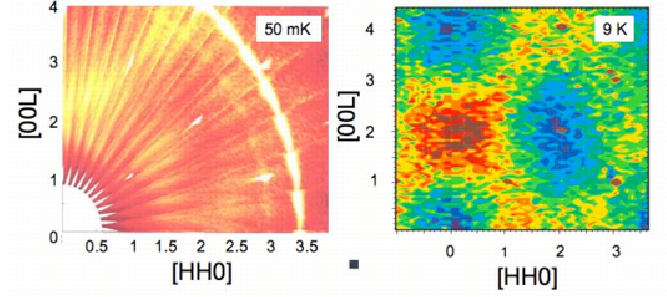


FIG. 51 Diffuse scattering from a single crystal of $\text{Tb}_2\text{Ti}_2\text{O}_7$ at 50 mK (left) and 9 K (right) (Gardner *et al.*, 2001, 2003). Sharp Bragg peaks can be seen at the appropriate reciprocal lattice positions in the 50 mK data set, but at 9 K, these have been subtracted out using a high temperature (100 K) data set.

conform to that expected for an Ising model with local $\langle 111 \rangle$ spin directions. Specifically, an Ising model with local $\langle 111 \rangle$ spins cannot simultaneously produce a large amount of scattering around 002 and null scattering at 000 (Enjalran and Gingras, 2004).

Single crystals also allow the study of the low-lying excitations as a function of \mathbf{Q} , (Gardner *et al.*, 2001, 2003) as opposed to the modulus $|Q|$ derived from powder samples. As was observed in powders (Gardner *et al.*, 1999), the dispersion develops below ~ 25 K. This low temperature dispersion is plotted along the three high symmetry directions within the (hhl) plane in Fig. 52, on which are overlaid cuts of $S(\mathbf{Q})$ along $[00l]$ (top), $[hhl]$ (middle), and $[hhh]$ (bottom). The diffuse scattering is well described by simple near-neighbor antiferromagnetic spin correlations on the pyrochlore lattice, as shown by the solid lines in Fig. 52. We also see that the minima in the dispersion of this low lying magnetic mode (closed symbols) correspond exactly with peaks in $S(\mathbf{Q})$, even though $S(\mathbf{Q})$ is anisotropic in \mathbf{Q} . Gardner *et al.* (2003) showed the gap between the first excited state and the ground state drops from 0.37 THz at 30 K to approximately 0.25 THz at 100 mK but does not soften further as the temperature is further decreased.

Neutron spin echo (Gardner *et al.*, 2003, 2004) and μSR (Gardner *et al.*, 1999; Keren *et al.*, 2004) measurements have also been carried out at mK temperatures to probe the dynamics of the magnetic moments. Both show large, fluctuating moments down to at least 17 mK (Gardner *et al.*, 1999), as expected for a cooperative paramagnet. However, below $T \approx 0.3$ K the $S(\mathbf{Q}, t)/S(\mathbf{Q}, 0)$ baseline is no longer zero indicating a proportion ($\approx 20\%$) of the magnetic moments are frozen in the neutron spin echo time window. This is consistent with the frequency dependence of the AC susceptibility shown in figure 49b (Gardner *et al.*, 2003; Luo *et al.*, 2001). However, we attribute this partial spin freezing to a small subset of magnetic moments distributed near a small number of defects. Evidence for spin freezing was

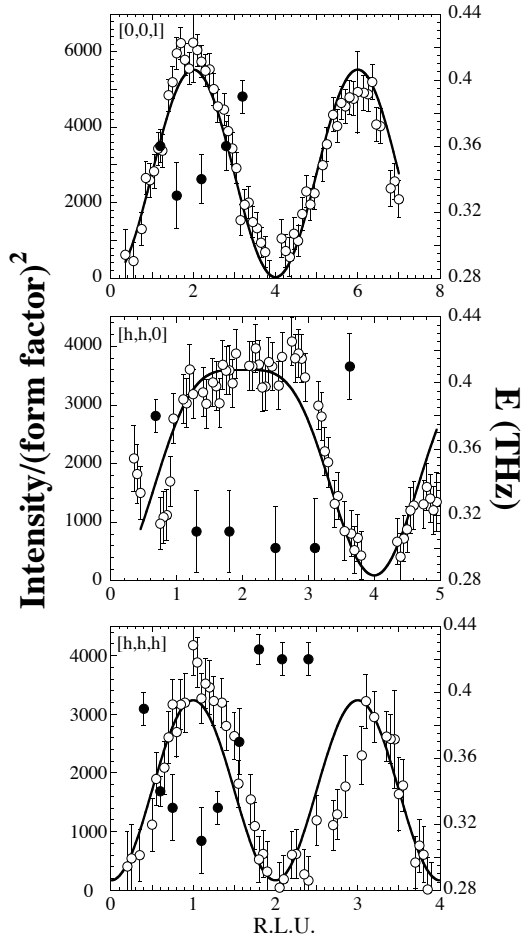


FIG. 52 Cuts through the checkerboard pattern of diffuse magnetic scattering (open symbols) along high symmetry directions of the cubic lattice. To complement these data, the dispersion of the lowest lying magnetic excitation, at 4 K, is also plotted (closed symbols). Fits to the diffuse scattering are shown and discussed in the text (Gardner *et al.*, 2001).

also found independently in neutron scattering experiments performed on other single crystal samples (Yasui *et al.*, 2002). In this case, hysteresis is observed in the scattering near 002 at temperatures less than ~ 1.7 K, but again most of the scattering remains diffuse in nature even below 1.7 K.

Dilution studies by Keren *et al.* (2004), perturbed the lattice through the percolation threshold but found that fluctuating moments prevail at all magnetic concentration as shown by the muon relaxation rate in Fig. 53. They also noted that the magnetic coverage of the lattice was important to the cooperative phenomenon but the percolation threshold played no critical role.

At first sight, it would be tempting to ascribe the failure of $\text{Tb}_2\text{Ti}_2\text{O}_7$ to develop long range order down to such a low temperature compared to θ_{CW} , to the collective paramagnetic behavior of the classical

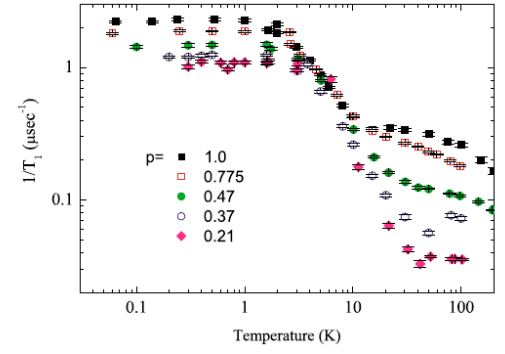


FIG. 53 Temperature dependence of the muon relaxation rate in a field of 50 G in various samples of $(\text{Tb}_p\text{Y}_{1-p})_2\text{Ti}_2\text{O}_7$ (Keren *et al.*, 2004).

pyrochlore Heisenberg antiferromagnet (Moessner and Chalker, 1998,a; Villain, 1979). However, consideration of the single-ion crystal field ground state doublet of Tb^{3+} in $\text{Tb}_2\text{Ti}_2\text{O}_7$ strongly suggests that, in absence of exchange and dipolar interactions, bare Tb^{3+} should be considered as an effective Ising spin (Gingras *et al.*, 2000; Rosenkranz *et al.*, 2000).

Considering only nearest-neighbor exchange and long-range dipolar interactions, the DSM of Eq. (12) would be the appropriate Hamiltonian to describe $\text{Tb}_2\text{Ti}_2\text{O}_7$ as an Ising system. On the basis of the estimated value of the nearest-neighbor exchange and dipolar coupling, $\text{Tb}_2\text{Ti}_2\text{O}_7$ would be predicted to develop a $\mathbf{k}_{\text{ord}} = 000$ four sublattice long-range Néel order at a critical temperature $T_c \approx 1$ K (den Hertog and Gingras, 2000), in dramatic contradiction with experimental results. Furthermore, the paramagnetic neutron scattering of such a classical Ising model is inconsistent with that observed in $\text{Tb}_2\text{Ti}_2\text{O}_7$ at 9 K as shown in Fig. 51. Mean field theory calculations on a Heisenberg model with dipolar and exchange interactions and with a simple single-ion anisotropy (Enjalran and Gingras, 2004) as well as a random phase approximation (RPA) calculation (Kao *et al.*, 2003) that considers a semi-realistic description of the crystal-field levels of Tb^{3+} show that the strong scattering intensity around 002 should be extremely weak for Ising spins. Rather, the intensity is caused by the finite amount of fluctuations perpendicular to the local (111) directions (Enjalran and Gingras, 2004). In the RPA calculations (Kao *et al.*, 2003), the scattering intensity near 002 originates from the contribution of the excited crystal field levels at an energy ~ 18 K to the susceptibility, which is made dispersive via the exchange and dipolar interactions. The experimental observation that the diffuse scattering intensity is largely unaltered down to a temperature of 50 mK, as shown in Fig. 51, suggests that the “restored” effective isotropicity of the spins is an intrinsic part of the effective low-energy theory that describes $\text{Tb}_2\text{Ti}_2\text{O}_7$. In that context, a recent paper by Molavian

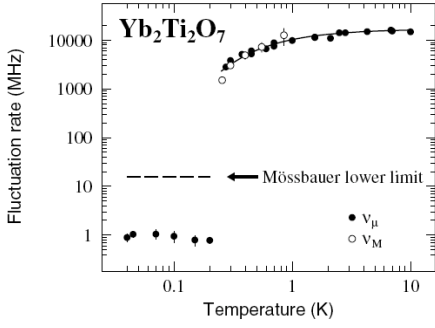


FIG. 54 Estimate fluctuation rate of the Yb^{3+} moment derived from muon (filled circles) and Mössbauer (open circles) spectroscopies (Hodges *et al.*, 2002). Note that the rate plateaus at 200 mK and does not go to zero.

et al. (2007) argues, on the basis of a calculation that considers non-interacting tetrahedra, that virtual fluctuations between the ground state and excited crystal field levels lead to an important renormalization of the coupling constants entering the effective low-energy theory. In particular, Molavian *et al.* (2007) propose that, for the simple model considered, the system is pushed to the spin ice side of the phase diagram by those quantum fluctuations. In other words, within that description, $\text{Tb}_2\text{Ti}_2\text{O}_7$ is a sort of quantum spin ice system where the spin ice like correlations remain hidden down to $T \lesssim 500$ mK.

In this discussion of the lack of order in $\text{Tb}_2\text{Ti}_2\text{O}_7$, it is not clear what is the role of the structural/lattice fluctuations very recently reported by Ruff *et al.* (2007). At this time, there is really no robust theoretical understanding of the physics at play in $\text{Tb}_2\text{Ti}_2\text{O}_7$ and more theoretical and experimental studies are required.

B. $\text{Yb}_2\text{Ti}_2\text{O}_7$

Ytterbium titanate is an insulator with lattice parameter $a_0 = 10.026(1)$ Å at room temperature (Brixner, 1964). Early work suggested an ordered magnetic state just below 0.2 K (Blöte *et al.*, 1969), where a sharp anomaly in the specific heat was observed. In a detailed magnetisation study, Bramwell *et al.* (2000) found a Curie-Weiss temperature of 0.59(1) K, indicative of weak ferromagnetic coupling and a free ion moment of $3.34(1) \mu_B$. Hodges *et al.* (2001) used Mössbauer spectroscopy to investigate the crystal field scheme and determined that the ground state Kramers doublet was separated by 620 K from the first excited state producing an easy plane anisotropy, like in $\text{Er}_2\text{Ti}_2\text{O}_7$. They also found the effective paramagnetic moment to be $3.05(8) \mu_B$.

Hodges and co-workers (Hodges *et al.*, 2002) extended their study of $\text{Yb}_2\text{Ti}_2\text{O}_7$ and found an abrupt change in the fluctuation rate of the Yb^{3+} spin at 0.24 K but not a frozen ground state as expected from the earlier studies (Blöte *et al.*, 1969). Using muon spin relaxation

and Mössbauer spectroscopies, they concluded that the Yb^{3+} spin fluctuations slow down by more than 3 orders of magnitude to several megahertz, without freezing completely. This was confirmed in their neutron powder diffraction, where no extra Bragg intensity was reported below 0.24 K. Single crystal neutron diffraction by Yasui *et al.* (2003) has revealed extra Bragg scattering below 0.24 K from a static ferromagnetic state, albeit with a reduced moment of $1.1 \mu_B$. The latter two studies motivated a polarised neutron scattering study by Gardner *et al.* (2004a). That work conclusively ruled out a frozen ferromagnetic state and confirmed that the majority of the spin system continues to fluctuate below the 240 mK transition while a small amount of magnetic scattering was observed at the 111 Bragg position at 90 mK.

C. $\text{Er}_2\text{Sn}_2\text{O}_7$

$\text{Er}_2\text{Sn}_2\text{O}_7$ and $\text{Er}_2\text{Ti}_2\text{O}_7$ are thought to constitute experimental realizations of the highly frustrated XY antiferromagnet on the pyrochlore lattice. Very little is known about $\text{Er}_2\text{Sn}_2\text{O}_7$ compared to the isostructural $\text{Er}_2\text{Ti}_2\text{O}_7$ compound which develops a non-collinear Néel state at 1.1 K, possibly via an order by disorder transition (see Section VIII.B (Champion *et al.*, 2003)). Bondah-Jagalu and Bramwell (2001) reported a pronounced field cooled - zero field cooled divergence in the susceptibility at 3.4 K. The temperature and field dependence of the bulk magnetization of $\text{Er}_2\text{Sn}_2\text{O}_7$ was more recently published by Matsuhira *et al.* (2002). At high temperatures $1/\chi(T)$ is linear and a fit to the Curie-Weiss law results in a ground state moment of $9.59 \mu_B$ appropriate for the $^4\text{I}_{15/2}$ ion. It also gives a Curie-Weiss temperature, $\theta_{\text{CW}} \approx -14$ K, suggestive of antiferromagnetic correlations. At 10 K $1/\chi(T)$ starts bending downwards, presumably due to crystal field effects. However, no anomaly indicative of a freezing into either a long or short range ordered system was seen down to 0.13 K, suggesting that geometrical frustration plays a large role in determining the magnetic ground state. μSR studies by Lago *et al.* (2005) revealed persistent spin dynamics at 20 mK in both Er based samples. While the temperature dependence of the muon relaxation rate is similar, the depolarisation curve for $\text{Er}_2\text{Sn}_2\text{O}_7$ remains exponential down to the lowest temperatures suggesting the system fails to enter an ordered state, while the titanate takes on a gaussian relaxation at early times.

Neutron diffraction results by Bramwell *et al.* (2004) and Shirai and Bramwell (2007) would however suggest that $\text{Er}_2\text{Sn}_2\text{O}_7$ enters a state with long-range order at ≈ 0.1 K. This ordered ground state is different that that of $\text{Er}_2\text{Ti}_2\text{O}_7$, which appears to be stable in the $\text{Er}_2(\text{Sn,Ti})_2\text{O}_7$ solid solution until 90% substitution of Ti for Sn.

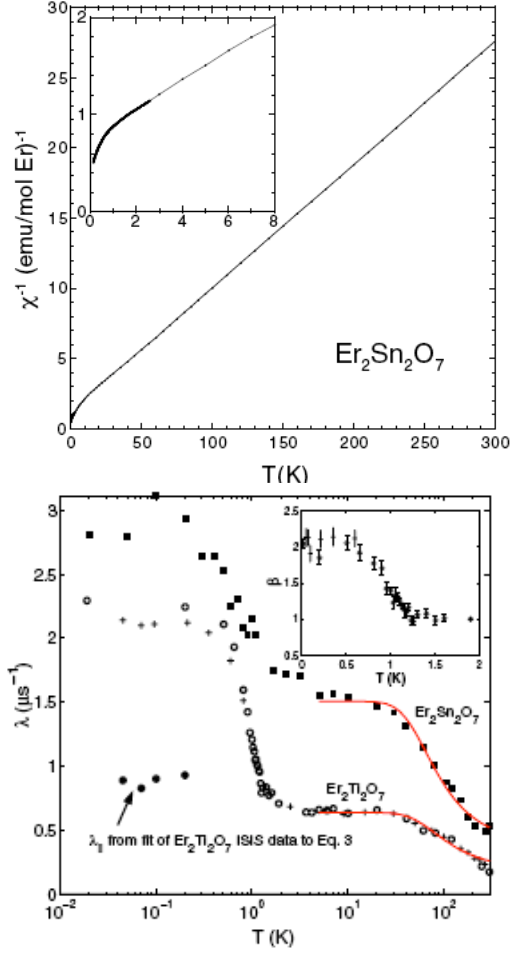


FIG. 55 Top: The temperature dependence of the inverse magnetic susceptibility from a powder sample of $\text{Er}_2\text{Sn}_2\text{O}_7$ (Matsuhira *et al.*, 2002). The inset shows the data down to 0.13 K. Bottom: Relaxation rates λ derived from muon spin relaxation measurements for $\text{Er}_2\text{Sn}_2\text{O}_7$ and $\text{Er}_2\text{Ti}_2\text{O}_7$ (Lago *et al.*, 2005). Solid curves are the fit of the high temperature data to an exponential activation function. λ_{\parallel} is the longitudinal relaxation rate for $\text{Er}_2\text{Ti}_2\text{O}_7$. Inset: thermal evolution of the order parameter critical exponent, β , for $\text{Er}_2\text{Ti}_2\text{O}_7$ showing the evolution from exponential to Gaussian curve shape across T_N . For $\text{Er}_2\text{Sn}_2\text{O}_7$, $\beta \approx 1$ for the entire temperature range.

D. $\text{Pr}_2\text{Ir}_2\text{O}_7$

Recently, much attention has been devoted to the metallic material $\text{Pr}_2\text{Ir}_2\text{O}_7$ which is reported to remain paramagnetic down to 0.3 K by Machida *et al.* (2005). From magnetization, specific heat and inelastic neutron scattering studies the Pr ground state was determined to be a well isolated doublet with Ising-like moments oriented along the local $\langle 111 \rangle$ axes. The antiferromagnetically coupled spins have an energy scale of ≈ 20 K and no freezing was observed. Subsequent studies carried out on crystals grown from a KF flux showed remarkably com-

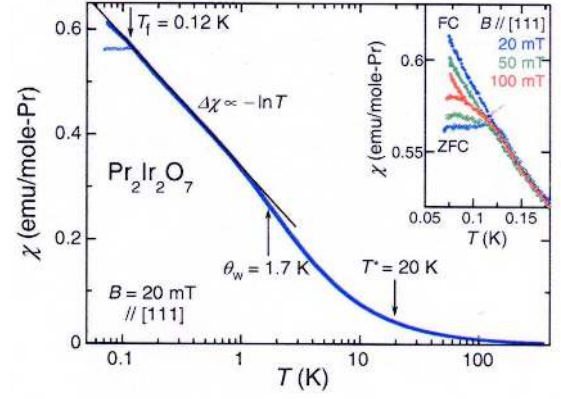


FIG. 56 DC susceptibility at a field of 20 mT applied along $[111]$ for $\text{Pr}_2\text{Ir}_2\text{O}_7$. Note the $\ln(T)$ dependence expected for the Kondo effect and (inset) evidence for spin freezing (Nakatsuji *et al.*, 2006).

plex behavior, including the Kondo effect and partial spin freezing below 120 mK (see Fig. 56) (Millican *et al.*, 2007; Nakatsuji *et al.*, 2006). The authors have concluded that a spin liquid state exists for the Pr moments but no studies of spin dynamics have yet been presented to support this claim.

Finally, a report of an unconventional anomalous Hall effect by Machida *et al.* (2007) has appeared very recently and a chirality mechanism, similar to that proposed for $\text{Nd}_2\text{Mo}_2\text{O}_7$ (Taguchi *et al.*, 2001, 2004), has been invoked.

XII. EXTERNAL PERTURBATIONS

Many studies have been performed on geometrically frustrated magnets where an external perturbation (apart from nonzero temperature) has been applied to the system. These perturbations can take the form of common variables like magnetic field and the chemical composition of the systems. Less common perturbations include applied pressure and irradiation damage and the effects of these too have been investigated on pyrochlore oxides. To date, no magnetic studies of irradiation damaged pyrochlores have been published, though several groups have studied the structural properties of pyrochlores after being bombarded with radiation (Ewing *et al.*, 2004; Sickafus *et al.*, 2000). Where appropriate, the results from changes in temperature or chemical composition have been mentioned in the previous sections and we will restrict ourselves here to those studies where profound changes to the magnetic nature of the frustrated magnet have been observed.

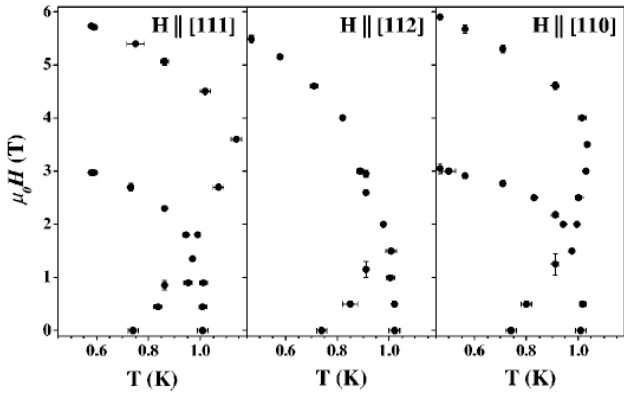


FIG. 57 Magnetic phase diagrams of the $\text{Gd}_2\text{Ti}_2\text{O}_7$ for three different orientations of an applied magnetic field (Petrenko *et al.*, 2004). These phase boundaries roughly approximate those seen by Ramirez *et al.* (2002) on a powder sample.

A. Magnetic Field

Most magnetic pyrochlore oxides have been subject to an applied field and their behavior monitored. In some cases, drastic effects have been observed. Indeed, one must remember that these systems are delicately balanced between several competing energy scales, and a magnetic field, even small fields, can alter the system significantly. For example, in the spin ices, $\text{Ho}_2\text{Ti}_2\text{O}_7$ and $\text{Dy}_2\text{Ti}_2\text{O}_7$, in a field as small as 100 Oe applied along [001] or [110], a few of the many ground states are favored creating metastable states, magnetization plateaus and slow spin dynamics but no elementary changes are observed (Fennell *et al.*, 2005). In a few cases, the application of a field can drive the system into a new ground state. These facts must be remembered when probing frustrated systems, possibly even in the remanent field of a magnet.

1. $\text{Gd}_2\text{Ti}_2\text{O}_7$

The magnetic field vs temperature phase diagram for the Heisenberg pyrochlore magnet $\text{Gd}_2\text{Ti}_2\text{O}_7$ was first determined on polycrystalline samples using specific heat and AC susceptibility (Ramirez *et al.*, 2002). A mean field model was used to justify the five phases found below 1 K and in fields up to 8 T. Petrenko *et al.* (2004) later reproduced these field induced transitions by measuring the specific heat along 3 different crystallographic directions on a single crystal (see Fig. 57).

To determine the magnetic structure in these phases, neutron powder diffraction measurements have been performed. Although significant differences can be seen in the diffraction patterns in every phase, only the zero field structures have been modeled successfully (Shirai and Bramwell, 2007; Stewart *et al.*, 2004).

With the recent knowledge that $\text{Gd}_2\text{Sn}_2\text{O}_7$ is a better

representation of a Heisenberg pyrochlore magnet with dipolar interactions and near neighbor exchange (Del Maestro and Gingras, 2007; Wills *et al.*, 2006) (see Section VIII.A), one would want to study it in single crystalline form and in a magnetic field.

2. Kagome ice

By applying a magnetic field along the [111] direction of single crystals of $\text{Dy}_2\text{Ti}_2\text{O}_7$ or $\text{Ho}_2\text{Ti}_2\text{O}_7$ one can induce a new microscopically degenerate phase, known as kagome ice. In this state the 2-in-2-out spin configuration, known as the ice-rules state, is still found, however one spin is pinned by the field and the number of possible ground states is lowered (Moessner and Sondhi, 2003). As shown in Fig. 4, the pyrochlore structure as observed along the [111] is comprised of stacked, alternating kagome and triangular planes. When the applied field exceeds 0.3 kOe the kagome ice phase is stable and exhibits a residual entropy of $\approx 40\%$ of that seen in zero field spin ice.

Matsuhira *et al.* (2002a) performed magnetisation and specific heat experiments on $\text{Dy}_2\text{Ti}_2\text{O}_7$, proving the existence of this phase. Since then, several pieces of work have been done, mainly on $\text{Dy}_2\text{Ti}_2\text{O}_7$, with probes like AC susceptibility and specific heat (Higashinaka *et al.*, 2004; Sakakibara *et al.*, 2004; Tabata *et al.*, 2006). Very recently Fennell *et al.* (2007) have performed neutron diffraction measurements on $\text{Ho}_2\text{Ti}_2\text{O}_7$ in the kagome ice phase and speculate that a Kasteleyn transition takes place. Wills *et al.* (2002) investigated via analytical and Monte Carlo calculations an ice-like state in a kagome lattice with local Ising anisotropy before one was experimentally realized. While the physics of kagome ice emerging from a spin ice single crystal subject to a [111] field is rather interesting, the behavior of spin ice subject to a magnetic field along one of the [110], [112] or [100] directions is also worthy of a brief comment.

The pyrochlore lattice can be viewed as two sets of orthogonal chains of spins. One set is parallel to the [110] direction and the other along $[1\bar{1}0]$. These two sets are referred to as α and β chains, respectively. The application of a field parallel to [110] and of strength slightly larger than 1 T leads to a pinning of the spins on the α chain, effectively freezing those spins. Both the net exchange and net dipolar field produced by the frozen spins on the α chains vanish by symmetry for the spins on the β chains. Since the β chains are perpendicular to the field along [110], the spins along those β chains are free to interact only among themselves. Just as a [111] field leads to a decomposition of the pyrochlore lattice into weakly coupled kagome planes with their normal along [111], a field along [110] induces a “magnetic break up” of an otherwise cubic pyrochlore system into a set of quasi one-dimensional β chains predominantly weakly coupled by dipolar interactions. On the basis of Monte Carlo simulations (Ruff *et al.*, 2005; Yoshida *et al.*, 2004) and chain mean field

theory (Ruff *et al.*, 2005), one expects that dipolar spin ice would have a transition to a long range ordered state, referred to as $\mathbf{q} = \mathbf{X}$ order (Harris *et al.*, 1997). However, while neutron scattering experiments on $\text{Ho}_2\text{Ti}_2\text{O}_7$ and $\text{Dy}_2\text{Ti}_2\text{O}_7$ (Fennell *et al.*, 2005) and specific heat measurements (Hiroi *et al.*, 2003a) on $\text{Dy}_2\text{Ti}_2\text{O}_7$ find some evidence for a transition with a field along $[110]$, the transition is not sharp. It is not known whether the apparent failure of the system to develop long range $\mathbf{q} = \mathbf{X}$ order is due to either an imperfect alignment of the field along $[110]$ or the inability of the system to properly equilibrate upon approaching the putative transition.

The $[100]$ field problem was probably the first one studied theoretically (Harris *et al.*, 1998). It was predicted on the basis of Monte Carlo simulations on the nearest-neighbor spin ice model that the system should exhibit a field-driven transition between a gas-like weakly magnetized ice-rule obeying state and a strongly polarized state. It was originally argued that this transition is first order and terminates at a critical point, similarly to the gas-liquid critical point (Harris *et al.*, 1998). However, recent work that combines numerical and analytical calculations argues for a more exotic topological Kastelyn transition driven by the proliferation of defects in the ice-state as the temperature or the field strength is varied (Jaubert *et al.*, 2007). The same work speculates that there exists preliminary evidence for such a rounded Kastelyn transition in the neutron scattering data on $\text{Ho}_2\text{Ti}_2\text{O}_7$ subject to a $[100]$ field (Fennell *et al.*, 2005). On the other hand, while the Monte Carlo data of Harris *et al.* (1998) find a sharp and a broad feature in the specific heat as a function of temperature for sufficiently low (but nonzero) $[100]$ field, specific heat measurements (Higashinaka *et al.*, 2003a) on $\text{Dy}_2\text{Ti}_2\text{O}_7$ only find one peak down to a temperature of 0.35 K. Perhaps long range dipolar interactions are of some relevance to the phenomenology at play for the case of a $[100]$ field. Indeed, long range dipole-dipole interactions are definitely crucial to the qualitative physics at play for fields along $[110]$ and near $[112]$ (Ruff *et al.*, 2005). Clearly, more experimental and theoretical work on the problem of spin ice in a $[100]$ magnetic field is called for.

3. $\text{Tb}_2\text{Ti}_2\text{O}_7$

Neutron diffraction and susceptibility data have recently been collected on the cooperative paramagnet $\text{Tb}_2\text{Ti}_2\text{O}_7$ in high magnetic fields (Rule *et al.*, 2006; Ueland *et al.*, 2006). In the AC susceptibility work by Ueland *et al.* (2006) unusual cooperative effects and slow spin dynamics were induced by applying fields as high as 9 T at temperatures above 1 K.

Rule *et al.* (2006) performed single crystal neutron scattering on $\text{Tb}_2\text{Ti}_2\text{O}_7$. They were able to show that the short range spin-spin correlations, discussed in Section XI (Gardner *et al.*, 2001, 2003), are very dynamic in origin and that they become of longer range as a field

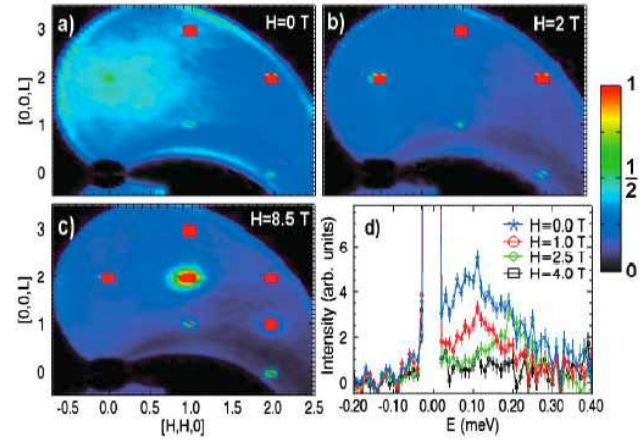


FIG. 58 Neutron scattering with $\Delta E = \pm 0.5$ meV from $\text{Tb}_2\text{Ti}_2\text{O}_7$ at 1 K (Rule *et al.*, 2006). In zero field (a), 2 T (b) and 8.5 T (c). In panel d) constant Q scans at 0.1 K are shown, indicating that the low lying magnetic scattering (slow spin dynamics) is quenched as the field increases.

is applied. Applying a fairly small field of 1000 Oe, at 400 mK, causes the magnetic diffuse scattering to condense into peaks (see Fig. 51), with characteristics similar to a polarised paramagnet. Figure 58 shows similar data at 1 K. In zero field, Bragg peaks are seen at 113 and 222 from the underlying nuclear structure and broad diffuse scattering, magnetic in origin is centered at 002. In a field up to 2 T (not shown) the diffuse scattering sharpens into a 002 peak and in higher fields ($\mu_0 H > 2$ T) a magnetically ordered phase is induced, with the development of true long range order accompanied by spin waves.

B. High Pressure

The study of pressure on samples in polycrystalline and single crystal form has become more common in recent years, with a paper on the pressure effect on the magnetoresistive material $\text{Tl}_2\text{Mn}_2\text{O}_7$ being among the earliest (Sushko *et al.*, 1996) in pyrochlore physics. More recently, studies have been performed on the transport, structural and magnetic properties of other pyrochlores (Mirebeau *et al.*, 2002; Saha *et al.*, 2006; Zhang *et al.*, 2007, 2006).

$\text{Sm}_2\text{Zr}_2\text{O}_7$ undergoes a structural distortion at low pressures. However, the distortion is not observed between 13.5 and 18 GPa. Above 18 GPa, the pyrochlore structure is unstable and a distorted fluorite structure, in which the cations and anion vacancies are disordered, is observed (Zhang *et al.*, 2007). Similar things happen to $\text{Cd}_2\text{Nb}_2\text{O}_7$ at 12 GPa (Samara *et al.*, 2006; Zhang *et al.*, 2006). $\text{Gd}_2\text{Ti}_2\text{O}_7$ undergoes a subtle distortion of the lattice at 9 GPa at room temperature (Saha *et al.*, 2006). Neutron diffraction at 1.4 K on $\text{Ho}_2\text{Ti}_2\text{O}_7$ at pressures up

to 6 GPa saw no change in the spatial correlations of this spin ice compound (Mirebeau and Goncharenko, 2004), but a recent study of $\text{Dy}_2\text{Ti}_2\text{O}_7$ observed a small change in the magnetisation at 13 kbar (Mito *et al.*, 2007).

1. $\text{Tb}_2\text{Ti}_2\text{O}_7$

The $\text{Tb}_2\text{Ti}_2\text{O}_7$ cooperative paramagnet has been studied by means of single-crystal and polycrystalline neutron diffraction for an unprecedented range of thermodynamical parameters combining high pressures, magnetic fields and low temperatures (Mirebeau *et al.*, 2002, 2004a). Mirebeau *et al.* (2002) found a long range, magnetically ordered state near 2 K for a hydrostatic pressure exceeding ~ 1.5 GPa. Powder neutron diffraction data as a function of pressure are shown in Fig. 59. Weak magnetic Bragg peaks occur at positions not associated with nuclear reflections although indexable to the $Fd\bar{3}m$ space group. They also found two small reflections that were attributed to a long range modulation of the main structure.

To investigate the transition further, Mirebeau *et al.* (2004a) studied single crystals where the ordered magnetic moment may be tuned by means of the direction of the anisotropic pressure component. It was shown that an anisotropic pressure component is needed to suppress the spin liquid state, but an anisotropic pressure alone with no hydrostatic component produced no effect at 1.4 K. When an ordered phase was induced, the direction of the anisotropic pressure was important with a factor of 30 difference seen in the strength of the magnetic scattering between different directions (Mirebeau *et al.*, 2004a). One wonders if the rich behavior of $\text{Tb}_2\text{Ti}_2\text{O}_7$ under pressure is related to the recent observations of seemingly dynamical lattice effects in zero applied pressure (Ruff *et al.*, 2007).

2. $\text{A}_2\text{Mo}_2\text{O}_7$ ($A = \text{Gd}$ and Tb)

The properties of $\text{Gd}_2\text{Mo}_2\text{O}_{7-x}$ change remarkably with pressure. Kim *et al.* (2005) applied moderate pressures of 1.6 GPa and found a significant decrease in the saturation moment at 4 K with increased hysteresis. Mirebeau *et al.* (2006a) and Miyoshi *et al.* (2006) extended the pressure range and were able to drive the system into a glassy state at 2.7 GPa. In the study by Mirebeau *et al.* (2006a) the melting of the magnetic structure was monitored by neutron diffraction (see Fig. 60). Thus, the application of pressure can change the sign of the Mo–Mo exchange interaction from ferromagnetic to antiferromagnetic. In addition, a phase with mixed Tb/La substitution on the A -site, namely $(\text{La}_{0.2}\text{Tb}_{0.8})_2\text{Mo}_2\text{O}_7$, was studied by Apetrei *et al.* (2007a). This material, which has nearly the same unit cell constant as $\text{Gd}_2\text{Mo}_2\text{O}_{7-x}$ [10.3787(8) Å], shows ferromagnetism with $T_c = 58$ K but with a different magnetic structure in

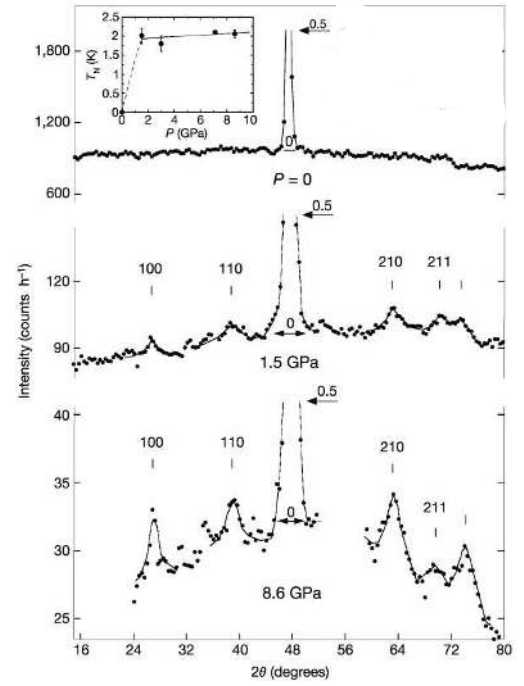


FIG. 59 Pressure induced magnetic Bragg scattering from polycrystalline $\text{Tb}_2\text{Ti}_2\text{O}_7$ at <2 K. The data shows the pressure evolution of static correlations in the cooperative paramagnet. The inset depicts the pressure dependence of the transition temperature (Mirebeau *et al.*, 2002).

which the Tb moments form the familiar two-in two-out Ising structure, but there is still ferromagnetic coupling between the A and B magnetic sublattices. It is also remarked that the ordered moments are reduced significantly from the free ion values by 50 percent for Tb, 30 percent for Gd and 70 percent for Mo. The case for Tb is not surprising and can be ascribed to crystal field effects, while the result for Mo is in line with previous reports (Gaulin *et al.*, 1992; Greedan *et al.*, 1991; Yasui *et al.*, 2001).

Part IV

Conclusions

We have highlighted most of the advances made over the past 20 years in classifying the magnetic ground state in many geometrically frustrated magnets with the pyrochlore lattice. An extensive review on other frustrated magnetic systems like the spinels and kagome lattice magnets would be most welcomed. Although significant advances have been made in the understanding and characterization of these pyrochlore magnets, much more work can be done. As the systems get more complicated (i.e. through dilution of the magnetic sublattice or mixing of magnetic species) we hope and expect to see more

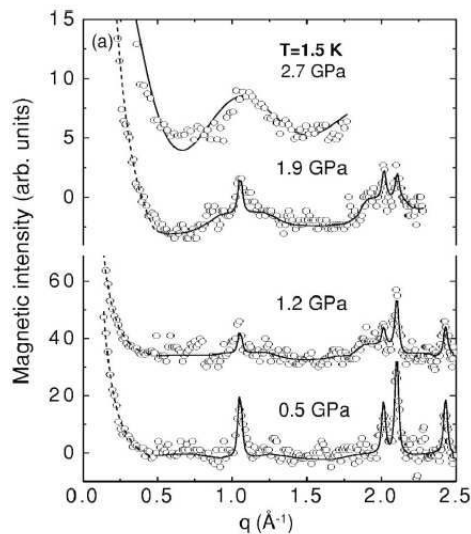


FIG. 60 Pressure dependence on the magnetic scattering from $\text{Gd}_2\text{Mo}_2\text{O}_7$. Note the broadening of the reflection near $q = 1 \text{ \AA}^{-1}$ which is complete by 2.7 GPa (Mirebeau *et al.*, 2006a)

new and exciting physics, but experimentalists will have to be more diligent in their characterization of their samples, since it is now clear that the magnetic ground state is very sensitive to small perturbations. Understanding the role local disorder and spin-lattice interactions play in these materials, as well as the origin of the persistent spin dynamics seen well below apparent ordering temperatures, usually by a local probe such as μSR is crucial in advancing this field. Another area that researchers should invest some time studying is the transport properties at metal/insulator or superconducting transitions. While a connection to geometric frustration is often a feature of the introduction to papers involving superconducting pyrochlores like $\text{Cd}_2\text{Re}_2\text{O}_7$ (Hanawa *et al.*, 2001; Sakai *et al.*, 2001) and the series MOs_2O_6 , where $M = \text{K}, \text{Rb}$ and Cs (Yonezawa *et al.*, 2004,a,b), there is no credible evidence yet that magnetism, frustrated or otherwise, plays any role in the superconducting phase. Finally, while the models, created by theorists, for understanding geometrically frustrated systems have become increasingly sophisticated, there persist many outstanding questions. What is the origin of the 15 K anomaly in the titanate spin ices? Why does $\text{Tb}_2\text{Ti}_2\text{O}_7$ remain dynamic and what is the true nature of the Tb^{3+} moments? What is the true ground state for $\text{Yb}_2\text{Ti}_2\text{O}_7$? Is the ground state of $\text{Er}_2\text{Ti}_2\text{O}_7$ truly selected by quantum order-by-disorder? These must be addressed in the near future.

Acknowledgements

We acknowledge here all our past and immediate collaborators, post-docs and students, too numerous to list

individually, and with whom we have enjoyed working over the years. Their contributions to this field are clear from the large number of citations of their work in the bibliography which follows. We also thank our many colleagues for hundreds of useful discussions and e-mail correspondences.

We acknowledge the generous financial support of: the NSERC of Canada, the Canada Research Chair program (M.G., Tier 1), the Research Corporation, the Canadian Institute for Advanced Research, Materials and Manufacturing Ontario, the Ontario Innovation Trust and the Canada Foundation for Innovation.

References

- Aharony, A. and E. Pytte, 1983, *Phys. Rev.* **27**, 5872.
- Ali N., M. P., Hill, S. Labroo, and J. E. Greedan, 1989, *J. Solid State Chem.* **83**, 178.
- Alonso, J. A., M. J. Martinez-Lope, M. T. Casais, and J. L. Martinez, 2000, *Chem. Mater.* **12**, 1127.
- Anderson, P. W., 1956, *Phys. Rev.* **102**, 1008.
- Anderson, P. W., 1973, *Mater. Res. Bull.* **8**, 153.
- Anderson, P. W., 1987, *Science* **235**, 1196.
- Apetrei, A., I., Mirebeau, I. Goncharenko, D. Andreica, and P. Bonville, 2007, *J. Phys.: Condens. Matter* **19**, 145214.
- Apetrei, A., I., Mirebeau, I. Goncharenko, D. Andreica, and P. Bonville, 2007a, *Phys. Rev. Lett.* **97**, 206401.
- Arai, M., Y. Ishikawa, N. Saito, and H. Takei, 1985, *J. Phys. Soc. Japan* **54**, 781.
- Balakrishnan, G., O. A. Petrenko, M. R. Lees, and D. M^cK. Paul, 1998, *J. Phys.: Condens. Matter* **10**, L723.
- Ballesteros, H. G., A. Cruz, L. A. Fernández, V. Martín-Mayor, J. Pech, J. J. Ruiz-Lorenzo, A. Tarancon, P. Téllez, C. L. Ullod, and C. Ungil, 2000, *Phys. Rev. B* **62**, 14237.
- Ballou, R., 2001, *Can. J. Phys.* **79**, 1475.
- Bansal, C., H. Kawanaka, H. Bando, and Y. Nishihara, 2002, *Phys. Rev. B* **66**, 052406.
- Bansal, C., K. Hirofumi, B. Hiroshi, and N. Yoshikazu, 2003, *Physica B* **329**, 1034.
- Barkema, G. T., and M. E. J. Newman, 1998, *Phys. Rev. E* **57**, 1155.
- Barton, W. A. and J. Cashion, 1979, *J. Phys. C* **12**, 2897.
- Bazuev, G. V., O. V. Makarova, V. Z. Oboldin, and G. P. Shveikin, 1976, *Doklady Akademii Nauk SSSR* **230**, 869.
- Bellier-Castella, L., M. J. P. Gingras, P. C. W. Holdsworth, and R. Moessner, 2001, *Can. J. Phys.* **79**, 1365.
- Berg, E., E. Altman, and A. Auerbach, 2003, *Phys. Rev. Lett.* **90**, 147204.
- Berman, D. L., R. Shindou, G. A. Fiete, and L. Balents, 2006, *Phys. Rev. B* **74**, 134409.
- Bert, F., P. Mendels, A. Olariu, N. Blanchard, G. Collin, A. Amato, C. Baines, and A. D. Hillier, 2006, *Phys. Rev. Lett.* **97**, 117203.
- Bertaut, E. F., F. Forrat, and M. C. Montmory, 1959, *Compt. Rend.* **249c**, 276.
- Bertin, E., P. Bonville, J.-P. Bouchaud, J. A. Hodges, J. P. Sanchez, and P. Vulliet, 2002, *Eur. Phys. J. B* **27**, 347.
- Billinge, S.J.L., 2004, *Z. Kristallogr.* **219**, 117.
- Binder, K., and A. P. Young, 1986, *Rev. Mod. Phys.* **58**, 801.
- Blacklock, K. and H. W. White, 1979, *J. Chem. Phys.* **71**, 5287.

- Blacklock, K. and H. W. White, 1980, *J. Chem. Phys.* **72**, 2191.
- Blöte, H. W. J., R. F. Wielinga, and W. J. Huiskamp, 1969, *Physica* **43**, 549.
- Bondah-Jagalu, V. and S. T. Bramwell, 2001, *Can. J. Phys.* **79**, 1381.
- Bonville, P., J. A. Hodges, M. Ocio, J. P. Sanchez, P. Vulliet, S. Sosin, and D. Braithwaite, 2003, *J. Phys.: Condens. Matter* **15**, 7777.
- Bonville, P., J. A. Hodges, E. Bertin, J.-Ph. Bouchaud, M. Ocio, P. Dalmas de Réotier, L. -P. Regnault, H. M. Rønnow, J. P. Sanchez, S. Sosin, A. Yaouanc, M. Rams, and K. Królas, 2003a, *Cond-mat/0306470*.
- Booth, C. H., J. S. Gardner, G. H. Kwei, R. H. Heffner, F. Bridges, and M. A. Subramanian, 2000, *Phys. Rev. B* **62**, R755.
- Bramwell, S. T., M. J. P. Gingras, and J. N. Reimers, 1994, *J. Appl. Phys.* **75**, 5523.
- Bramwell, S. T., M. N. Field, M. J. Harris, and I. P. Perkin, 2000, *J. Phys.: Condens. Matter* **12**, 483.
- Bramwell, S. T. and M. J. P. Gingras, 2001, *Science* **294**, 1495.
- Bramwell, S. T., M. J. Harris, B. C. den Hertog, M. J. P. Gingras, J. S. Gardner, D. F. McMorrow, A. R. Wildes, A. L. Cornelius, J. D. M. Champion, R. G. Melko, and T. Fennell, 2001a, *Phys. Rev. Lett.* **87**, 047205.
- Bramwell, S. T., M. Shirai, and C. Ritter, 2004, *Institut Laue-Langevin Experimental Reports*, 5-31-1496.
- Bombardi, A., J. Rodriguez-Carvajal, S. Di Matteo, F. de Bergevin, L. Paolasini, P. Carretta, P. Millet, and R. Caciuffo, 2004, *J. Phys. Soc. Jpn.* **93**, 027202.
- Brixner, L. H., 1964, *Inorg. Chem.* **3**, 1065.
- Canals, B. and C. Lacroix, 1998, *Phys. Rev. Lett.* **80**, 2933.
- Canals, B. and C. Lacroix, 2000, *Phys. Rev. B* **61**, 1149.
- Cannella, V. and J. A. Mydosh, 1972, *Phys. Rev. B* **6**, 4220.
- Cao, N., T. Timusk, N. P. Raju, J. E. Greedan, and P. Gougeon, 1995, *J. Phys.: Condens. Matter* **7**, 2489.
- Carcia, P. F., A. Ferretti, and A. Suna, 1982, *J. Appl. Phys.* **53**, 5282.
- Cashion, J. D., D. B. Prowse, and A. Vas, 1973, *J. Phys. C* **6**, 2611.
- Castelnovo, C., R. Moessner, and S. L. Sondhi, 2008, *Nature* **451**, 42.
- Cépas, O., and B. S. Shastry, 2004, *Phys. Rev. B* **69**, 184402.
- Cépas, O., A. P. Young, and B. S. Shastry, 2005, *Phys. Rev. B* **72**, 184408.
- Chalker, J. T., P. C. W. Holdsworth, and E. F. Shender, 1992, *Phys. Rev. Lett.* **68**, 855.
- Champion, J. D. M., A. S. Wills, T. Fennell, S. T. Bramwell, J. S. Gardner, and M. A. Green, 2001, *Phys. Rev. B* **64**, 140407R.
- Champion, J. D. M., M. J. Harris, P. C. W. Holdsworth, A. S. Wills, G. Balakrishnan, S. T. Bramwell, E. Čížmár, T. Fennell, J. S. Gardner, J. Lago, D. F. McMorrow, M. Orendáč, A. Orendáčová, D. M^cK. Paul, R. I. Smith, M. T. F. Telling, and A. Wildes, 2003, *Phys. Rev. B* **68**, 020401.
- Champion, J. D. M. and P. C. W. Holdsworth, 2004, *J. Phys.: Condens. Matter* **16**, S665.
- Chandra, P. and P. Coleman, 1995, in *Strongly Interacting Fermions and High Temperature Superconductivity*, edited by B. Douçot and J. Zinn-Justin (North-Holland), p. 495.
- Chapuis, Y., A. Yaouanc, P. Dalmas de Réotier, S. Pouget, P. Fouquet, A. Cervellino, and A. Forget, 2007, *J. Phys.: Condens. Matter* **19**, 446206.
- Chen, D. and R. Xu, 1998, *Mat. Res. Bull.* **33**, 409.
- Cheong, S.-W., H. Y. Hwang, B. Batlogg, and L. W. Rupp, Jr., 1996, *Solid State Comm.* **98**, 163.
- Coey, J. M. D., 1987, *Can. J. Phys.* **65**, 1210.
- Cornelius, A. L., and J. S. Gardner, 2001, *Phys. Rev. B* **64**, 060406.
- Corruccini, L. R., and S. J. White, 1993, *Phys. Rev. B* **47**, 773.
- Dalmas de Réotier, P., A. Yaouanc, P. C. M. Gubbens, C. T. Kaiser, C. Baines, and P. J. C. King, 2003, *Phys. Rev. Lett.* **91**, 167201.
- Dalmas de Réotier, P., A. Yaouanc, L. Keller, A. Cervellino, B. Roessli, C. Baines, A. Forget, C. Vaju, P. C. M. Gubbens, A. Amato, and P. J. C. King, 2006, *Phys. Rev. Lett.* **96**, 127202.
- Del Maestro, A. G. and M. J. P. Gingras, 2004, *J. Phys.: Condens. Matter* **16**, 3339.
- Del Maestro, A. G. and M. J. P. Gingras, 2007, *Phys. Rev. B* **76**, 064418.
- den Hertog B. C. and M. J. P. Gingras, 2000, *Phys. Rev. Lett.* **84**, 3430.
- Diep, H. T., Ed., 1994, *Magnetic Systems with Competing Interactions (Frustrated Spin Systems)*, (World Scientific, Singapore).
- Diep, H. T., Ed., 2004, *Frustrated Spin Systems*, (World Scientific Publishing, Singapore).
- Donohue, P. C., J. M. Longo, R. D. Rosenstein, and L. Katz, 1965, *Inorg. Chem.* **4**, 1152.
- Dunsiger, S. R., R. F. Kiefl, K. H. Chow, B. D. Gaulin, M. J. P. Gingras, J. E. Greedan, A. Keren, K. Kojima, G. M. Luke, W. A. MacFarlane, N. P. Raju, J. E. Sonier, Y. Uemura, and W. D. Wu, 1996, *Phys. Rev. B* **54**, 9019.
- Dunsiger, S. R., R. F. Kiefl, K. H. Chow, B. D. Gaulin, M. J. P. Gingras, J. E. Greedan, A. Keren, K. Kojima, G. M. Luke, W. A. MacFarlane, N. P. Raju, J. E. Sonier, Y. Uemura, and W. D. Wu, 1996a, *J. Appl. Phys.* **79**, 6636.
- Dunsiger S. R., J. S. Gardner, J. A. Chakhalian, A. L. Cornelius, J. Jaime, R. F. Kiefl, R. Movshovich, W. A. MacFarlane, R. I. Miller, J. E. Sonier, and B. D. Gaulin, 2000, *Phys. Rev. Lett.* **85**, 3504.
- Dunsiger, S. R., R. F. Kiefl, J. A. Chakhalian, J. E. Greedan, W. A. MacFarlane, R. I. Miller, G. D. Morris, A. N. Price, N. P. Raju, and J. E. Sonier, 2006, *Phys. Rev. B* **73**, 172418.
- Dupuis, V., E. Vincent, J. Hammann, J. E. Greedan, and A. S. Wills, 2002, *J. Appl. Phys.* **91**, 8384.
- Ehlers, G., A. L. Cornelius, M. Orendáč, M. Kajnaková, T. Fennell, S. T. Bramwell, and J. S. Gardner, 2003, *J. Phys.: Condens. Matter* **15**, L9.
- Ehlers, G., A. L. Cornelius, T. Fennell, M. Koza, S. T. Bramwell, and J. S. Gardner, 2004, *J. Phys.: Condens. Matter* **16**, S635.
- Ehlers, G., 2006, *J. Phys.: Condens. Matter* **18**, R231.
- Ehlers, G., J. S. Gardner, C. H. Booth, M. Daniel, K. C. Kam, A. K. Cheetham, D. Antonio, H. E. Brooks, A. L. Cornelius, S. T. Bramwell, J. Lago, W. Haussler, and N. Rosov, 2006a, *Phys. Rev. B* **73**, 174429.
- Elhajal, M., B. Canals, R. Sunyer, and C. Lacroix, 2005, *Phys. Rev. B* **71**, 094420.
- Enjalran, M. and M. J. P. Gingras, 2003, *arXiv:cond-mat/0307152*.
- Enjalran, M. and M. J. P. Gingras, 2004, *Phys. Rev. B* **70**, 174426.

- Erwing, R. C., W. J. Weber, and J. Lian, 2004, *J. Appl. Phys.* **95**, 5949.
- Fazekas, P. and P. W. Anderson, 1974, *Philos. Mag.* **30**, 432.
- Fennell, T., O. A. Petrenko, B. Fåk, S. T. Bramwell, M. Enjalran, T. Yavors'kii, M. J. P. Gingras, R. G. Melko, and G. Balakrishnan, 2004, *Phys. Rev. B* **70**, 134408.
- Fennell, T., O. A. Petrenko, B. Fåk, J. S. Gardner, S. T. Bramwell, and B. Ouladdiaf, 2005, *Phys. Rev. B* **72**, 224411.
- Fennell, T., S. T. Bramwell, D. F. McMorrow, P. Manuel, and A. R. Wildes, 2007, *Nature Physics* **3**, 566.
- Finn, C. P. B., R. Orbach, and W. P. Wolf, 1961, *Proc. Phys. Soc.* **77**, 261.
- Flood, D. J., 1974, *J. Appl. Phys.* **45**, 4041.
- Fujinaka, H., N. Kinomura, M. Koizumi, Y. Miyamoto, and S. Kume, 1979, *Mat. Res. Bull.* **14**, 1133.
- Fukazawa, H., and Y. Maeno, 2002, *J. Phys. Soc. Jpn.* **71**, 2578.
- Fukazawa, H., R. G. Melko, R. Higashinaka, Y. Maeno, and M. J. P. Gingras, 2002a, *Phys. Rev. B* **65**, 054410.
- Gaertner, H. R., 1930, *Neues Jb. Mineralog., Geol. Palaontol., Beilage-Bd. Abt. A* **61**, 1.
- Gardner, J. S., B. D. Gaulin, and D. M. Paul, 1998, *J. Crystal Growth* **191**, 740.
- Gardner, J. S., S. R. Dunsiger, B. D. Gaulin, M. J. P. Gingras, J. E. Greedan, R. F. Kiefl, M. D. Lumsden, W. A. MacFarlane, N. P. Raju, J. E. Sonier, I. Swainson, and Z. Tun, 1999, *Phys. Rev. Lett.* **82**, 1012.
- Gardner, J. S., B. D. Gaulin, S.-H. Lee, C. Broholm, N. P. Raju, and J. E. Greedan, 1999a, *Phys. Rev. Lett.* **83**, 211.
- Gardner, J. S., B. D. Gaulin, A. J. Berlinsky, P. Waldron, S. R. Dunsiger, N. P. Raju, and J. E. Greedan, 2001, *Phys. Rev. B* **64**, 224416.
- Gardner, J. S., G. Ehlers, R. H. Heffner, and F. Mezei, 2001a, *J. Magn. Magn. Mater.* **226-230**, 460.
- Gardner, J. S., A. Keren, G. Ehlers, C. Stock, E. Segal, J. M. Roper, B. Fåk, P. R. Hammar, M. B. Stone, D. H. Reich, and B. D. Gaulin, 2003, *Phys. Rev. B* **68**, 180401.
- Gardner, J. S., G. Ehlers, S. T. Bramwell, and B. D. Gaulin, 2004, *J. Phys.: Condens. Matter* **16**, S643.
- Gardner, J. S., G. Ehlers, N. Rosov, R. W. Erwin, and C. Petrovic, 2004a, *Phys. Rev. B* **70**, 180404(R).
- Gardner, J. S., A. L. Cornelius, L. J. Chang, M. Prager, Th. Brökel, and G. Ehlers, 2005, *J. Phys.: Condens. Matter* **17**, 7089.
- Gaulin, B. D., J. N. Reimers, T. E. Mason, J. E. Greedan, and Z. Tun, 1992, *Phys. Rev. Lett.* **69**, 3244.
- Gaulin, B. D., 1994, *Hyperfine Interactions* **85**, 159.
- Ghosh, S., R., Parthasarathy, T. F. Rosenbaum, and G. Aeppli, 2002, *Science* **296**, 2195.
- Gingras, M. J. P., C. V. Stager, B. D. Gaulin, N. P. Raju, and J. E. Greedan, 1996, *J. Appl. Phys.* **79**, 6170.
- Gingras, M. J. P., C. V. Stager, N. P. Raju, B. D. Gaulin, and J. E. Greedan, 1997, *Phys. Rev. Lett.* **78**, 947.
- Gingras, M. J. P., B. C. den Hertog, M. Faucher, J. S. Gardner, S. R. Dunsiger, L. J. Chang, B. D. Gaulin, N. P. Raju, and J. E. Greedan, 2000, *Phys. Rev. B* **68**, 6496.
- Gingras M. J. P., and B. C. den Hertog, 2001, *Can. J. Phys.* **79**, 1339.
- Greedan, J. E., M. Sato, X. Yan, and F. S. Razavi, 1986, *Sol. State Comm.* **59**, 895.
- Greedan, J. E., M. Sato, N. Ali, and W. R. Datars, 1987, *J. Solid State Chem.* **68**, 300.
- Greedan, J. E., J. N. Reimers, S. L. Penny, and C. V. Stager, 1990, *J. Appl. Phys.* **67**, 5967.
- Greedan, J. E., J. N. Reimers, C. V. Stager, and S. L. Penny, 1991, *Phys. Rev. B* **43**, 5682.
- Greedan, J. E., 1992a, in *Landolt-Bornstein New Series*, ed. H. P. J. Wijn (Springer-Verlag Berlin Heidelberg.), **27**, 100.
- Greedan, J. E., J. Avelar and M. A. Subramanian, 1992b, *Sol. State Comm.* **82**, 797.
- Greedan, J. E., N. P. Raju, A. Maignan, C. Simon, J. S. Pedersen, A. M. Niraimathi, E. Gmelin and M. A. Subramanian, 1996, *Phys. Rev. B* **54**, 7189.
- Greedan, J. E., N. P. Raju, and M. A. Subramanian, 1996a, *Solid State Comm.* **99**, 399.
- Greedan, J. E., 2001, *J. Materials Chem.* **11**, 37.
- Greedan, J. E., 2006, *J. Alloys and Compounds.* **408**, 444.
- Gurgul, J., M. Rams, Ż. Świątkowska, R. Kmieć, and K. Tomala, 2007, *Phys. Rev. B* **75**, 064426.
- Han, S.-W., J. S. Gardner, and C. H. Booth, 2004, *Phys. Rev. B* **69**, 024416.
- Haldane, F. D. M., 1983, *Phys. Rev. Lett.* **50**, 1153.
- Hanasaki, N., M. Kinuhara, I. Kézsmárki, S. Iguchi, S. Miyasaka, N. Takeshita, C. Terakura, H. Takagi, and Y. Tokura, 2006, *Phys. Rev. Lett.* **96**, 116403.
- Hanasaki, N., K. Watanabe, T. Ohtsuka, I. Kezmarki, S. Iguchi, S. Miyasaka, and Y. Tokura, 2007, *Phys. Rev. Lett.* **99**, 086401.
- Hanawa, M., Y. Muraoka, T. Sakakibara, T. Yamaura, and Z. Hiroi, 2001, *Phys. Rev. Lett.* **87**, 187001.
- Harris, A. B., A. J. Berlinsky, and C. Bruder, 1991, *J. Appl. Phys.* **69**, 5200.
- Harris, M. J., M. P. Zinkin, Z. Tun, B. M. Wanklyn, and I. P. Swainson, 1994, *Phys. Rev. Lett.* **73**, 189.
- Harris, M. J., S. T. Bramwell, D. F. McMorrow, T. Zeiske, and K. W. Godfrey, 1997, *Phys. Rev. Lett.* **79**, 2554.
- Harris, M. J., S. T. Bramwell, P. C. W. Holdsworth, and J. D. Champion, 1998, *Phys. Rev. Lett.* **81**, 4496.
- Harris, M. J., S. T. Bramwell, T. Zeiske, D. F. McMorrow, and P. J. C. King, 1998a, *J. Magn. Magn. Mater.* **177**, 757.
- Harrison, A., 2004, *J. Phys.: Condens. Matter* **16**, S553.
- Hassan, A. K., L. P. Levy, C. Darie, and P. Strobel, 2003, *Phys. Rev. B* **67**, 214432.
- He, J., R. Jin, B. C. Chakoumakos, J. S. Gardner, D. Mandrus, and T. M. Tritt, 2007, *J. Electronic Materials* **36**, 740.
- Higashinaka, R., H. Fukazawa, D. Yanagishima, and Y. Maeno, 2002, *J. Phys. Chem. Solids* **63**, 1043.
- Higashinaka, R., H. Fukazawa, and Y. Maeno, 2003, *Phys. Rev. B* **68**, 014415.
- Higashinaka, R., H. Fukazawa, and Y. Maeno, 2003a, *Physica B* **329**, 1040.
- Higashinaka, R., H. Fukazawa, K. Deguchi, and Y. Maeno, 2004, *J. Phys.: Condens. Matter* **16**, S679.
- Hiroi, Z., K. Matsuhira, S. Takagi, T. Tayama, and T. Sakakibara, 2003, *J. Phys. Soc. Jpn.* **72**, 411.
- Hiroi, Z., K. Matsuhira, and M. Ogata, 2003a, *J. Phys. Soc. Jpn.* **72**, 3045.
- Hizi, U., and C. L. Henley, 2007, *J. Phys.: Condens. Matter* **19**, 145268.
- Hodges, J. A., P. Bonville, A. Forget, M. Rams, K. Królas, and G. Dhalenne, 2001, *J. Phys.: Condens. Matter* **13**, 9301.
- Hodges, J. A., P. Bonville, A. Forget, A. Yaouanc, P. Dalmás de Réotier, G. André, M. Rams, K. Królas, C. Ritter, P. C. M. Gubbens, C. T. Kaiser, P. C. King, and C. Baines,

- 2002, Phys. Rev. Lett. **88**, 077204.
- Hodges, J. A., P. Bonville, A. Forget, J. P. Sanchez, P. Vulliet, M. Rams, and K. Królas, 2003, Eur. Phys. J. B **33**, 173.
- Hoekstra, H. R., and F. Gallagher, 1968, Inorg. Chem. **7**, 2553.
- Horowitz, H. S., J. M. Longo, and H. H. Horowitz, 1983, J. Electrochem. Soc. **130**, 1851.
- Houtappel, R. M. F., 1950, Physica B **16**, 425.
- Hubert, P. H., 1974, Bull. Chim. Soc. Fr. **11**, 2385.
- Hubert, P. H., 1975, Bull. Chim. Soc. Fr. **11-1**, 2463.
- Hüfner, S., 1978, *Optical Spectra of Transparent Rare Earth Compounds*, (Academic Press), 38.
- Iikubo, S., S. Yoshii, T. Kageyama, K. Oda, Y. Kondo, K. Murata, and M. Sato, 2001, J. Phys. Soc. Jpn. **70**, 212.
- Isakov, S. V., R. Moessner, and S. L. Sondhi, 2005, Phys. Rev. Lett. **95**, 217201.
- Ito, M., Y. Yasui, M. Kanada, H. Harashina, S. Yoshii, K. Murata, M. Sato, H. Okumura, and K. Kakurai, 2001, J. Phys. Chem. Solids **62**, 337.
- Jana, Y. M., A. Sengupta, and D. Ghosh, 2002, J. Magn. Magn. Materials **248**, 7.
- Jaubert, L., J. T., Chalker, P. C. W., Holdsworth, and R., Moessner, 2008, Phys. Rev. Lett. **100**, 067207.
- Jin, R., J. He, S. McCall, C. S. Alexander, F. Drymiotis, and D. Mandrus, 2001, Phys. Rev. B **64**, 180503.
- Jönsson, P. E., R. Mathieu, W. Wernsdorfer, A. M. Tkachuk, and B. Barbara, 2007, Phys. Rev. Lett. **98**, 256403.
- Kadowaki, H., Y. Ishii, K. Matsuhira, and Y. Hinatsu, 2002, Phys. Rev. B **65**, 144421.
- Kageyama, T., S. Iikubo, S. Yoshii, Y. Kondo, M. Sato, and Y. Iye, 2001, J. Phys. Soc. Jpn. **70**, 3006.
- Kao, Y.-J., M. Enjalran, A. G. Del Maestro, H. R. Molavian, and M. J. P. Gingras, 2003, Phys. Rev. B **68**, 172407.
- Katsufuji, T., H. Y. Hwang, and S.-W. Cheong, 2000, Phys. Rev. Lett. **84**, 1998.
- Kawamura, H., 1988, Phys. Rev. B **38**, 4916.
- Ke, X., R. S., Freitas, B. G. Ueland, G. C. Lau, M. L. Dahlberg, R. J. Cava, R. Moessner, and P. Schiffer, 2007, Phys. Rev. Lett. **99**, 137203.
- Keren, A., and J. S. Gardner, 2001, Phys. Rev. Lett. **87**, 177201.
- Keren, A., J. S. Gardner, G. Ehlers, A. Fukaya E. Segal, and Y. J. Uemura, 2004, Phys. Rev. Lett. **92**, 107204.
- Kézsmárki, I., N., Hanasaki, D., Hashimoto, S., Iguchi, Y., Taguchi, S. Miyasaka, and Y. Tokura, 2004, Phys. Rev. Lett. **93**, 266401.
- Kézsmárki, I., S., Onoda, Y., Taguchi, T., Ogasawara, M., Matsubara, S., Iguchi, N., Hanasaki, N. Nagaosa, and Y. Tokura, 2005, Phys. Rev. B **72**, 094427.
- Kézsmárki, I., N. Hanasaki, K. Watanabe, S. Iguchi, Y. Taguchi, S. Miyasaka, and Y. Tokura, 2006, Phys. Rev. B **73**, 125122.
- Kido, H., S. Komarneni, and R. Roy, 1991, J. Am. Cer. Soc. **74**, 422.
- Kim, H. C., Y. Jo, J. G. Park, S. W. Cheong, M. Ulharz, C. Pfleiderer, and H. V. Lohneysen, 2005, Physica B **359**, 1246.
- Kmieć, R., Ż. Świątkowska, J. Gurgul, M. Rams, A. Zarzycki, and K. Tomala, 2006, Phys. Rev. B **74**, 104425.
- Kwei, G. H., C. H. Booth, F. Bridges, and M. A. Subramanian, 1997 Phys. Rev. B **55**, R688.
- Ladieu, F., F. Bert, V. Dupuis, E. Vincent, and J. Hammann, 2004, J. Phys. Condens. Matter **16**, S735.
- Lago, J., T. Lancaster, S. J. Blundell, S. T. Bramwell, F. L. Pratt, M. Shirai, and C. Baines, 2005, J. Phys.: Condens. Matter **17**, 979.
- Lago, J., S. J. Blundell, and C. Baines, 2007, J. Phys.: Condens. Matter **19**, 326210.
- Läuchli, A., S. Dommanger, B. Normand, and F. Mila, 2007, Phys. Rev. B **76**, 144413.
- Lau, G. C., R. S. Freitas, B. G. Ueland, B. D. Muegge, E. L. Duncan, P. Schiffer, and R. J. Cava, 2006, Nature Physics **2**, 249.
- Lau, G. C., B. D. Muegge, T. M. McQueen, E. L. Duncan, and R. J. Cava, 2006a, J. Solid State Chem. **179**, 3126.
- Lau, G. C., R. S. Freitas, B. G. Ueland, M. L. Dahlberg, Q. Huang, H. W. Zandbergen, P. Schiffer, and R. J. Cava, 2007, Phys. Rev. B. **76**, 054430.
- Lazarev, V. B., and V. B. Shaplygin, 1978, Mat. Res. Bull. **13**, 229.
- Lecheminant, P., P. Bernu, C. Lhuillier, L. Pierre, and P. Sindzingre, 1997, Phys. Rev. B **56**, 2521.
- Lee, S. H., C. Broholm, T. H. Kim, W. Ratcliff, and S.-W. Cheong, 2000, Phys. Rev. Lett. **84**, 3718.
- Lee, S. H., C. Broholm, W. Ratcliff, G. Gasparovic, Q. Huang, T. H. Kim, and S.-W. Cheong, 2002, Nature **418**, 856.
- Lee, L. W. and A. P. Young, 2003, Phys. Rev. Lett. **90**, 227203.
- Lee, Seongsu, J.-G.. Park, D. T. Adroja, D. Khomskii, S. Streltsov, K. A. McEwen, H. Sakai, K. Yoshimura, V. I. Anisimov, D. Mori, R. Kanno, and R. I. Ibberson, 2006, Nature Materials **5**, 471.
- Lee, L. W., and A. P. Young, 2007, Phys. Rev. B **76**, 024405.
- Lozano, A. D., J. E. Greedan, and T. Proffen, 2007, unpublished.
- Luo, G., S. T. Hess, and L. R. Corruccini, 2001, Phys. Lett. A **291**, 306.
- Lynn, J. W., L. Vasiliiu-Doloc, and M. A. Subramanian, 1998, Phys. Rev. Lett. **80**, 4582.
- Machida, Y., S. Nakatsuji, H. Tonomura, T. Tayama, T. Sakakibara, J. van Duijn, C. Broholm, and Y. Maeno, 2005, J. Phys. Chem. Solids **66**, 1435.
- Machida, Y., S. Nakatsuji, Y. Maeno, T. Yamada, T. Tayama, and T. Sakakibara, 2007, J. Magn. Magn. Mater. **310**, 1079.
- Mailhot, A. and M. L. Plumer, 1993, Phys. Rev. B **48**, 9881.
- Mandiram, A. and A. Gopalakrishnan, 1980, Indian J. Chem. **19A**, 1042.
- Mandrus, D., J. R.. Thompson, R. Gaal, L. Forro, J. C. Bryan, B. C. Chakoumakos, L. M. Woods, B.C. Sales, R. S. Fishman, and V. Keppens, 2001, Phys. Rev. B **63**, 195104.
- Matsuda, M., H. Ueda, A. Kikkawa, Y. Tanaka, K. Katsumata, Y. Narumi, T. Inami, Y. Ueda, and S.-H. Lee, 2007, Nature Physics **3**, 397.
- Matsuhira, K., Y. Hinatsu, K. Tenya, and T. Sakakibara, 2000, J. Phys.: Condens. Matter **12**, L649.
- Matsuhira, K., Y. Hinatsu, and T. Sakakibara, 2001, J. Phys.: Condens. Matter **13**, L737.
- Matsuhira, K., Y. Hinatsu, K. Tenya, H. Amitsuka, and T. Sakakibara, 2002, J. Phys. Soc. Jpn. **71**, 1576.
- Matsuhira, K., Z. Hiroi, T. Tayama, S. Takagi, and T. Sakakibara, 2002a, J. Phys.: Condens. Matter **14**, L559.
- Matsuhira, K., C. Sekine, C. Paulsen, and Y. Hinatsu, 2004, J. Magn. Magn. Matter. **272**, E981.
- Matsuhira, K., M. Wakeshima, R. Nakanishi, T. Yamada, W. Kawano, S. Tagaki, and Y. Hinatsu, 2007, J. Phys. Soc. Jpn. **76**, 043706.
- McCarthy, G. J., 1971, Mat. Res. Bull. **6**, 31.

- Melko, R. G., B. C. den Hertog, and M. J. P. Gingras, 2001, Phys. Rev. Lett. **87**, 067203.
- Melko, R. G. and M. J. P. Gingras, 2004, J. Phys.: Condens. Matter **16**, R1277.
- Mila, F., Ed., 2008, *Highly Frustrated Magnetism*, (Springer, Berlin).
- Millican, J. N., R. T. Macaluso, S. Nakatsuji, Y. Machida, Y. Maeno, and J. Y. Chan, 2007, Mat. Res. Bull. **42**, 928.
- Minervini, L., R. W. Grimes, Y. Tabira, R. L. Withers, and K. E. Sickafus, 2002, Philos. Magazine A **82**, 123.
- Mirebeau, I., I. N. Goncharenko, P. Cadavez-Peres, S. T. Bramwell, M. J. P. Gingras, and J. S. Gardner, 2002, Nature **420**, 54.
- Mirebeau, I. and I. N. Goncharenko, 2004, Physica B **350**, 250.
- Mirebeau, I., I. N. Goncharenko, D. Dhailenne, and A. Revcolevschi, 2004a, Phys. Rev. Lett. **93**, 187204.
- Mirebeau, I., A. Apetrei, J. Rodríguez-Carvajal, P. Bonville, A. Forget, D. Colson, V. Glazkov, J. P. Sanchez, O. Isnard, and E. Suard, 2005, Phys. Rev. Lett. **94**, 246402.
- Mirebeau, I., A. Apetrei, I. N. Goncharenko, and R. Moessner, 2006, Physica B **385**, 307.
- Mirebeau, I., A. Apetrei, I. N. Goncharenko, D. Andreica, P. Bonville, J. P. Sanchez, A. Amato, E. Suard, W. A. Crichton, A. Forget, and D. Colson, 2006a, Phys. Rev. B **74**, 174414.
- Mirebeau, I., P. Bonville, and M. Hennion, 2007, Phys. Rev. B **76**, 184436.
- Mito, M., S. Kuwabara, K. Matsuhira, H. Deguchi, S. Takagi, and Z. Hiroi, 2007, J. Magn. Mag. Mater. **310**, e432.
- Miyoshi, K., Y. Nishimura, K. Honda, K. Fujiwara, and J. Takeuchi, 2000, J. Phys. Soc. Jpn. **69**, 3517.
- Miyoshi, K., T. Yamashita, K. Fujiwara, and J. Takeuchi, 2002, Physica B **312**, 706.
- Miyoshi, K., Y. Takamatsu, and J. Takeuchi, 2006, J. Phys. Soc. Jpn. **75**, 065001.
- Moessner, R. and J. T. Chalker, 1998, Phys. Rev. B. **58**, 12049.
- Moessner, R. and J. T. Chalker, 1998a, Phys. Rev. Lett. **80**, 2929.
- Moessner, R., 2001, Can. J. Phys. **79**, 1283.
- Moessner, R. and S. L. Sondhi, 2003, Phys. Rev. B. **68**, 064411.
- Moessner, R., S. L. Sondhi, and M. O. Goerbig, 2006, Phys. Rev. B **73**, 094430.
- Molavian H. R., M. J. P. Gingras, and B. Canals, 2007, Phys. Rev. Lett. **98**, 157204.
- Moritomo, Y., Sh. Xu, A. Machida, T. Katsufuji, E. Nishibori, M. Takata, S. Sakata, and S.-W. Cheong, 2001, Phys. Rev. B. **63**, 144425.
- Munenaka, T. and Hirohiko S., 2006, J. Phys. Soc. Jpn. **75**, 103801.
- Nakatsuji, S., Y. Machida, Y. Maeno, T. Tayama, T. Sakakibara, J. van Duijn, L. Balicas, J. N. Millican, R. T. Macaluso, and J. Y. Chan, 2006, Phys. Rev. Lett. **96**, 087204.
- Néel, L., 1948, Ann. Phys. **3**, 137.
- Nussinov, Z., C. D. Batista, B. Normand, and S. A. Trugman, 2007, Phys. Rev. B **75**, 094411.
- Obradors, X., A. Labarta, A. Isalgue, J. Tejada, J. Rodriguez, and M. Pernet, 1988, Solid State Commun. **65**, 189.
- Okamoto, Y., M. Nohara, H. Aruga-Katori, and H. Takagi, 2007, Phys. Rev. Lett. **99**, 137207.
- Orbach R., 1961, Proc. Phys. Soc. **77**, 821.
- Orendác, M., J. Hanko, E. Čizmar, A. Orendáčová, J. Shirai, and S. T. Bramwell, 2007, Phys. Rev. B. **75**, 104425.
- Palmer, S. E. and J. T. Chalker, 2000, Phys. Rev. B **62**, 488.
- Park, J. G., Y. Jo, J. Park, H. C. Kim, H. C. Ri, S. Xu, Y. Moritomo, and S. W. Cheong, 2003, Physica B **328**, 90.
- Pauling, L., 1935, J. Am. Chem. Soc. **57**, 2680.
- Penc, K., N. Shannon, and H. Shiba, 2004, Phys. Rev. Lett. **93**, 197203.
- Petrenko O. A., C. Ritter, M. Yethiraj, and D. M. Paul, 1998, Phys. Rev. Lett. **80**, 4570.
- Petrenko, O. A., M. R. Lees, G. Balakrishnan, and D. M^cK Paul, 2004, Phys. Rev. B **70**, 012402.
- Pike, G. E. and C. H. Seager, 1977, J. Appl. Phys. **53**, 5152.
- Pinettes, C., B. Canals, and C. Lacroix, 2002, Phys. Rev. B **66**, 024422.
- Poole, A., A. S. Wills, and E. Lelièvre-Berna, 2007, J. Phys.: Condens. Matter **19**, 452201.
- Proffen, Th., S. J. L. Billinge, T. Egami, and D. Louca, 2003, Z. Kristallogr. **218**, 132.
- Quilliam, J. A., K. A. Ross, A. G. Del Maestro, M. J. P. Gingras, L. R. Corruccini, and J. B. Kycia, 2007, Phys. Rev. Lett. **99**, 097201.
- Ramirez, A.P., 1994, Ann. Rev. Mater. Sci. **24**, 453.
- Ramirez, A. P. and M. A. Subramanian, 1997, Science **277**, 546.
- Ramirez, A. P., A. Hayashi, R. J. Cava, R. Siddharthan, and B. S. Shastry, 1999, Nature **399**, 333.
- Ramirez, A. P., B. S. Shastry, A. Hayashi, J. J. Krajewski, D. A. Huse, and R. J. Cava, 2002, Phys. Rev. Lett. **89**, 067202.
- Ranganathan, R., G. Rangarajan, R. Srinivasan, M. A. Subramanian, and G. V. Subba Rao, 1983, J. Low Temp. Phys. **52**, 481.
- Raju, N. P., E. Gmelin, and R. Kremer, 1992, Phys. Rev. B **46**, 5405.
- Raju, N. P., J. E. Greedan, and M. A. Subramanian, 1994, Phys. Rev. B **49**, 1086.
- Raju, N. P. and P. Gougeon, 1995, unpublished
- Raju, N. P., M. Dion, M. J. P. Gingras, T. E. Mason, and J. E. Greedan, 1999, Phys. Rev. B **59**, 14489.
- Reich, D. H., T. F. Rosenbaum, and G. Aeppli, 1987, Phys. Rev. Lett. **59**, 1969.
- Reich, D. H., B. Ellman, Y. Yang, T. F. Rosenbaum, G. Aeppli, and D. P. Belanger, 1990, Phys. Rev. B **42**, 4631.
- Reimers, J. N., J. E. Greedan, and M. Sato, 1988, J. Solid State Chem. **72**, 390.
- Reimers, J. N., J. E. Greedan, R. K. Kremer, E. Gmelin, and M. A. Subramanian, 1991, Phys. Rev. B **43**, 3387.
- Reimers, J. N., A. J. Berlinsky, and A.-C. Shi, 1991a, Phys. Rev. B **43**, 865.
- Reimers, J. N., 1992, Phys. Rev. B **45**, 7287.
- Reimers, J. N., J. E. Greedan, and M. Björgvinsson, 1992, Phys. Rev. B **45**, 7295.
- Reimers, J. N., and A. J. Berlinsky, 1993, Phys. Rev. B **48**, 9539.
- Rhyne, J. J., 1985, IEEE Trans. Magn. **21**, 1990.
- Rhyne, J. J. and G. E. Fish, 1985, J. Appl. Phys. **57**, 3407.
- Rosenfeld, H. D. and M. A. Subramanian, 1996, J. Solid State Chem. **125**, 278.
- Rosenkranz, S., A. P. Ramirez, A. Hayashi, R. J. Cava, R. Siddharthan, and B. S. Shastry, 2000, J. Appl. Phys. **87**, 5914.
- Roth, R. S., 1956, J. Res. Natl. Bur. Stds. **56**, 17.
- Ruff, J. P. C., R. G. Melko, and M. J. P. Gingras, 2005, Phys. Rev. Lett. **95**, 097202.

- Ruff, J. P. C., B. D. Gaulin, J. P. Castellan, K. C. Rule, J. P. Clancy, J. Rodrigues, and H. A. Dabkowska, 2007, *Phys. Rev. Lett.* **99**, 237202.
- Rule, K. C., J. P. C. Ruff, B. D. Gaulin, S. R. Dunsiger, J. S. Gardner, J. P. Clancy, M. J. Lewis, H. A. Dabkowska, I. Mirebeau, P. Manuel, Y. Qiu, and J. R. D. Copley, 2006, *Phys. Rev. Lett.* **96**, 177201.
- Rushbrooke, G. S., and P. J. Wood, 1958, *Mol. Phys.* **1**, 257.
- Sagi, E., O. Ofer, A. Keren, and J. S. Gardner, 2005, *Phys. Rev. Lett.* **94**, 237202.
- Saha, S., D. V. S. Muthu, C. Pascanut, N. Dragoe, R. Suryanarayanan, G. Dhalenne, A. Revcolevschi, S. M. Karmakar, S. Sharma, and A. K. Sood, 2006, *Phys. Rev. B* **74**, 064109.
- Sakai, H., K. Yoshimura, H. Ohno, H. Kato, S. Kambe, R. E. Walstedt, T. D. Matsuda, and Y. Haga, 2001, *J. Phys.: Condens. Matter* **13**, L785.
- Sakakibara, T., T. Tayama, K. Matsuhira, S. Takagi, and Z. Hiroi, 2004, *J. Magn. Mag. Matter.* **272**, 1312.
- Samara, G. A., E. L. Venturini, and L. A. Boatner, 2006, *J. Appl. Phys.* **100**, 074112.
- Sato, M., X. Yan, and J. E. Greedan, 1986, *Z. Anorg. Allg. Chem.* **540**, 177.
- Sato, M. and J. E. Greedan, 1987, *J. Sol. State Chem.* **67**, 248.
- Saunders, T. E. and J. T. Chalker, 2007, *Phys. Rev. Lett.* **98**, 157201.
- Schnelle, W. and R. K. Kremer, 2004, *J. Phys. Condens. Matter* **16**, S685.
- Schuck, G., S. M. Kazakov, K. Rogacki, N. D. Zhigadlo, and J. Karpinski, 2006, *Phys. Rev. B* **73**, 144506.
- Schiffer, P., A. P. Ramirez, D. A. Huse, and A. J. Valentino, 1994, *Phys. Rev. Lett.* **73**, 2500.
- Schiffer, P., A. P. Ramirez, W., Bao, and S.-W. Cheong, 1995, *Phys. Rev. Lett.* **75**, 3336.
- Schiffer, P., A. P. Ramirez, D. H., Huse, P. L. Gammel, U., Yaron, D. J. Bishop, and A. J. Valentino, 1995a, *Phys. Rev. Lett.* **74**, 2379.
- Schiffer, P., and A. P. Ramirez, 1996, *Comments Condens. Matter Phys.* **18**, 21.
- Schnelle, W., and R. K. Kremer, 2004, *J. Phys.: Condens. Matter* **16**, S685.
- Shender, E. F., V. P. Cherepanov, P. C. W. Holdsworth, and A. J. Berlinsky, 1993, *Phys. Rev. Lett.* **70**, 3812.
- Sherrington, D. and B. W. Southern, 1975, *J. Phys. F: Met. Phys.* **5**, L49.
- Shi, J., Z. Tang, B. P. Zhu, P. Huang, D. Yin, C. Z. Li, Y. Wang, and H. Wen, 2007, *J. Magn. Mag. Mate.* **310**, 1322.
- Shiga, M., K. Fujisawa, and H. Wada, 1993, *J. Phys. Soc. Jpn.* **62**, 1329.
- Shimakawa, Y., Y. Kubo, and T. Manako, 1996, *Nature* **379**, 53.
- Shimakawa, Y., Y. Kubo, N. Hamada, J. D. Jorgensen, Z. Hu, S. Short, M. Nohara, and H. Takagi, 1999, *Phys. Rev. B* **59**, 1249.
- Shimiz, Y., K. Miyagawa, K. Kanoda, M. Mitsuhiro, and M. Saito, 2006, *Phys. Rev. B* **73**, 140407(R).
- Shin-ike, T., G. Adachi, and J. Shiokawa, 1977, *Mat. Res. Bull.* **12**, 1149.
- Shirai, M. and S. T. Bramwell, 2007, Thesis Chapter, UCL and private communication.
- Shlyakhtina, A. V., L. G. Shcherbakova, A. V. Knotko, and A. V. Steblevskii, 2004, *J. Solid State Electrochem.* **8**, 661.
- Sickafus, K. E., L. Minervini, R. W. Grimes, J. A. Valdez, M. Ishimaru, F. Li, K. J. McClellan, and T. Hartmann, 2000, *Science* **289**, 748.
- Siddharthan, R., B. S. Shastry, A. P. Ramirez, A. Hayashi, R. J. Cava, and S. Rosenkranz, 1999, *Phys. Rev. Lett.* **83**, 1854.
- Sleight, A. W., and P. J. Bouchard, 1972, *Proc. 5th Mater. Res. Symp.* **364**, 227.
- Sleight, A. W., J. L. Gillson, J. F. Weiher, and W. Bindloss, 1974, *Solid State Commun.* **14**, 357.
- Snyder, J., J. S. Slusky, R. J. Cava, and P. Schiffer, 2001, *Nature* **413**, 48.
- Snyder, J., J. S. Slusky, R. J. Cava, and P. Schiffer, 2002, *Phys. Rev. B* **66**, 064432.
- Snyder, J., B. G. Ueland, J. S. Slusky, H. Karunadasa, R. J. Cava, A. Mizel, and P. Schiffer, 2003, *Phys. Rev. Lett.* **91**, 107201.
- Snyder, J., B. G. Ueland, J. S. Slusky, H. Karunadasa, R. J. Cava, and P. Schiffer, 2004, *Phys. Rev. B* **69**, 064414.
- Snyder, J., B. G. Ueland, A. Mizel, J. S. Slusky, H. Karunadasa, R. J. Cava, and P. Schiffer, 2004a, *Phys. Rev. B* **70**, 184431.
- Soderholm, L., J. E. Greedan, and M. F. Collins, 1980, *J. Solid State Chem.* **35**, 385.
- Solovyev, I., 2003, *Phys. Rev. B* **67**, 174406.
- Sosin, S. S., A. I. Smirnov, L. A. Prozorova, G. Balakrishnan, and M. E. Zhitomirsky, 2006, *Phys. Rev. B* **73**, 212402.
- Sosin, S. S., A. I. Smirnov, L. A. Prozorova, O. A. Petrenko, M. E. Zhitomirsky, and J. -P. Sanchez, 2006a, *J. Magn. Magn. Mater.* **310**, 1590.
- Sosin, S. S., L. A. Prozorova, A. I. Smirnov, P. Bonville, G. Jasmin -Le Bras, and O. A. Petrenko, 2007, *Cond-Mat.* 0709.4379.
- Stevens, K. W. H., 1952, *Proc. Phys. Soc. (London)* **A65**, 209.
- Stewart, J. R., G. Ehlers, A. S. Wills, S. T. Bramwell, and J. S. Gardner, 2004, *J. Phys.: Condens. Matter* **16**, L321.
- Stewart, J. R., G. Ehlers, and J. S. Gardner, 2004a, private communication.
- Subramanian, M. A., G. Aravamudan, and G. V. Subba Rao, 1983, *Prog. Solid State Chem.* **15**, 55.
- Subramanian, M. A., C. C. Torardi, D. C. Johnson, J. Pannetier, and A. W. Sleight, 1988, *J. Solid State Chem.* **72**, 24.
- Subramanian, M. A., and A. W., Sleight, 1993, in *Handbook on the Physics and Chemistry of Rare Earths*, ed. K. A. Gschneidner and L. Eyring (Elsevier Science Publishers B.V.), p. 225.
- Subramanian, M. A., B. H. Toby, A. P. Ramirez, W. J. Marshall, A. W. Sleight, and G. H. Kwei, 1996, *J. Solid State Chem.* **72**, 24.
- Sushko, Yu. V., Y. Kubo, Y. Shimakawa, and T. Manako, 1996, *Czechoslovak J. Phys.* **46**, 2003.
- Sushkov, A. B., O. Tchernyshyov, W. Ratcliff II, S. W. Cheong, and H. D. Drew, 2005, *Phys. Rev. Lett.* **94**, 137202.
- Tabata, Y., H. Kadowaki, K. Matsuhira, Z. Hiroi, N. Aso, E. Ressouche, and B. Fåk, 2006, *Phys. Rev. Lett.* **97**, 257205.
- Taguchi, Y. and Y. Tokura, 1999, *Phys. Rev. B* **60**, 10280.
- Taguchi, Y. and Y. Tokura, 2000, *Physica B* **284**, 1448.
- Taguchi, Y., Y. Oohara, H. Yoshizawa, N. Nagaosa, and Y. Tokura, 2001, *Science* **291**, 2573.
- Taguchi, Y., K. Ohgushi, and Y. Tokura, 2002, *Phys. Rev. B*

- 65**, 115102.
- Taguchi, Y., Y. Oohara, H. Yoshizawa, N. Nagaosa, T. Sasaki, S. Awaji, Y. Iwasa, T. Tayama, T. Sakakibara, S. Iguchi, K. Ohgushi, T. Ito, and Y. Tokura, 2004, *J. Phys.: Condens. Matter* **16**, S599.
- Taira, N., M. Wakeshima, and Y. Hinatsu, 1999, *J. Solid State Chem.* **144**, 216.
- Taira, N., M. Wakeshima, and Y. Hinatsu, 2001, *J. Phys.: Condens. Matter* **13**, 5527.
- Taira, N., Makoto W., Yukio H., Aya T., and Kenji O., 2003, *J. Solid State Chem.* **176**, 165.
- Tang, Z., C. Z. Li, D. Yin, B. P. Zhu, L. L. Wang, J. F. Wang, R. Xiong, Q. Q. Wang, and J. Shi, 2006, *Acta Physica Sinica* **55**, 6532.
- Tchernyshyov, O., R. Moessner, and S. L. Sondhi, 2002, *Phys. Rev. B* **66**, 064403.
- Tchernyshyov, O., R. Moessner, and S. L. Sondhi, 2006, *Europhys. Lett.* **73**, 278.
- Toulouse, G., 1977, *Commun. Phys.* **2**, 115.
- Troyanchuk, I. O., and V. N. Derkachenko, 1988, *Sov. Phys. Solid State* **30**, 2003.
- Troyanchuk, I. O., 1990, *Inorganic Materials* **26**, 182.
- Troyanchuk, I. O., N. V. Kasper, D. D. Khalyavin, H. Szymczak, and A. Nabialek, 1998, *Phys. Stat. Sol. A* **167**, 151.
- Tsuneishi, D., M. Ioki, and H. Kawamura, 2007, *J. Phys.: Condens. Matter* **19**, 145273.
- Ueda, H., H. A. Katori, H. Mitamura, T. Goto, and H. Takagi, 2005, *Phys. Rev. Lett.* **94**, 047202.
- Ueland, B. G., G. C. Lau, R. J. Cava, J. R. O'Brien, and P. Schiffer, 2006, *Phys. Rev. Lett.* **96**, 027216.
- Ueland, B. G., G. C. Lau, R. S. Freitas, J. Snyder, M. L. Dahlberg, B. D. Muegge, E. L. Duncan, R. J. Cava and P. Schiffer, 2008, *Phys. Rev. B* **77**, 144412.
- van Duijn, J., N. Hur, J. W. Taylor, Y. Qiu, Q. Huang, S. W. Cheong, C. Broholm, and T. Perring, 2008, *Phys. Rev. B* **77**, 020405.
- Velasco, P., J. A. Alonso, M. T. Casais, M. J. Martínez-Lope, J. L. Martínez, and M. T. Fernández-Díaz, 2002, *Phys. Rev. B* **66**, 174408.
- Villain, J., 1977, *J. Phys. C: Solid State Phys* **10**, 1717.
- Villain, J., 1979, *Z. Phys. B* **33**, 31.
- Wang, R. and A. W. Sleight, 1998, *Mater. Res. Bull.* **33**, 1005.
- Wanklyn, B., 1968, *J. Mater. Sci.* **3**, 395.
- Wannier, G. H., 1950, *Phys. Rev.* **79**, 357.
- Wannier, G. H., 1973, *Phys. Rev. B* **7**, 5017.
- White, S. J., M. R. Roser, J. Xu, J. T. van der Norrdaa, and L. R. Corruccini, 1993, *Phys. Rev. Lett.* **71**, 3553.
- Wiebe, C. R., J. S. Gardner, S.-J. Kim, G. M. Luke, A. S. Wills, B. D. Gaulin, J. E. Greedan, I. Swainson, Y. Qiu, and C. Y. Jones, 2004, *Phys. Rev. Lett.* **93**, 076403.
- Wills, A. S., R. Ballou, and C. Lacroix, 2002, *Phys. Rev. B* **66**, 144407.
- Wills, A. S., M. E. Zhitomirsky, B. Canals, J. P. Sanchez, P. Bonville, P. Dalmas de Réotier and A. Yaouanc, 2006, *J. Phys.: Condens. Matter* **18**, L37.
- Wu, W., D. Bitko, T. F. Rosenbaum, and G. Aeppli, 1993, *Phys. Rev. Lett.* **71**, 1919.
- Yafet, Y. and C. Kittel, 1952, *Phys. Rev.* **87**, 290.
- Yamamoto, A., P. A. Sharma, Y. Okamoto, A. Nakao, H. A. Katori, S. Niitaka, D. Hashizume, and H. Takagi, 2007, *J. Phys. Soc. Jpn.* **76**, 043703.
- Yamashita, Y., and K. Ueda, 2000, *Phys. Rev. Lett.* **85**, 4960.
- Yanagishima, D. and Y. Maeno, 2001, *J. Phys. Soc. Jpn.* **70**, 2880.
- Yaouanc, A., P. Dalmas de Réotier, V. Glazkov, C. Marin, P. Bonville, J. A. Hodges, P. C. M. Gubbens, S. Sakarya, and C. Baines, 2005, *Phys. Rev. Lett.* **95**, 047203.
- Yasui, Y., Y. Kondo, M. Kanada, M. Ito, H. Harashina, M. Sato, and K. Kakurai, 2001, *J. Phys. Soc. Japan* **70**, 284.
- Yasui, Y., M. Kanada, M. Ito, H. Harashina, M. Sato, H. Okumura, K. Kakurai, and H. Kadowaki, 2002, *J. Phys. Soc. Jpn.* **71**, 599.
- Yasui, Y., M. Soda, S. Iikubo, M. Ito, M. Sato, N. Hamaguchi, T. Matsushita, N. Wada, T. Takeuchi, N. Aso, and K. Kakurai, 2003, *J. Phys. Soc. Jpn.* **72**, 3014.
- Yasui, Y., S. Iikubo, H. Harashina, T. Kageyama, M. Ito, M. Sato, and K. Kakurai, 2003a, *J. Phys. Soc. Jpn.* **72**, 865.
- Yasui, Y., T. Kageyama, T. Moyoshi, H. Harashina, M. Soda, M. Sato, and K. Kakurai, 2006, *J. Phys. Soc. Jpn.* **75**, 084711.
- Yavors'kii, T., M. Enjalran, and M. J. P. Gingras, 2006, *Phys. Rev. Lett.* **97**, 267203.
- Yavors'kii, T., W. Apel, and H.-U. Everts, 2007, *Phys. Rev. B* **76**, 064430.
- Yavors'kii, T., T. Fennell, M. J. P. Gingras, and S. T. Bramwell, 2008, *Phys. Rev. Lett.* **101**, 037204.
- Yonezawa, S., Y. Muraoka, Y. Matsushita, and Z. Hiroi, 2004, *J. Phys.: Condens. Matter* **16**, L9.
- Yonezawa, S., Y. Muraoka, Y. Matsushita, and Z. Hiroi, 2004a, *J. Phys. Soc. Jpn.* **73**, 819.
- Yonezawa, S., Y. Muraoka, and Z. Hiroi 2004b, *J. Phys. Soc. Jpn.* **73**, 1655.
- Yoshida, S.-i., K. Nemoto, and K. Wada, 2004, *J. Phys. Soc. Jpn.* **73**, 1619.
- Yoshii, S. and M. Sato, 1999, *J. Phys. Soc. Jpn.* **68**, 3034.
- Yoshii, S., S. Iikubo, T. Kageyama, K. Oda, Y. Kondo, K. Murata, and M. Sato, 2000, *J. Phys. Soc. Jpn.* **69**, 3777.
- Zhang, F. X., J. Lian, U. Becker, L. M. Wang, J. Z. Hu, S. Saxena, and R. C. Ewing, 2007, *Chem. Phys. Lett.* **441**, 216.
- Zhang, F. X., J. Lian, U. Becker, R. C. Ewing, L. M. Wang, L. A. Boatner, J. Z. Hu, and S. Saxena, 2006, *Phys. Rev. B* **74**, 174116.
- Zhou, H. D., C. R. Wiebe, Y. J. Jo, L. Balicas, Y. Qiu, J. R. D. Copley, G. Ehlers, P. Fouquet, and J. S. Gardner, 2007, *J. Phys.: Condens. Matter* **10**, 342201.